Helsinki University of Technology Publications in Foundry Technology

Teknillisen korkeakoulun Valimotekniikan laboratorion julkaisuja

Espoo 2006 TKK-VAL-1/2006

MOLD-METAL REACTIONS IN MAGNESIUM INVESTMENT CASTINGS

Celal Cingi

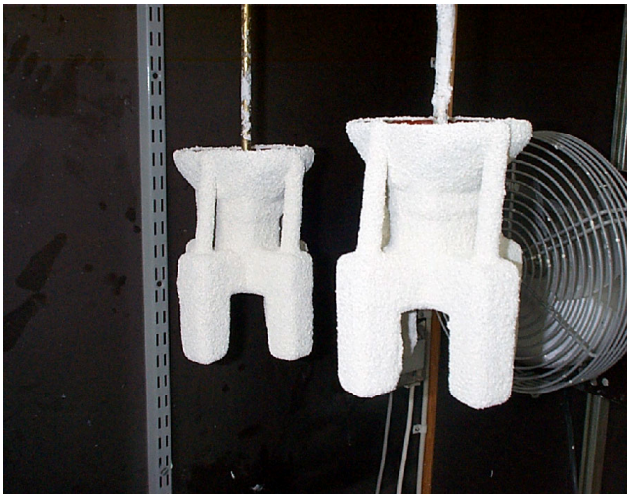

TEKNILLINEN KORKEAKOULU
TEKNISKA HÖGSKOLAN
HELSINKI UNIVERSITY OF TECHNOLOGY
TECHNISCHE UNIVERSITÄT HELSINKI
UNIVERSITE DE TECHNOLOGIE D'HELSINKI

Helsinki University of Technology Publications in Foundry Technology

Teknillisen korkeakoulun Valimotekniikan laboratorion julkaisuja

Espoo 2006 TKK-VAL-1/2006

MOLD-METAL REACTIONS IN MAGNESIUM INVESTMENT CASTINGS

Celal Cingi

Dissertation for the degree of Doctor of Technology to be presented with due permission for public examination and debate in Auditorium K216 at Helsinki University of Technology (Espoo, Finland) on the 10th of November 2006, at 12 o'clock noon.

Helsinki University of Technology
Department of Mechanical Engineering
Laboratory of Foundry Engineering

Teknillinen korkeakoulu
Konetekniikan osasto
Valimotekniikan laboratorio

Distribution:
Helsinki University of Technology
Laboratory of Foundry Engineering
P.O.Box 4100
FIN-02015 HUT
Tel. 358-9-4513939
Fax. 358-9-4513518
E-mail: celal.cingi@hut.fi

ISBN 978-951-22-8434-4
ISBN 951-22-8434-0
ISBN 978-951-22-8435-1 (electronic version)
ISBN 951-22-8435-9 (electronic version)

ISSN 1456-3568

Picaset Oy
Espoo 2006

Cingi, C., **Mold-Metal Reactions in Magnesium Investment Castings**

Keywords: magnesium, investment casting, mold-metal reactions

ABSTRACT

Mold-metal reactions can be encountered during the investment casting of magnesium alloys. This study was carried out for investigating the degree of reactions between the various refractory materials and the magnesium alloy AZ91E, and for finding new techniques to reduce these reactions.

Investment casting molds containing multiple test pieces with the dimensions of 25x25x60mm in dimension were used. The wax pattern of each test piece was coated with a different ceramic face coat in mold fabrication and the resulting differences on cast metal surfaces were studied. The backup layers of the shell were the same for all test pieces. Fused alumina, fused silica, molochite, zircon, yttria, zirconia and fused magnesia were the ceramics studied as face coat materials.

Digital pictures of the cast surfaces were taken and an image analyzer was used to a quantitatively assess the reacted areas. The results show that fused magnesia and yttria were the best face coat materials to resist molten magnesium. Fused alumina and zircon were the next best materials. Molochite and zirconia were ranked as moderate to poor in resisting reactions. Strong mold-metal reactions were seen in the case of fused silica. Shell permeability measurements suggest that the degree of reactivity is not related to the shell permeability. It can however be correlated to the free energy of formation of the refractory. The excellent reaction resistance of magnesia and yttria observed in the experiments can be explained by the strongly negative Gibb's free energy of formation and consequent stability of these materials.

HSC software was used to calculate theoretically the free energy of formation for the refractories studied in this work. The obtained results were compared to experimental values. Analysis with EDS indicated that the reaction layers consisted mostly of oxides.

Ceramic test bars coated with various refractories were dipped in magnesium melt to study for reactions. It was seen that none of the tested refractories reacted with magnesium as a result of the dipping operation. It was concluded that oxygen is required for the mold-metal reactions to be initiated.

It was verified that the atmosphere surrounding the shell also influenced the observed reactions. In molds containing both normal and reduced permeability shells around the test pieces, the surfaces cast in reduced permeability shells showed large reductions in reactivity. It is suggested that reactions in investment casting molds occur in two stages: 1. During pouring and filling 2. After the filling is complete by the effect of external oxygen.

The cooling curves of magnesia-coated test bars were compared with those of silica-coated test bars. Analysis shows that heat is released during the mold-metal reactions.

An attempt was made to incorporate the inhibitor KBF_4 in the mold structure in the form of first coat stucco. Rough cast surfaces were obtained, which indicated that the used high sintering temperature was not compatible with this inhibitor. Similarly, when the preheated investment-casting mold was placed in a bed of KBF_4 before casting, only small reductions in reactivity were obtained.

Reactivity was reduced in shells buried in a bed of Croning sand. Then, however, the cast pieces contained gas holes.

$NaBF_4$ produced better results as an inhibitor. It was first dissolved in water and then the sintered molds were dipped in this solution. Large reductions in reactivity were observed. The inhibiting effect of this chemical can be attributed to the liberation of BF_3 gas during mold preheating.

PREFACE

The research work for this thesis was carried out in a EU project on magnesium: IDEA (Integrated Design and Product Development for the Eco-efficient Production of Low-weight Aeroplane Equipment) Project Number: FP6-503826. I would like to acknowledge the IDEA project leaders for providing the financial support and permission to publish the results as dissertation. The cooperation and encouragement of Jukka Vainölä from VTT is particularly acknowledged.

I would like to thank my supervisor Prof. Juhani Orkas for his guidance in all stages of this work and for reading the manuscript. Thanks are also due to my colleagues in the HUT Laboratory of Foundry Technology. Special thanks are due to our laboratory manager Eero Niini for his suggestions and help.

I wish to express my gratitude to Petri Koivu from Helsinki Polytechnic for EDS work, to Dr. Outi Söderberg from HUT Laboratory of Materials Science for XRD work, and to Dr. Mamdouh El Haj Assad from HUT Laboratory of Applied Thermodynamics for the use of HSC software.

Finally, I would like to thank my wife Kristiina and my daughters for their support and belief in me.

CONTENTS

ORIGINAL FEATURES

Following aspects are original:

1. The experimental approach is original. The influence of a particular refractory and inhibitor on mold-metal reactions was studied by using a single mold containing multiple test pieces. Then, the casting parameters including melt and mold temperature, pouring rate and the amount of protective gas were the same for all test pieces. This enabled a more reliable comparison of the mold-metal reactions resulting from different refractories as each separate test piece was coated with a different refractory. Treatments for reducing the reactions, such as use of inhibitors were applied only on one half of the shell and then the differences between pieces from differently treated halves could be compared.

2. The extent of mold metal-reactions was assessed quantitatively. An image analyzer was used to measure the reacted surface area in each piece.

3. The influence of external oxygen on mold-metal reactions was addressed by shell permeability measurements. Although foundries know this effect, there is no previous work, where this would have been shown by measurements. It is suggested that the mold-metal reactions in investment casting molds occur in two stages: a) during pouring and filling and b) after the filling is complete by the influence of external oxygen. It was shown that the presence of oxygen is essential for the mold-metal reactions to start.

4. It was found that $NaBF_4$ could have an inhibiting influence on mold-metal reactions in ceramic shells during magnesium casting. Method of incorporating this chemical in the mold structure is original. The chemical was first dissolved in water and then the sintered molds were dipped in this solution.

1 INTRODUCTION

Magnesium is the lightest of all commonly used metals. It is one third lighter than aluminum. This property is one of the reasons for selecting magnesium for a structural component. Due to its excellent damping capacity, which provide vibration absorption ability, corrosion resistance and excellent machining characteristics, use of magnesium in industry, particularly in automobile industry is consistently increasing.

Magnesium melts at 650^{o}C which is about the same as the required to melting point of aluminum. Unlike aluminum, during melting, the molten magnesium must be prevented to come into contact with the oxygen in air. It reacts spontaneously with oxygen, and therefore the melting and casting of magnesium alloys are carried out under a protective gas.

All known casting processes including investment casting can be used for to production of magnesium castings. However there are only a limited number of investment foundries, which are casting magnesium at this moment. The foundries producing aluminum investment castings are not necessarily familiar with magnesium investment casting. With the increasing general demand for magnesium parts, the number of magnesium investment foundries is expected to increase in future.

Mold-metal reactions in magnesium investment castings have not been studied in detail. Main reason for this is again the fact that magnesium must be melted and cast in a protective atmosphere to avoid the rapid oxidation and consequent catastrophic burning of the mold. This makes the subject difficult to study. The similar light metal aluminum has been the research subject in many universities and research organizations mainly due to its easy melting and casting. This has resulted in a huge amount of knowledge on the properties, melting and casting of aluminum alloys. Magnesium reacts practically with all refractories which the shell molds are made of. In order to assess these reactions in more detail, quantitative methods must be applied for comparing the extent of reactions for each refractory. Quantitative measurements are essential also for determining the efficiency of methods and chemicals in preventing the mold burning.

1.1 Review of Earlier Work on Mold-metal Reactions in Magnesium Investment Castings

There are only a few published papers specifically concentrating on the mold-metal reactions in the investment casting of magnesium alloys. The results and conclusions obtained in these studies are reviewed on the following pages.

Mold-metal reactions have been generally explored on the basis of the free energy of formation of refractories and of the tendency of the melt to react with the mold material and producing oxides. Therefore, the review of earlier work begins with a section discussing the free energy of formation and stability of oxides.

Some part of the earlier research work has been directed to understanding and explaining the mechanisms of melt and mold protection by using protective gas atmospheres on magnesium melts (1,2,3,4).

There are also some general articles on mold-metal reactions in investment castings (5,6). These review articles mostly give examples of reactions in either titanium casting or superalloy casting. Most of the research work on mold-metal reactions has been carried out for explaining mold-metal reactions in sand castings.

1.1.1 Stability of Oxides (7)

In order to understand mold-metal reactions, we must start by considering the stability of oxides and chemical compounds in general.

Theoretically a refractory oxide can be produced directly from its elements, for example for producing magnesia:

$$2Mg + O_2 \longrightarrow 2MgO$$

If this equation is written in reverse direction, it represents the decomposition of magnesia:

$2MgO \longrightarrow 2\,Mg + O_2$

The Gibbs free energy change for this kind of chemical reaction is called the free energy of formation, denoted as ΔG^o_f. A large negative value of ΔG^o_f indicates a strong driving force for compound formation. It also shows a high resistance of the compound to thermal decomposition (reverse reaction). For the stability comparison of oxides, it is sufficient to compare the values of ΔG^o_f of room temperature, denoted as $\Delta G^o_{f,298}$.

Generally the chemical stability increases with increasing melting point. Figure 1 is a plot of $\Delta G^o_{f,298}$ vs $10^4/T_m$ (where T_m is the melting point in degrees K) for binary oxides. The dashed line in the middle, which is chosen arbitrarily, separates acceptable refractory compounds (above the dashed line) from unacceptable ones (below the dashed line). Unacceptable compounds are disqualified by the combined criteria of both melting point and chemical stability.

Some high melting point oxides, including MgO and Y_2O_3 are among the most stable oxides (large negative values for $\Delta G^o_{f,298}$) . For magnesium casting, high melting point is not very critical due to relatively low casting temperatures, but chemical stability is of importance.

In general terms, a chemical reaction can be written as follows:

$xA + uB \longrightarrow yC + zD$

where

A and B are reactants, and C and D are products

x,u,y,z: number of moles

Gibbs free energy change for the above reaction is

$\Delta G^o_T = \Sigma \Delta G^o$ (products)- $\Sigma \Delta G^o$ (reactants)

$\Delta G^o_T = y\Delta G^o(C) + z\Delta G^o(D) - x\Delta G^o(A) - u\Delta G^o(B)$

Gibbs free energy change can also be written as

$\Delta G^{o}_{T} = \Delta H + T\Delta S$

ΔH= enthalpy change; ΔS = entropy change; T= Temperature

ΔH and ΔS values for different reactions can be found in JANAF tables (8,9) and consequently ΔG^{o}_{T} versus T can be drawn for oxides. Figure 2 and Figure 3 show the free energies of formation of simple (binary) oxides and the free energies of formation of ternary oxides respectively. At magnesium melting temperature MgO is one of the most stable oxides.

Some oxides even though they are very stable may have other properties, which make them difficult to use in any application. For instance as listed in reference 7:

BeO - Toxic dust, human carcinogen

ThO_2, UO_2 - Radioactivity

BaO, SrO - Slaking susceptibility (a concern for CaO as well)

La_2O_3, Y_2O_3, CeO_2, HfO_2, ThO_2, UO_2 – High costs (also for BaO, BeO, and SrO)

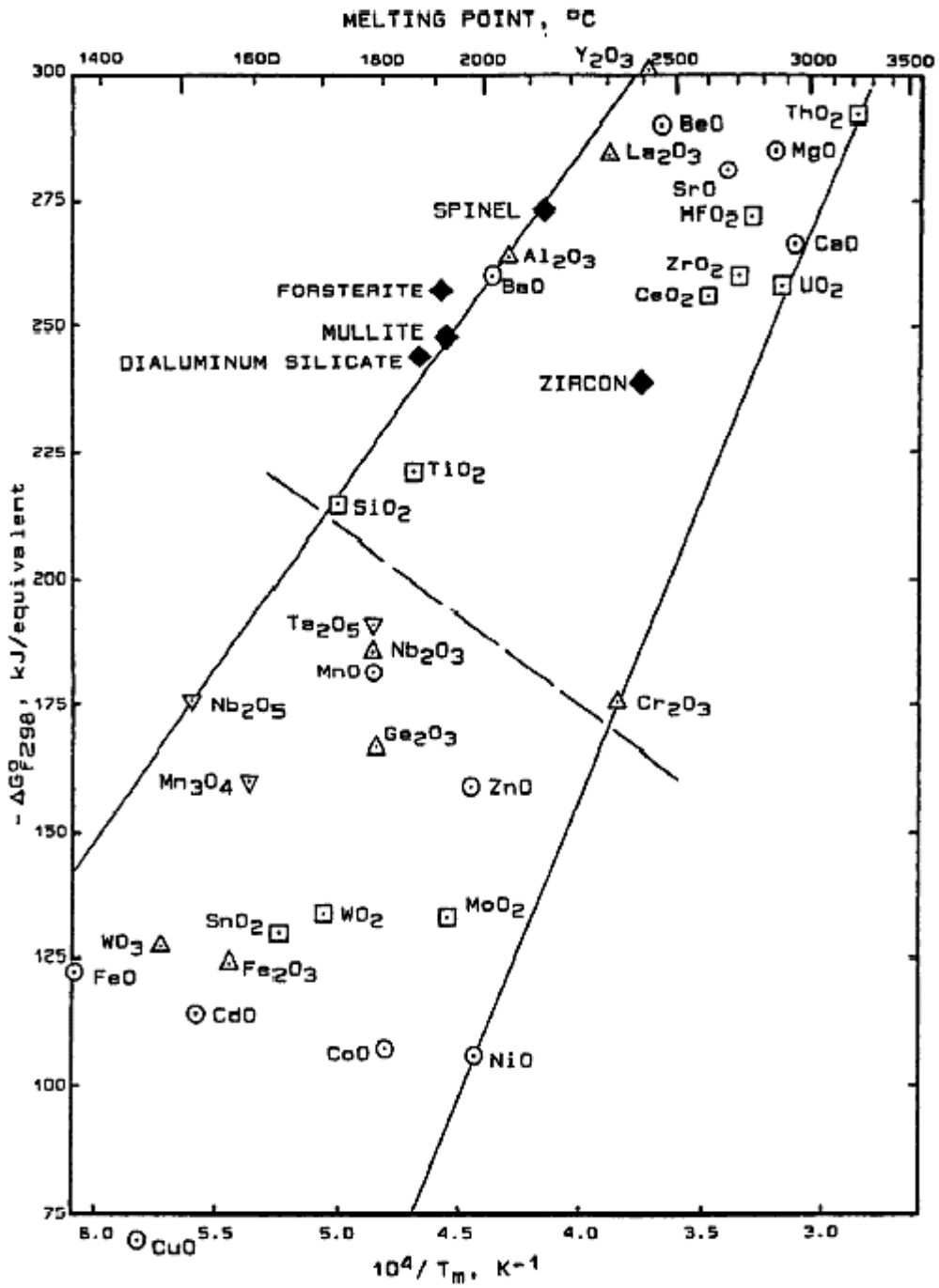

Figure 1. Standard free energy of formation of oxides (at room temperature) vs oxide melting point. (9). MgO and Y_2O_3 are among the most stable oxides (very large negative values for $\Delta G^o_{f,298}$)

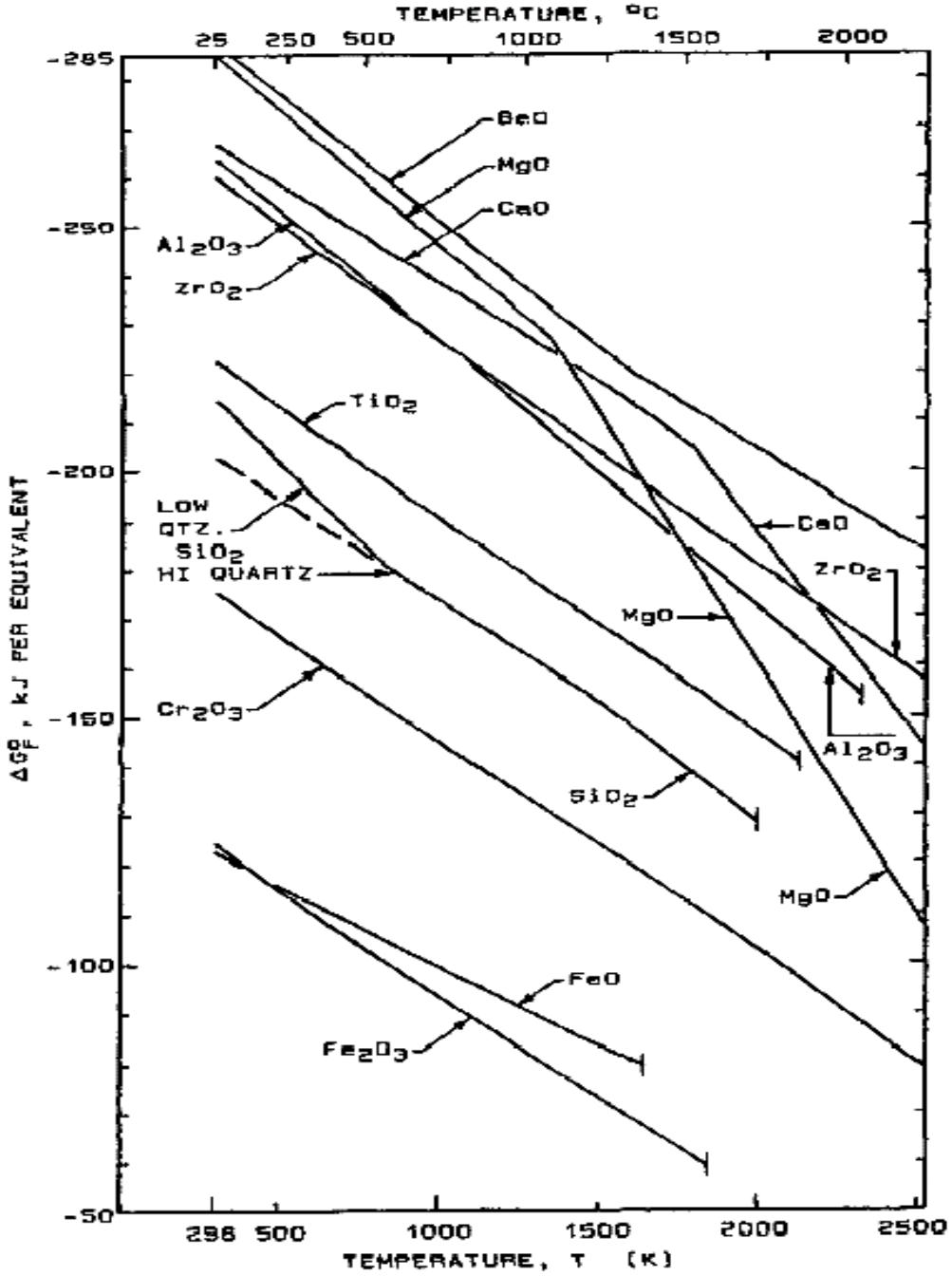

Figure 2. Free energies of formation of simple oxides vs temperature (8)

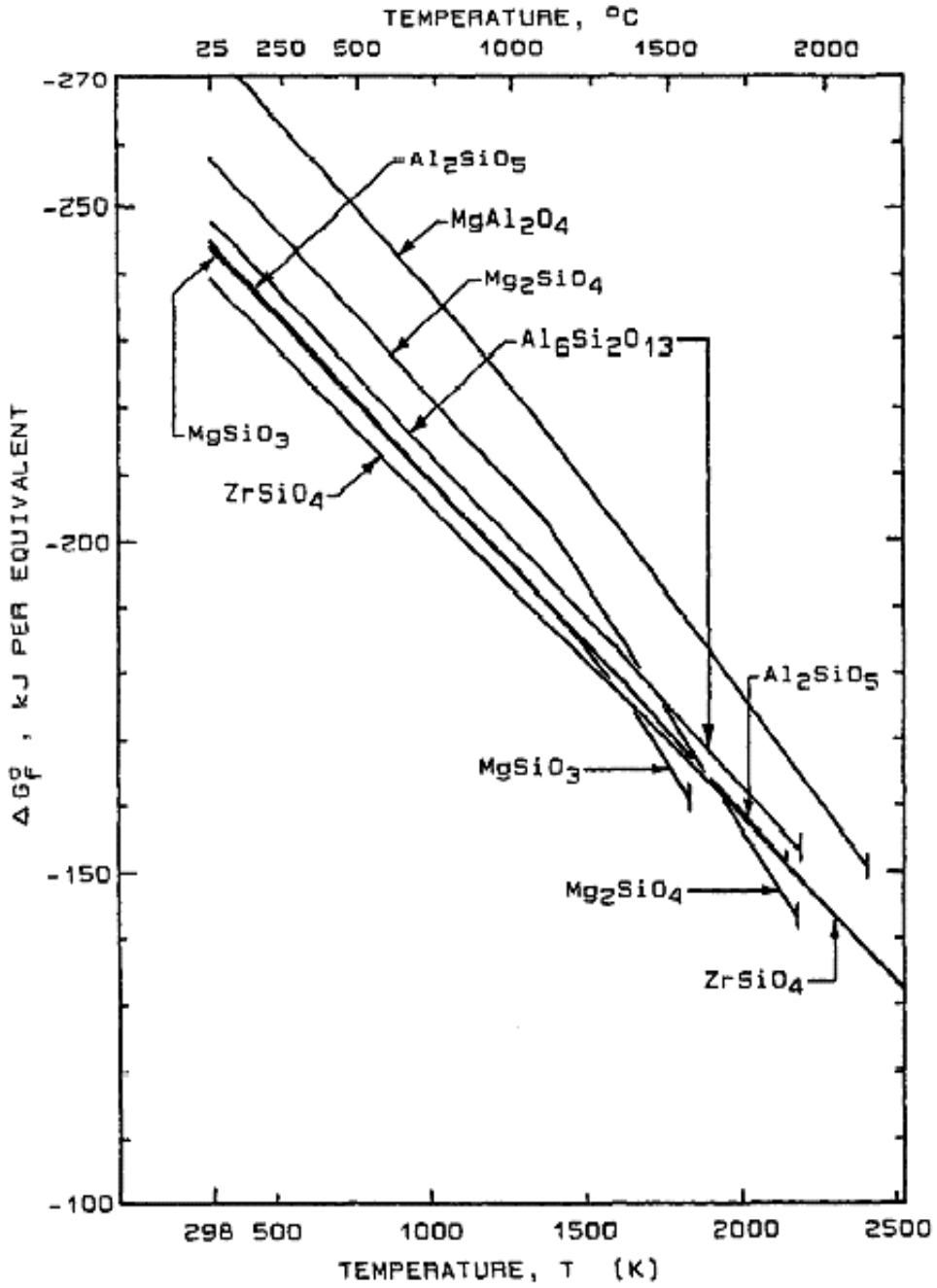

Figure 3. Free energies of formation of ternary oxides vs temperature (8)

1.1.2 Classification of Mold-Metal Reactions in Investment Castings

Frye, Yasrebi, and Sturgis (6) classified the mold-metal reactions as follows:

1. M_xO_y = xM(dissolved) + yO (dissolved)
2. M_xO_y + z MA (dissolved) = MA_zO_y (g) + xM (dissolved)
3. M_xO_y + zMA (dissolved) = MA_zO_y + xM (dissolved)
4. M_xO_y + zMA (dissolved) = $MA_zM_{x-w}O_y$ + wM (dissolved)
5. M_xO_y = xM (g) + yO (dissolved)
6. M_xO_y = M_xO_y (l) where

M_xO_y= an oxide; MA= an element in the alloy

Reaction 1 describes the dissolution of shell material into the liquid metal. For instance

Al_2O_3 = 2Al + 3O

If titanium is melted in an alumina crucible, substantial amounts of oxygen and aluminum metal dissolves into molten titanium regardless of the fact that the ΔG of alumina is more negative than that of TiO_2. The reason for this is the formation of sub-oxides. The ΔG for the formation of sub-oxides of titanium (i.e. TiO) is more negative than the ΔG of alumina.

Reactions 2, 3, and 4 characterize the reaction of the molten metal with the mold.

An example of reaction 2 is the rapid decarburization of NiTaC alloy based on the following reaction

M_xO_y + z C (in the alloy)= yCO(g) + xM(dissolved) (10)

Reaction 3 involves reduction of the mold by the metal to form another metal oxide. For example:

Al_2O_3 + 3Mg = 3MgO + 2Al

Another good example is the reaction between Ti, Al, or Hf in superalloys with the mold oxides (5). The above reactions normally produce thin layers of molten metal oxide at the metal-mold interface. Such interfacial reactions are commonly stable and may be beneficial for the cast part by hindering further reactions between mold and the molten metal. Another example of reaction 3 is the reaction between the titanium and the mold oxides in molten titanium alloys to form TiO or TiO_2. The above oxides are frequently not seen because these oxides dissolve rapidly in the molten metal.

Molten metal may form double oxides with the mold material as shown in reaction 4. An example is the reaction between Al and rare earth oxides:

$Y_2O_3 + Al = YAlO_3 + Y$

The ΔG of rare earth oxides is normally more negative than the ΔG of alumina. Therefore the ΔG of double oxides comprised of alumina and a rare earth oxide are more negative than those for pure Al_2O_3. This explains why the molten Al is more reactive with rare earth shell molds than it appears to be on the basis of the single oxide ΔG data.

Reaction 5 shows a gaseous reaction product in the cast part. An example of such reaction is shown by Ingo and co-workers (11). The authors showed that the $CaSO_4$-SiO_2 -based mold materials used for casting alloys of Au or Pd decompose according to the following reaction:

$CaSO_4 = CaO + SO_2$ (g) + O (dissolved)

The produced oxygen dissolves into the alloy and forms oxides with the alloying elements such as Cu, Ag, and Zn. For instance

O (dissolved) + Zn = ZnO

The dissociation of $CaSO_4$ is further catalyzed by the presence of SiO_2 and ZnO in the melt and a high concentration of SO_2 gas in the cast results.

Reaction 6 represents solid to liquid transformation of ceramic components in the shell mold. Solid to liquid transformation does not contribute to a substantial change in the ΔG of oxides (12). However the formation of the liquid phase increases the oxide mobility. Consequently, the kinetics of the reactions increases the formation of the liquid phase also lowers the mechanical stability of the shell mold. Consequently the surface erosion and penetration of the metal into the mold may result.

Mold-metal reactions in investment castings were also reviewed by Piwonka (5). According to this researcher, the following classification can be made:

1. Molten metal dissolves the mold: A well-known case of molten metal dissolving the mold is found in titanium castings. When molten titanium dissolves the mold, oxygen from the mold goes into solution in the titanium, and when the oxygen content of titanium exceeds 250 ppm,

the hardness level of the solidified metal increases. When this occurs on the surface of the casting, this hard outer "case" (the "alpha case") can cause premature failure of the cast component. The formation of alpha case is a function of the temperature of the liquid metal and the time, which the casting spends above 500^{o}C. Below this temperature the rate of oxygen diffusion in titanium becomes negligible.

The primary parameters, which influence the formation of the alpha case on the exterior surface of cast titanium are related to the strong affinity of titanium to oxygen. The sources of oxygen include:

a. Initial oxygen content of the melt.
b. The oxygen picked up by the metal as it travels through the gating system.
c. Oxygen picked up from the furnace atmosphere. This is negligible in vacuum melting.
d. The oxygen dissolved from the mold when the metal comes to rest in the casting.

According to Piwonka, only the last is of significance. When the molten metal comes to rest there is no oxygen gradient in the metal. However, as the metal lies against the mold surface, the mold dissolves in the molten titanium alloy, and oxygen begins to diffuse into the casting. Even if titanium reacts with some mold elements, such as silica, to form TiO_2, as the free energy of formation of TiO_2 is more negative than that of SiO_2, TiO_2 is also soluble in the molten titanium (13), little TiO_2 is found on the surface of the casting.

2. Molten metal reacts with the mold: The actual reaction of molten metal with the mold material may also occur but it is rare. What is usually considered to be a mold/metal reaction is actually often a reaction with the atmosphere in the mold. However the titanium and aluminum in superalloys can react with the silica in the mold to form a thin reaction layer at the interface. Also Hf in superalloys may react with molds and cores.

$Hf + SiO_2 = Si + 2HfO$

Hf reacts also with zirconia to form hafnium oxide. The formation of hafnia is good for the quality of the castings; as it is stable it can stop further reactions between metal, mold and core.

3. Molten metal dissolves the mold material and reacts with it: This is the main reaction in titanium castings. However, the products of the reactions (where TiO and TiO_2 are formed) are frequently not seen as these oxides dissolve rapidly in the metal. Mold dissolution was found to be more dominant than mold reaction.

4. Molten metal reacts with the atmosphere in the mold: Most of the mold/metal reactions which are encountered depend on the reactions of the metal with the gas (usually air) in the atmosphere. In fact the resulting metal oxide causes often the most severe problems. E.g. oxide inclusions in steel (14,15), and oxide films in aluminum castings (16).

5. Molten metal physically penetrates the mold, causing a rough surface: This is more prevalent in sand castings (17,18,19). As the investment casting molds are made with fine grain refractories in the prime dip, the mechanical penetration of metal into the mold is actually impossible.

6. Molten metal reacts with gas in the mold and the reaction product reacts with the mold: A well-known example is the oxidation of iron, which can be followed by the reaction of iron oxide and silica to form fayalite (Figure 4). Fayalite is a low melting point mixture of iron oxide and silica, it can dissolve both silica and iron oxide.

   This reaction never occurs in cast iron, as the carbon in the alloy reacts with oxygen in the mold atmosphere and depletes the mold atmosphere from oxygen before fayalite can form.

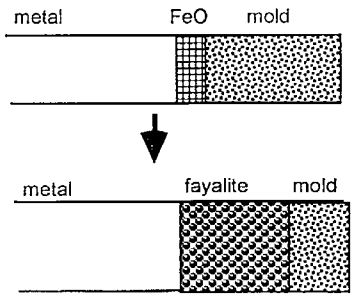

Figure 4. Fayalite formation at the mold-metal interface of ferrous castings (5)

In steels, where the carbon content is much lower, oxidation of iron to iron oxide can occur. The iron oxide can, in turn, react with silica in the prime dip to yield a mold reaction. Even if

silica is minimized in the prime dip, its presence in the binder (colloidal silica or ethyl silicate) still leaves for the mold a possibility to react with iron oxide.

7. Solid metal reacts with the atmosphere: A casting cooling in a mold may react with oxygen in the case of steels the metal is usually decarburized. As the investment castings are usually small, they tend to cool so quickly that the decarburization is not a problem.

There are also beneficial mold-metal surface reactions in investment castings. The best known beneficial reaction is the effect of $CoAl_2O_4$ in controlling the grain size in nickel-base alloys. In this case, cobalt aluminate crystals act as nuclei for the heterogeneous nucleation of nickel grains on the surface of the castings.

1.1.3 The Wettability of Ceramic Materials by Liquid Metals

When a liquid droplet is placed on a solid, the equilibrium shape of the droplet will result from the balance of the surface energy of the three different surfaces, liquid/solid (LS), liquid/vapor (LG) and, and solid/vapor (SG). The equilibrium shape of the drop minimizes the surface energy (19,20,21). This shape is originally a sphere but under gravitational forces the sphere flattens to an ellipsoid. The equilibrium between the surface energies of the three interfaces is described by Young's equation:

$$\gamma_{LG} \cos\theta = \gamma_{SG} - \gamma_{LS}$$

where γ is the surface energy, and θ is the contact angle between the liquid and the solid.

If the contact angle θ is smaller than 90^o then the liquid wets the solid. If θ is greater than 90^o, we have conditions of non-wetting. If $\gamma_{SG} > (\gamma_{SL} + \gamma_{LG})$, no nonzero value of θ will satisfy Young's equation. The liquid will cover the whole surface, and complete wetting result (spreading). If $\gamma_{SL} > (\gamma_{SG} + \gamma_{LG})$ again no equilibrium value of θ can be found. In this case no contact area can form and the liquid will not wet the solid at all.

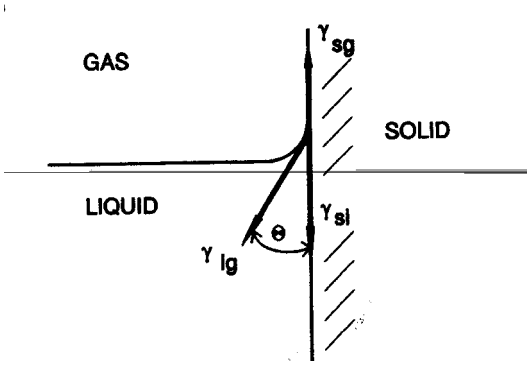

Figure 5. Forces acting on solid-liquid-vapor contact line (20)

Wettability is significantly influenced by many factors. Even in the same solid-liquid system the obtained results have been different among different investigators. Wettability is affected by key factors such as alloying elements, roughness and crystal orientation of solid material, and impurities (22).

It has been found that the additions of Ni, Cu and Si to liquid iron slightly reduce the surface energy of iron, whereas Ca, Mg, Ce, S, Se, and Te have a much stronger influence (23).

The surface energy and consequent surface tension decrease with increasing temperature. This has been shown by several investigators (24).

Wettability is enhanced by the addition of impurities in the liquid in several systems. For instance, oxides of transition metals such as Ta_2O_5 can be added to glass to increase the wettability when coating stainless steels with glass (25).

In galvanizing, hot-rolled steel is immersed in an aqueous solution of zinc and ammonium chloride salts. On withdrawal, the flux solution evaporates leaving a thin crystalline deposit of fluxing salts, this enables the uniform wetting of steel by molten zinc (26).

In sand casting, a method known to successfully prevent the penetration is the coating of the mold cavity[1]. Recommended coatings include talc, coke dust, graphite, zircon sand and colloidal silica. The efficiency of coatings or washes can be addressed to decreased wettability and to the higher bulk density of the mold surface (27,28,29,19).

Some refractories are known to be "non-wettable" by definite metal alloys. This is a useful property when the refractory is used as a melting crucible. For instance, (contrary to alumina crucibles), zirconia crucibles are not wetted by nickel-base superalloys. This increases crucible life.

1.1.4 Melting of Magnesium

Molten magnesium reacts with oxygen and oxygen containing materials. Reactions are exothermic. The following reactions may occur during the melting of magnesium (30):

1. Burning/oxidation
   $Mg + O_2 = 2MgO$
2. Rapid evaporation (expansion) of water entrapped by liquid magnesium
   $Mg\ (liq) + H_2O\ (liq) = H_2O\ (vapour) + Mg$
3. Water reaction/Hydrogen explosion
   $Mg + H_2O = MgO + H_2$
   $2H_2 + O_2 = 2H_2O$
4. Thermite reaction
   $3Mg + Fe_2O_3 = 3MgO + 2Fe$
5. Silica reaction
   $2Mg + SiO_2 = 2MgO + Si$

Magnesium reacts not only with silica but also with most of the other oxide based refractories. Therefore, an oxide based refractory crucible is not suitable for magnesium melting.

[1] Investment molds are made with layers of fine grain refractories in the face coat. Therefore the mechanical penetration of the molten metal into the mold wall is almost impossible (5)

Possible crucible materials for melting of magnesium melting are (31,32):

1. Wrought or cast iron or steel: Iron does not react with magnesium
2. Low alloy steels (low chromium steels). Nickel and copper contents must be restricted to max 0.10%.

Cast iron crucibles can be prepared with an outer nickel layer cladded to the crucible in order to reduce scaling.

1.1.5 Protective Gases

A protective flux or a protective gas must cover the molten magnesium to prevent burning. There are a few available gas and flux systems in use today:

1. Sulfur hexafluoride SF_6 (33): This is a colourless, odourless and non-toxic gas. The protective power of SF_6 was discovered at the end of the 1970's and SF_6 was considered as an ideal protection system except for the high costs, and a certain tendency to attack the crucible walls when the concentration and/or humidity was too high. It was later discovered that SF_6 is a very effective greenhouse gas: 23,900 times worse than CO_2. The present trend in some countries of Europe is to ban its use in magnesium casting due to its strong greenhouse effect.

   SF_6 is normally used as mixed with a carrier gas. For die casting operations the SF_6 content can be as low as 0.6% (vol), whereas for sand casting and investment casting where the pouring temperatures are considerably higher, the SF_6 content needs to be up to 2% of the gas mixture. Air, CO_2, argon or nitrogen can be used as the carrier gas (34).

2. Sulfur dioxide SO_2: This is not a greenhouse gas. However, it is toxic and its concentration in the working atmosphere should be monitored continuously. The recommended concentration is 0.5-0.7% by volume of dry air (33).

3. Hydrofluorocarbon gas 1,1,1,2-tetrafluoroethane HFC-134a: This is a new and patented protective gas. It is environmentally friendly and it is used by a limited number of installations at the moment. The recommended concentration of the gas is 0.5-0.7% by volume of dry air (35).

4. Magshield system (36): It is based on the decomposition of boron bearing powder KBF_4.

   $$KBF_4 \xrightarrow{375\text{-}900\ C} BF_3\ (gas) + KF$$

   BF_3 is as effective as SF_6 in magnesium melt protection. However it is a toxic gas. Its concentration in the atmosphere should be therefore continuously monitored. The recommended concentration is 0.4-0.8% by volume of dry air.

1.1.6 Flux Materials

Instead of a protective gas, a powder flux can be used to prevent burning. A suitable flux prevents burning and it can also remove non-metallic impurities. There are several proprietary fluxes (34), but KBF_4 can also be used (37). KBF_4 produces protective BF_3 gas on heating (see 1.1.5). Protection from burning is satisfactory with flux, but the flux inclusions trapped in the casting may be a problem.

1.1.7 State of the Art: Commercially Available Shells for Magnesium Casting

The commercially available shell systems for investment casting can in general be described as follows:
The most universal ceramic for the face coating in investment casting molds is zircon ($ZrSiO_4$). Fused silica is also used, particularly in the USA. For the back-up coatings, alumino-silicates are widely used both in the USA and Europe. Molochite is an alumino-silicate based material.

The shell systems used for magnesium castings in investment foundries can be described as follows:

According to a U.K manufacturer of binders (38), there are two alternatives for the shell systems and casting methods used in investment casting of magnesium:

1. The use zircon-aluminosilicate standard shells for investment castings. An additional sealing of the exterior surface of the mold before pouring for reducing metal-mold reactions. For sealing, a layer of (porcelain) glazing is applied on the shell (39). Before pouring, the mold cavity is flushed with SF_6.
2. The use of a silica-free binder for instance the ammonium zirconium carbonate. The use of zirconia ceramics for mold material.

The first method is less costly and therefore it is more commonly used. The second method involves more expensive materials.

1.1.8 The Mold-Metal Reactions in the Investment Casting of Magnesium

Idris and Clegg (40) studied the mold-metal reactions both in Shaw-type[2] molds and ceramic shell molds. They also showed the effectiveness of the protection provided by SF_6 and the importance of the amount of SF_6 in the gas mixture.

The mold-metal reactions in alumino-silicate molds (ceramic shell molds) were reduced by flushing the mold with SF_6 gas before pouring. The use of CO_2/SF_6 gas mixture was studied at three different flow rates. The first mold was flushed at a rate of 25 liters/min, the second at 15 liters/min and the third at 5 liters/min. The flushing gas was flowing for approximately 30 seconds. The melt was poured at a temperature of $730^oC \pm 5^oC$.

The casting formed in the mold flushed with the flow rate of 25 liters/min exhibited a clean metallic finish. There was no sign of a mold-metal reaction. The castings produced at the flow rates of 15 and 5 liters/min demonstrated dull metallic surfaces.

[2] In the Shaw process (48) a permanent pattern is used to produce a jointed mold, whereas in the investment casting process an expendable wax pattern is used which permits a single-piece mold to be produced. Similar refractory and binder materials are used in each of the two processes, to produce after firing, strong and inert molds suitable for casting a wide range of alloys. Shaw process uses a liquid ethyl-silicate binder and a gelling agent. Hardening time of the slurry is controlled by the amount of the gelling agent. After hardening the mold is immediately torched to remove evolved alcohol. Shaw type molds are then sintered to remove combustible materials and to improve strengh.

When the molds were flushed directly in air with CO_2/SF_6 gas, reactions were observed in both Shaw molds and ceramic molds. When the mold was flushed within a closed container, a clean metallic surface was obtained. There were no signs of black spots indicating mold-metal reaction. The authors suggested that although the protective gas is heavier than air, it does not remain inside the mold, since it might be pushed out by the dynamic turbulence of the incoming gas. The method of putting the ceramic mold inside an enclosure and flushing the whole system (both the mold cavity and the enclosure) was considered more reliable. It 'ensured that the flushing gas remains both within the enclosure and the mold'.

It was also observed that when the pouring temperature was reduced, the severity of reaction seemed to also reduce.

The researchers (40) also studied the mold-metal reactions in Shaw molds made of magnesium oxide, calcium oxide, silicon carbide, calcium carbonate, graphite and anhydrous calcium sulphate (plaster). The Shaw molds, which were produced by using magnesium oxide, calcium oxide and calcium carbonate burned away and disintegrated slowly after the magnesium melt was poured into the molds. The authors had anticipated that the magnesium alloy would not be oxidized by these materials, because they all are stable compounds when compared to magnesium alloy. The reason for the unexpected result is explained as follows: The molds burned away immediately after the magnesium melt was poured into the mold because during the torching state for removing the alcohol, the bonding agent might have disintegrated. Therefore, the use of ethyl silicate for bonding these materials is inappropriate. And furthermore, even though the three materials mentioned above are stable compounds by themselves, when bonded with ethyl silicate, a reaction might take place between the magnesium alloy and the silica of the binder.

The castings produced by using graphite and silicon carbide molds also exhibited burns all around their upper surface. This is also explained by insufficient bonding provided by the ethyl silicate binder.

Kim et al (41,42,43,44) compared the mold-metal reactions in ceramic shell molds made of Al_2O_3 and $ZrSiO_4$ bonded with colloidal silica, of $CaZrO_3$ bonded with a silica free binder, and of CaO[3] molds. When the mold temperature was below 400°C, no reactions occurred between the melt and the Al_2O_3, $ZrSiO_4$ and $CaZrO_3$ molds. For CaO molds reactions were observed at 350°C and reactions were observed even when the mold was at the room temperature before pouring.

When the mold temperature was above 600°C, significant reactions occurred between the melt and the conventional silica-bonded Al_2O_3 and $ZrSiO_4$ molds. $CaZrO_3$ molds were reaction free even at this high temperature.

The above results were obtained by comparing the photographs and by judgements based on visual observations. It was concluded that the relative stability of oxides can be ranked in the order of increasing stability as follows: $CaO \rightarrow ZrSiO_4 \rightarrow Al_2O_3 \rightarrow CaZrO_3$. The grading corresponded to the free energy data for the formation of these oxides calculated by the authors, except for CaO mold. The unexpectedly poor performance of CaO was explained by the hydration susceptibility of this material in air.

[3] For CaO, it was not possible to make a shell mold with CaO, so a rammed mold was used for comparisons (42), because calcium oxide has a very high affinity for water (hydration). For this reason, CaO-based refractories have not yet found a widespread use (45). Hydration is a problem also for MgO.

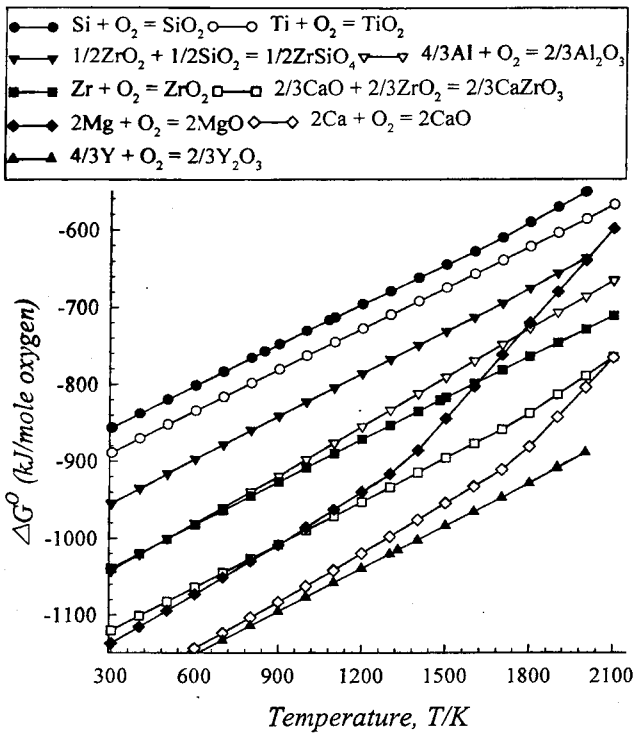

Figure 6. The standard free energy change for the formation of oxides as calculated by Kim et al (42)

The magnesium alloy did not show any reaction with CaO mold when the alloy was melted in plasma arc furnace in vacuum and was immediately poured into a CaO mold. The authors concluded that there is a possibility that the reaction of the melt with the CaO mold in air could have been occurred by the reaction of CaO with MgO that was generated on the surface of the casting at an early stage of mold filling.

Zhang et al (46,47) studied the reactions of magnesium with colloidal silica-bonded zircon shells and zirconia sol-bonded zirconia shells. The molds were preheated to 650^{o}C before casting.

In both shell systems mold-metal reactions were observed. The mapping of elements Mg, O, Si and Zr by electron probe microanalysis (EPMA) showed that there was magnesium oxide layer in the shell mould and that the thickness of the magnesium oxide layer was more than 100 μm.

In another set of experiments, molds were flushed for 40 seconds with a mixture of CO_2/SF_6 protective gas before pouring. Excellent casting surfaces were observed. However there were some signs of reaction. It was found that there were reactions between the magnesium and zircon shells and that a compound of magnesium, oxygen and fluorine appeared on the inside surface and on the wall of the zircon shell.

The influence of concentration of SF_6 in the protective gas was also studied by the same investigators (47). When the amount of SF_6 was 1%, magnesium melt–mold reactions were observed in zircon shells. There were no reactions in zirconia shells. When the amount of SF_6 was over 1%, a clean casting surface was obtained also in zircon shells.

Based on the measurements of the content variations of Mg, O, F, Si, Al, S, C and N across the reaction depth, the following model for the reactions was proposed:

1. When no protective gas is used, magnesium reacts with oxygen and yields a magnesium oxide film. As this film is porous, magnesium or magnesium vapor will penetrate the oxide layer to react further with shell materials.
2. When the inhibitor gas is used, fluorine and sulfur from SF_6 react with magnesium or magnesium oxide. These reactions enhance the apparent density of the porous oxide film (less pores). Aluminum could also participate in the reactions as it appears in the special layer. However the role of aluminum in the reaction prevention is not clear. The improved oxide layer makes the penetration of atoms such as magnesium and passing through the film more difficult. As the concentration of SF_6 in the inhibitor mixture is increased, the content ratio of fluorine to oxygen in the special layer increases. This would further enhance the quality of the special layer.

The protective surface films formed on molten magnesium were investigated by Cashion, Ricketts, and Hayes (2,3). The XPS (X-ray photoelectron spectroscopy) analysis indicated that MgO and MgF_2 were the only chemical compounds present in the film when the air+SF_6 protective atmosphere was used. Sulfur and sulfur containing compounds were not detected. The

types of the chemical compounds present in the protective film do not change with the concentration of the SF_6 in the protective gas or with the time of exposure to the protective gas.

When molten magnesium is exposed to a protective gas mixture containing SF_6 and oxygen, a layer of MgO crystal particles form on the melt surface due to the initial reaction between the oxygen and magnesium. Under the SF_6 containing gaseous environment, the liquid magnesium **wets** the solid magnesium oxide. The magnesium metal is drawn up between the MgO particles by capillary action. The MgO particles form a cohesive *raft* on the melt surface (Figure 7). This minimizes the exposed surface area of the melt, reduces significantly further magnesium vaporization and prevents the subsequent rapid oxidation and burning. The decomposition of SF_6 provides fluorine for the formation of MgF_2. The fluorine also can be integrated in the product layer.

If the protective gas mixture does not contain SF_6, the experimental observations show that the oxidation of magnesium produces a fine MgO fume. The MgO particles do not form a stable layer on the melt surface, which allows the rapid oxidation of the melt to continue. The SEM micrographs showed a porous reaction layer which did not adhere to the metal surface. The porous layer allows the rapid vaporization of magnesium to continue.

Pettersen, Ovrelid, Tranell, Fenstad, and Gjestland (1) came to similar conclusions. The MgO crystals are formed first. The amount of fluorine increases with time as the film grows thicker. After a long time exposure to SF_6, the surface turns grey. This is explained by the increasing film thickness and by the transformation into the thermodynamically more stable MgF_2 phase. It was also found that under an N_2 atmosphere, SF_6 did not protect magnesium. This indicates that the rapid initial formation of the MgO film is necessary for the protective action of SF_6. The NF_3 compound protects the surface also very well. This gives a strong indication that the fluorine is the active element in the protection.

In the atmosphere consisting of SO_2 and air the melt was also well protected and the casting surface remained shiny even after extended exposure. The thin surface film was found to be dense

and continuous similarly to what was observed in fluorine containing atmospheres. It consisted of small grains of MgO with some dissolved sulfur.

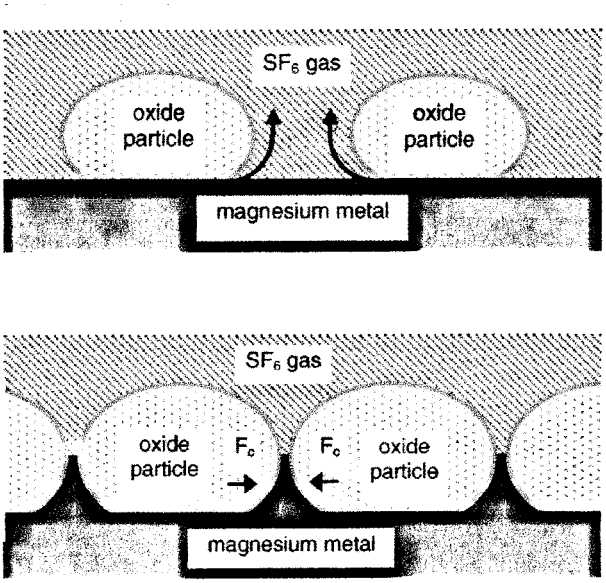

Figure 7. Under SF_6 -containing atmosphere, molten magnesium wets the MgO particles. The oxide particles on the molten metal surface are drawn together by capillary forces (3)

The protective film formed by SF_6 was further investigated by Aarstad, Tranell, Pettersen, and Engh (4). The initiation stage of film was followed closely under a hot-stage microscope. It was observed that on heating the magnesium, dark spots with elevated fluorine contents started to appear on the interface between the magnesium bulk metal and the magnesium oxide formed on the surface already below the magnesium melting point. The number of (MgF_2) spots was seen to increase with time. The fraction of surface covered by the oxide layer as a function of time was calculated both by manually and by using an image analyzer.

The thickness of protective film was measured by TEM and, also by EPMA (electron probe microanalyzer).

1.1.9 Inhibitors for Magnesium Casting

Inhibitors are chemicals which reduce the rate or prevent completely a definite chemical reaction.

KBF_4 (potassium tetra fluoroborate) is used as an additive in sand castings and plaster mold castings to prevent magnesium metal-mold reactions.

Other chemicals, which have been suggested and used as inhibitors are sulphur, boric acid, ammonium fluorosilicate, sodium fluorosilicate, ammonium bifluoride (NH_4FHF), and different combinations of these (34,48,61).

In sand castings, any of the above or a combination can be used in varying amounts usually ranging from 0.5% to 2%. Cores can also contain inhibitors. For cores, KBF_4 is known to cause misruns (49); therefore often only sulfur and boric acid are used in cores when casting light sections.

KBF_4 is supplied under the trade name "Sand Inhibitor K" by John Winter &Co. Ltd, UK. It is used by some sand foundries in U.K., and by at least one plaster mold foundry in Denmark (Temponik Metal). The marketing company does not know any user of this material in investment castings. KFB_4 is also used as a flux on magnesium melts to prevent burning (37).
$NaBF_4$ (sodium tetra fluoroborate) is also used as an inhibitor in sand castings. This chemical is not as effective as KBF_4, therefore larger amounts are added to the sand mixture. A typical amount is 2%, as compared to 1%, which is sufficient for the KBF_4 (39).

Idris and Clegg (40) tried KBF_4 as an inhibitor in Shaw molds (block molds). Molds were produced with additions of 2,4,6,8,20,30,40,and 50% by weight KBF_4. After sintering at 1000^oC, it was observed that molds containing more than 30% of inhibitor had disintegrated. The remaining molds were cast. Apart from the casting produced in the mold containing 20% KBF4, all castings exhibited heavy reactions on the surfaces, i.e., a dark "burn-like" appearance. The bottom parts of the castings showed a better finish (metallic surface). Generally, it was observed that, with the increasing amounts of KBF_4 addition, the severity of reactions seemed to be reduced. The casting produced in the mold containing 20% KBF_4 exhibited a metallic appearance with black spots all over its surface.

Fluoroborates dissociate upon heating according to the reaction:

$$KBF_4 \xrightarrow{350\text{-}750^{o}C} BF_3\ (gas) + KF$$

$$NaBF_4 \longrightarrow BF_3\ (gas) + NaF$$

BF_3 is known to be equally effective to SF_6 as a protective gas. Magshield system (36) which was introduced as an alternative to SF_6 uses this protective property of BF_3.

There is also a present study where a preheated ceramic shell is placed in resin sand or foam before the pouring with the aim to reduce mold-metal reactions (50).

1.2 Aim of the Work

The aim of the work carried out for this thesis was:

1. To study the severity of reactions between the various refractory mold materials and the magnesium alloy AZ91E
2. To find new techniques for reducing these reactions.
3. To provide a better understanding of the mold-metal reactions in magnesium investment casting.

2 EXPERIMENTAL PROCEDURE

2.1 Selection of Test Method

There is no universal test method for studying the metal-mold reactions in investment castings. A test method proposed by Investment Casting Institute (test #855-82 in the publication"Ceramic Test Procedures") was employed in this work with certain modifications (52). The mold contained a main wax sprue and multiple test pieces. This can be called as a modified Mock-Casting test. In this method, it is possible to apply manually a different ceramic on the mold of each test piece.

An alternative test method is the so-called "Metal-Dunk Test" in which a ceramic sample is immersed in a melt and the reaction products on the sample surface are studied. This method was not used in this work (except in section 2.9), as in Mock-casting test molds are poured under conditions similar to those in foundry production. This is particularly important in magnesium casting due to the fact that the reactions of molten magnesium with refractories depend on the use of a protective gas. As the later sections will show, some experiments, like the influence of inhibitors and the dependence of reactions on shell permeability could not have been carried out with the Metal-Dunk test. In fact, other investigators, except for the work done on SF_6 protective films on magnesium melts, used also ceramic shell molds simulating the casting conditions in foundries.

2.2 Mold Design

The molds were symmetrical. This assured that the test pieces (dimensions 25x25x60mm) received the molten magnesium at exactly the same temperature. Vents were attached to each test piece in order to ease filling and to remove the reaction gases if any (Figure 8).

Figure 8. 7-piece molds used in the study. Face coats have been applied. Each test piece has a different refractory face coat.

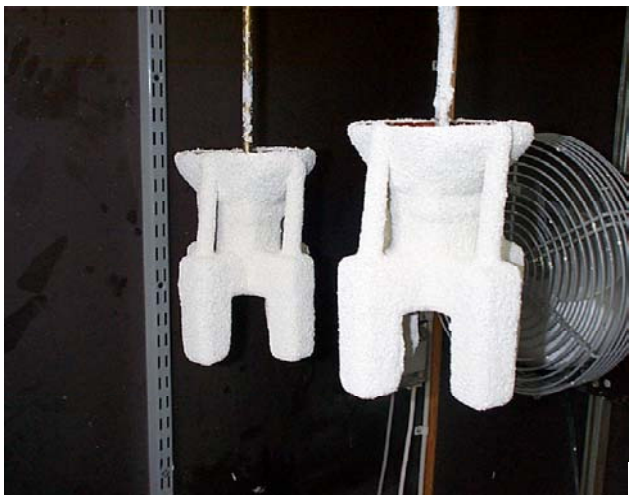

Figure 9. 4-piece molds used in the study as ready for dewaxing. Molds were dewaxed by flash dewaxing method at 750^{o}C and subsequently sintered for about 2 hours in a sintering furnace at 800-950^{o}C.

2.3 Ceramic Materials Selected for Molds

1. Fused alumina Al_2O_3
2. Fused silica, SiO_2
3. Zircon, $ZrSiO_4$
4. Molochite Al_2O_3(ab.42%).SiO_2(ab.54.5%)
5. Zirconia, ZrO_2

6. Yttria, Y_2O_3
7. Fused magnesia MgO

Besides yttria the selected ceramics are the most commonly used ceramics in foundries. Fused alumina, fused silica, zircon, and molochite are employed in shell production. Zirconia is also used in shell production and as melting crucible/furnace lining material but for shells it is considered as expensive. Yttria is also very expensive and it is used only for special cases. Magnesia is used mainly in steel melting operations as crucible and furnace lining material and as furnace bricks.

Some of the materials mentioned in the reports of other investigators are used industrially for block molds, for instance the plaster in reference 40. Two experimental mold materials, which are not included in this work are CaO and $CaZrO_3$ (41,42,43).

2.4 Composition of Slurry

Small batches of slurry (ab. 200 cc) were prepared of each refractory to be used as the face coat for the test pieces. The compositions of the slurries are shown in Table 1.

For the preparation of slurry, ceramic powder was gradually added to the binder until the slurry with a suitable viscosity for shell production was obtained. No viscosity measurements were carried out, but the density of each slurry was measured immediately when the slurry was ready.

The large differences between the densities of different slurries are mainly due to the differences in the densities of the dry powders.

Table 2 shows the powders and stuccos used for each layer. Each material supplied by the manufacturer has a specific grain size distribution. For example the grain size distribution of fused silica 50-100 is shown in the fourth column of Table 3.

Table 1. The compositions of the face-coat slurries

Slurry	**Binder**	**Powder**	**Density of Slurry (g/mm^3)**	**Wetting Agent (few drops)**
Fused Alumina	Ludox SK-R 110g	Alumina –325 279g	2.3857	Victawet 12
Fused Magnesia	Silester XAR 80g	Magnesia –200 261.8g	2.13	-
Molochite	Ludox SK-R 108.4g	Molochite –200 185.35g	1.81	Victawet 12
Fused Silica	Ludox SK-R 110g	Fused silica –325 149g	1.61	Victawet 12
Yttria	Silester XAR 80g	Yttria 5-8 microns 351g	2.76	-
Zircon	Ludox SK-R 110g	Zircon –200 328g	2.77	Victawet 12
Zirconia	Ludox SK-R 110g	Zirconia <50 microns 380g	3.06	Victawet 12

Table 2. Mold making program

First Slurry	First Stucco	Second Slurry	Second Stucco	Third slurry	Third Stucco	Fourth Slurry	Fourth Stucco	Fifth Slurry	Fifth Stucco
F.Alumina -325	F.Alumina 110	F.Alumina - 325	F.Alumina 110	Zircon -200	Zircon Sand	Molochite -200	Molochite 30-80	Molochite -200	Molochite 16-30
F.Magnesia -200	F.Magnesia 50-80	F.Magnesia -200	FMagnesia 50-80	Zircon -200	Zircon Sand	Molochite -200	Molochite 30-80	Molochite -200	Molochite 16-30
Molochite -200	Molochite 30-80	Molochite -200	Molochite 30-80	Zircon -200	Zircon Sand	Molochite -200	Molochite 30-80	Molochite -200	Molochite 16-30
F. Silica -325	F. Silica 50-100	F. Silica -325	F. Silica 50-100	Zircon -200	Zircon Sand	Molochite -200	Molochite 30-80	Molochite -200	Molochite 16-30
Yttria 5-8 microns	F.Alumina 110	Yttria 5-8 microns	F.Alumina 110	Zircon -200	Zircon Sand	Molochite -200	Molochite 30-80	Molochite -200	Molochite 16-30
Zircon -200	Zircon Sand	Zircon -200	Zircon Sand	Zircon -200	Zircon Sand	Molochite -200	Molochite 30-80	Molochite -200	Molochite 16-30
Zirconia <50microns	Zirconia Sand	Zirconia <50microns	Zirconia Sand	Zircon -200	Zircon Sand	Molochite -200	Molochite 30-80	Molochite -200	Molochite 16-30

Remarks:

a. 6^{th} and 7^{th} layers are repetitions of 5^{th} layer.

b. The selected stucco sizes are the closest sizes to the stuccos used in the zircon-molochite system.

c. For yttria, no stuccos were available. Fused alumina was used instead.

d. Ludox SK-R is a colloidal silica binder. Silester XAR is an ethyl silicate binder.

Table 3. Each stucco material supplied by the manufacturer has a specific grain size distribution. This table shows the grain size distribution of fused silica stuccos. Size 50-100 was used in this work.

U.S. Std. Sieve%	10-20	30-50	50-100	F100
8	<2	-	-	-
12	6 – 25	-	-	-
16	33 – 50	-	-	-
20	25 – 45	<1	-	-
30	<13	15 – 30	-	-
40	-	38 – 50	-	-
50	<4	20 – 35	<13	-
70	-	-	30 – 60	-
80	-	<10	-	-
100	-	-	28 – 51	<15
140	-	-	4 – 16	17 – 40
200	-	-	<2	19 – 34
325	-	-	-	14 – 30
Pan	<3	<2	<1	4 – 20
Magnetics ppm	<50	<50	<50	<50

2.5 Casting Experiments

Figure 10. The test arrangement in casting experiments. Mold was not flushed with SF_6 before casting. During pouring a mixture of 2%SF_6+98%CO_2 *was applied to the pouring cup.*

Magnesium alloy AZ91E[4] was used for all castings. The alloy was melted under a protective gas containing approximately 2%SF_6 and 98%CO_2. All castings were poured at $740^{o}\pm10^{o}$C. Mold temperature at the mold-metal interface was controlled at $450^{o}\pm2^{o}$C. Figure 10 shows a ceramic mold at the casting station immediately after the pouring.

Preliminary trials showed that smaller mold temperatures resulted in surfaces with minor amounts of mold-metal reactions, which made the comparisons difficult. On the other hand, higher mold temperatures resulted in very severe reactions and complete mold-metal sintering in most of the specimens, which also made the comparisons difficult.

The molds were not flushed with protective gas before the pouring, but the protective gas was blown into the pouring cup during the pouring.

Distinct differences were seen between the cast test pieces regarding to the reacted surface area. Therefore all comparisons of the face coat refractories and the studies of the influence of inhibitors in this work were carried out by comparing the reacted surface areas.

[4] This alloy contains aluminum: 8.1-9.3%, zinc: 0.4-1%, manganese: 0.17-0.35, magnesium: balance.

It was also observed that small changes in the pouring temperature or the mold temperature resulted in changes in the reacted surface area. Therefore comparisons were made only within the same mold because then all parameters, particularly the metal and mold temperatures are exactly the same for all test pieces. The pictures showing the surface reactions were taken from the test pieces cast in the same mold.

2.6 Cooling Curves

For a few castings, a K-type thermocouple (chromel-alumel) was located just at the metal-mold interface in the mold cavity, and the temperatures were recorded continuously from the beginning of mold heating to the end of alloy solidification. A Data logger[5] was used for recording the temperatures. For the rest of the castings, mold temperature was controlled with a thermocouple located at the metal-mold interface. The thermocouple was connected to a hand-held temperature measuring device but no continuous recording was carried out.

2.7 Method of Evaluation[6]

After the casting, all refractory material on the cast test piece was carefully removed and digital pictures of all 4 faces were taken. For the removal of the refractory, high-pressure water blast, and very light rubbing with sand paper/wire brush/knife were used. Then, in order to reduce errors, gray areas of each picture were removed[7] for revealing only the reacted areas (black) and unreacted areas (white). This was possible by carrying out the brightness/contrast adjustments by an image processing software[8]. In this adjustment, the final image on the computer monitor was adjusted to be the same as the visual appearance of the actual cast piece.

[5] Intab PC-logger 2100 with EasyTherm Software
[6] A more detailed, step-by-step explanation of the method is given in APPENDIX C.
[7] It was found that the removal of the gray areas from the digital pictures reduced the errors. In the absence of this step, image analyzer gives smaller values because it interprets the black pixels within the unreacted areas as reacted pixels.
[8] Adobe Photoshop 5.0

An image analyzer[9] was then used to measure the cumulative amounts of white areas and black areas. The method is based on the count of black and white pixels. An example of the procedure is shown in Figure 11. The number given under each refractory is the value given by the image analyzer. Maximum possible value for this number is 255 (all white). Minimum value is zero (all black). This number is called arbitrarily as "quality index". It is possible to convert this number to "reacted surface area" and "unreacted surface area" if the total area of the test piece or the total number of pixels in the analyzed area is known, or to express the readings in terms of percentages.

Most previous investigators have assessed mold-metal reactions qualitatively by visual comparisons of digital photographs. As compared to these studies the method used in this work can be considered as quantitative and original[10].

The sources of errors in the quality index measurements are originating from following factors:

1. Incomplete cleaning of refractory materials from cast surfaces and the unclear boundaries between reacted and unreacted areas. These are probably the most important factors. An estimate of about ±10% error margin can be given at the medium values of quality index.
2. Errors made during digital photographing, particularly unbalanced illumination.
3. Errors in the use of image analyzer.

All digital photos which are used in this work in the comparisons of different samples for revealing e.g. the influence of different refractories on the mold-metal reactions are taken from the same sample set cast in a multi-piece mold (see figures 8 and 9). Since all parameters are exactly the same for all test pieces in a specific multipiece casting, the variations in metal-mold reactions on the test pieces can be considered to originate from the various face-coat materials.

[9] Image Analyzer 1.22.2. Internet http://meesoft.logicnet.dk/Analyzer/

[10] There is however one research work where an image analyzer was used in a similar task:
Aarstad et al (4) observed microscopically dark spots on the surfaces of magnesium samples heated under SF_6 gas. These spots were found to be MgF_2. Both manual methods and an image analyzer method were used to determine the fraction of surface covered by dark spots.

Alumina Zircon Molochite Fused silica

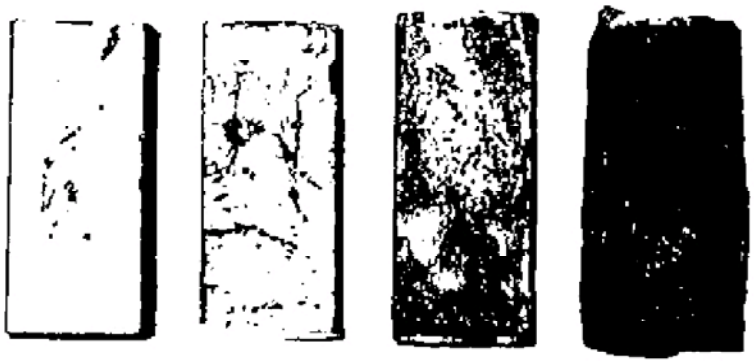

Alumina Zircon Molochite Fused silica

249 228 103 2

Figure 11. Digital pictures of test pieces cast in the same multipiece mold, where each mold cavity had a different refractory face coat to reveal the influence of different refractories on mold-metal reactions. In the lower picture gray areas have been removed. The number under each test piece in the lower picture is the quality index value measured by the image analyzer.

2.8 Chemical Analysis Work

2.8.1 EDS Analysis of reaction layers: A scanning electron microscope equipped with an energy dispersive X-ray spectrometer (EDS) was used for studying the mold-metal reaction layers on the surfaces of cast test pieces. For some samples, two different acceleration voltages were used to change the penetration depth in order to make sure that the observed elements are from the reaction layers and not from the alloy matrix. Beam area was kept at about 2 mm^2.

2.8.2 XRD for silica face coated test pieces: Philips PW1710 diffractometer with

CuKα radiation (40 kilovolts) was used in X ray diffraction.

2.9 Direct Reaction of Magnesium Melt With the Mold Refractories

In order to study possible mold-metal reactions in the absence of oxygen, the following options were considered:

1. Casting under vacuum or in an atmosphere of inert gas, in a vacuum melting and casting furnace
2. Dipping the refractory concerned in a magnesium melt for a predetermined time and examine the reactions occurred on the refractory surfaces. In this case, free oxygen content of the melt is assumed to be zero

The second approach was chosen in this work. Samples to be dipped were produced by the following method:

Alumina or fused silica bars with the dimensions 150x15x5mm were produced in a metal mold. The slurry for the test bars was hardened by the Shaw process. They were subsequently sintered in a furnace at 800-900^{o}C. After sintering, they were used as they were, or they were coated with another refractory by dipping them in a slurry of this refractory and then re-sintering to remove combustibles and to render some strength. Figure 12 shows refractory coated bars used for dipping experiments.

The bars were dipped in an AZ91E melt at **700^{o}C** for **30 seconds** and then they were taken out of the melt to check for the reactions. After removal from the melt, a thin skin of magnesium melt was observed to stay on the surface of the test bar.

In order to avoid the burning of the magnesium skin, an experimental setup, which is shown in the Figure 13 and Figure 14, was used. A gas mixture of 2-3% SF_6+ 98% CO_2 was blown into the cooling tube. This protective gas prevented burning of the magnesium skin and at the same time, the sample cooled down. Reactions between the melt and the refractory, which had occurred inside the melt, were preserved on the surface of the refractory.

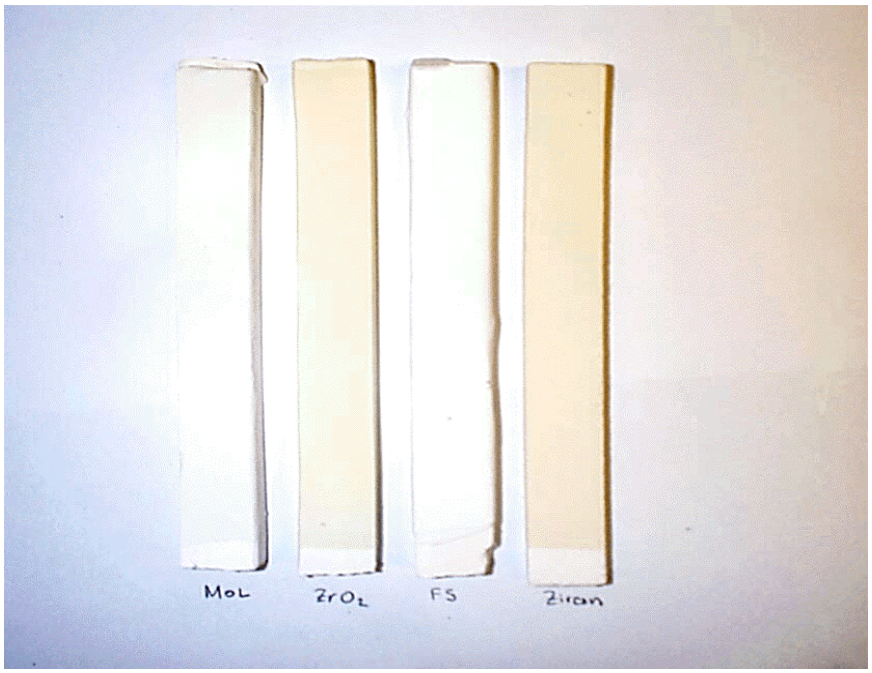

Figure 12. Refractory coated bars used for dipping experiments.

Figure 13. The dipping experiments set-up

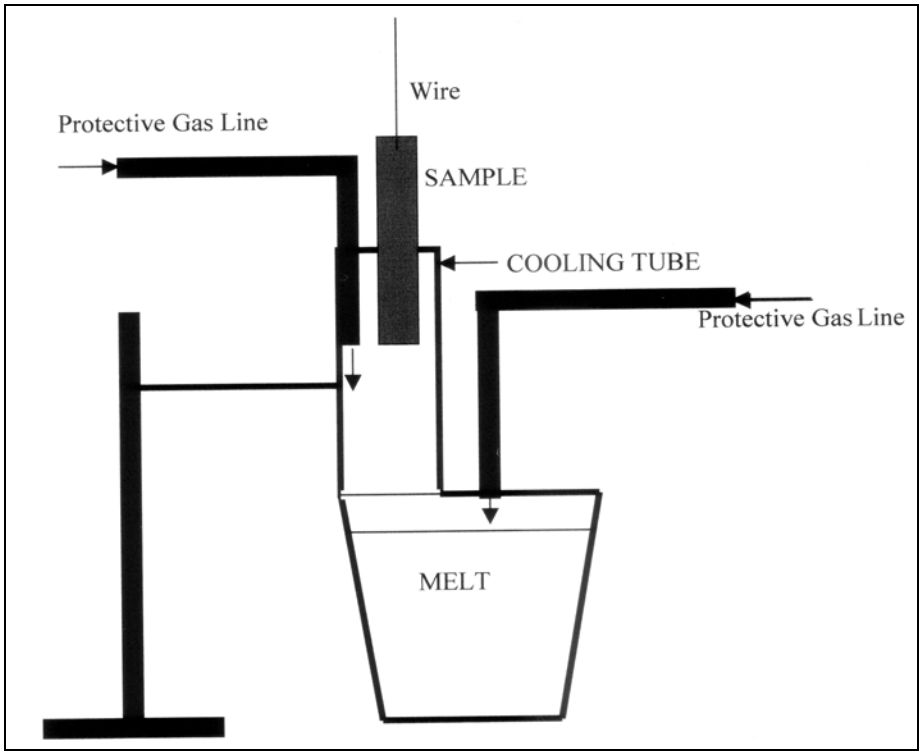

Figure 14. Schematic for the dipping experiments

2.10 The Influence of External Oxygen

To study the influence of external oxygen, molds containing 4 test pieces were used. Molochite was used as the face coat material.

Only one half of the **sintered** mold was dipped in a viscous zircon slurry. Dipping was repeated until an extra mold wall thickness of 3-4 mm was produced around the test pieces. No stucco or a minimum amount of (fine) zircon stucco was used between the dips. A completed mold is seen in Figure 15a.

The permeability of the standard mold and the reduction in the permeability caused by the application of additional zircon layers were measured by the shell permeability measurement method suggested in reference 12. In this method, a ceramic shell is built on a composite ping-pong ball/refractory tube pattern (Figure 15b). The shell is sintered by the standard method during which the ping-pong ball is burned out. Then, the rate of nitrogen flow through the shell is measured at either room temperature or at elevated temperature using a custom built apparatus.

In this work, the gas permeabilities were measured at room temperature.

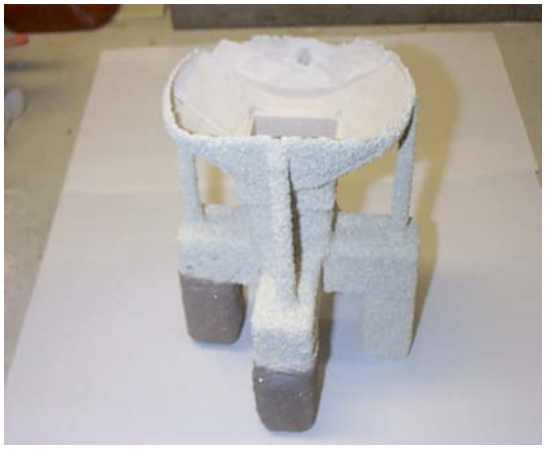

Figure 15a. An extra zircon layer with the thickness of 3-5 mm was applied on two of the test pieces for reducing the mold permeability.

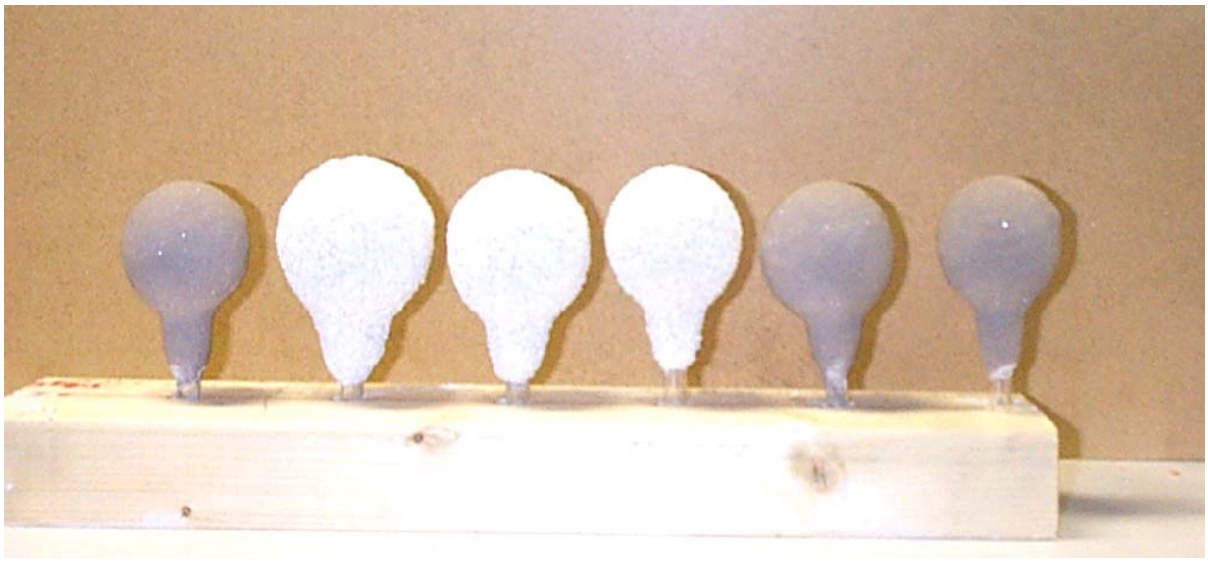

Figure 15b. Gas permeability specimens prepared in this work. These specimens were built on a ping-pong ball as described in the test #775-83 in "Ceramic Test Procedures" (52).

2.11 Heat Release During Mold-Metal Reaction

To study heat evolution or heat absorption, a ceramic shell mold shown in Figure 16 was prepared. This mold contained two fused magnesia-coated test pieces and two fused silica-coated test pieces. Slurry compositions and mold making programs were as in Table 1 and Table 2.

Two thermocouples on one of the fused magnesia-coated test pieces (No.1 and No.2), and two thermocouples on one of the fused silica-coated test pieces (No. 3 and No. 4) were attached as shown in Figure 16. Figure 17 shows the location of the attached thermocouples.

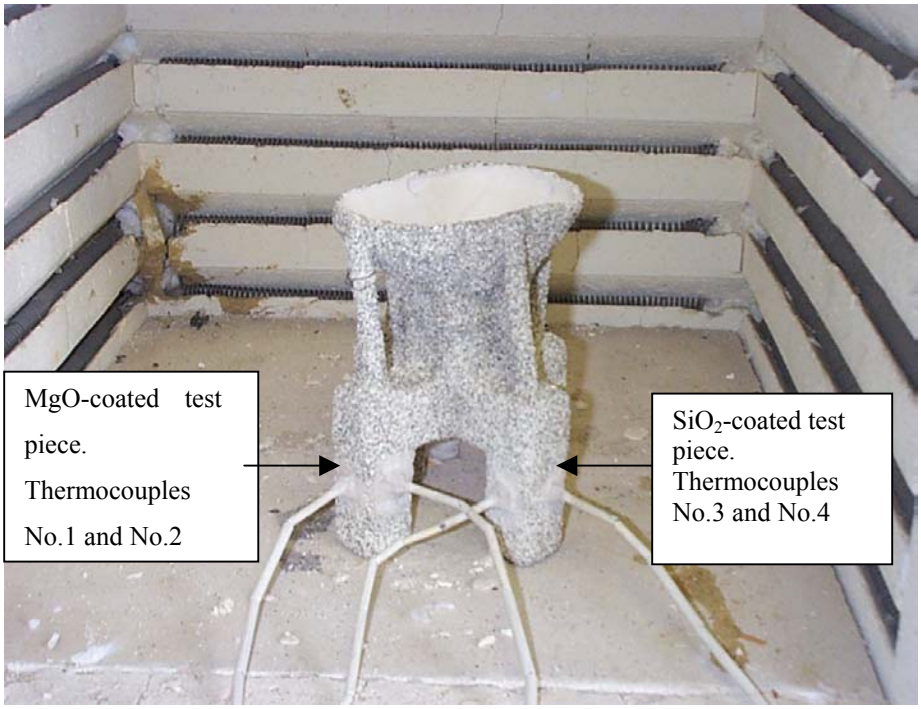

Figure 16. Mold in the preheating furnace

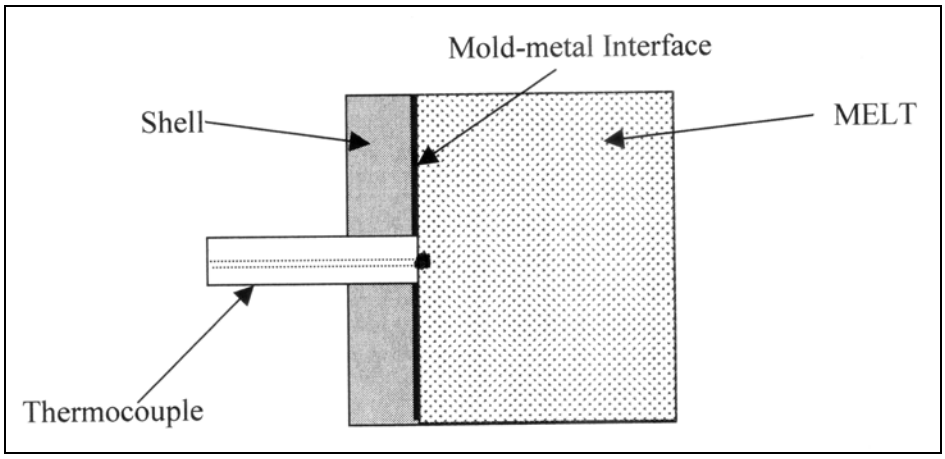

Figure 17. Location of thermocouples

Molds were preheated before casting to about 465^{o}C. Casting temperature was 755^{o}C. Alloy was AZ91E.

In a separate experiment, in order to find out the effect of the difference in heat conductivity values of magnesia and silica on the cooling curves, AlSi10Mg[11] alloy was cast into an identical mold.

2.12 Inhibitor experiments

The use of SF_6 as an inhibitor was not studied in this work, as this inhibitor has been previously studied by other researchers and it is in industrial use. Instead, the influences of KBF_4, $NaBF_4$, and the resin sand were investigated.

In all inhibitor experiments, the molochite was used as the face coat material, since this refractory was found to react easily with magnesium and it was thought that any improvement due to an inhibitor would then be readily observable.

2.12.1 KBF_4 as an inhibitor

The following methods were used to study the efficiency of KBF_4 as an inhibitor:

Addition to the mold as a stucco: One half of a standard shell mold was produced so that, for the first and third coat stuccos, KBF_4 grains were used. The rest of the mold making program was the same standard procedure which was used in the fabrication of the second half of the mold.

Buried in KBF_4: One half of a preheated mold was immersed in KBF_4 grains of inhibitor just before pouring (Figure 18). Since the temperature of the preheated mold was 450^{o}C, it was anticipated that KBF_4 would liberate BF_3 gas upon contact with hot mold surfaces, which might reduce the mold-metal reactions.

[11] Composition of this alloy is given as Si: 9-11%, Mg: 0.15-0.40%, Fe.=0-0.60, Mn: 0-0.60%, Al: Balance.

Figure 18. One half of the preheated mold was buried in KBF_4 just before pouring. It was anticipated that the BF_3 gas, which evolves from the inhibitor due to contact with hot mold would diffuse through the shell and consequently reduce the mold-metal reactions.

2.12.2 Croning Sand as an Inhibitor

One half of the preheated mold was buried in Croning sand before pouring the melt**.**

2.12.3 $NaBF_4$ as an Inhibitor

KBF_4 and $NaBF_4$ are similar chemicals in their properties. One noticeable difference is the solubility of these salts in water. KBF_4 is only slightly soluble in water (4.4 g/l at 20^{o}C) (51). The solubility of $NaBF_4$ in water is high: 973 g/l at 20^{o}C. High solubility of this chemical makes it possible to prepare aqueous $NaBF_4$ solutions.

The following procedure was used for this chemical:

1. Dissolve 42g $NaBF_4$ dry powder in 115g warm water.
2. Dip one half of the **sintered** mold in this solution for 2-3 minutes.

During dipping, the wetting and absorption of the solution by the shell mold were visible.

Casting ingate(s) and air vents were covered by isolation wool to prevent the escape of evolving gases. Molds were heated to 450^{o}C in the preheating furnace. Isolation wool was removed just before pouring.

The standard mold design, which was used throughout this work proved unsatisfactory for this type of experiment. If only two test pieces (out of four) are dipped in the solution and the common ingate is sealed with isolation wool, the gases generated during heating will fill the entire mold, and consequently the difference between the dipped and undipped test pieces can not be revealed.

Therefore, a new mold with two ingates was designed (Figure 19). In this mold design, the gas generated on one side of the mold cannot influence the other side of the mold (two isolated chambers are cast at the same time).

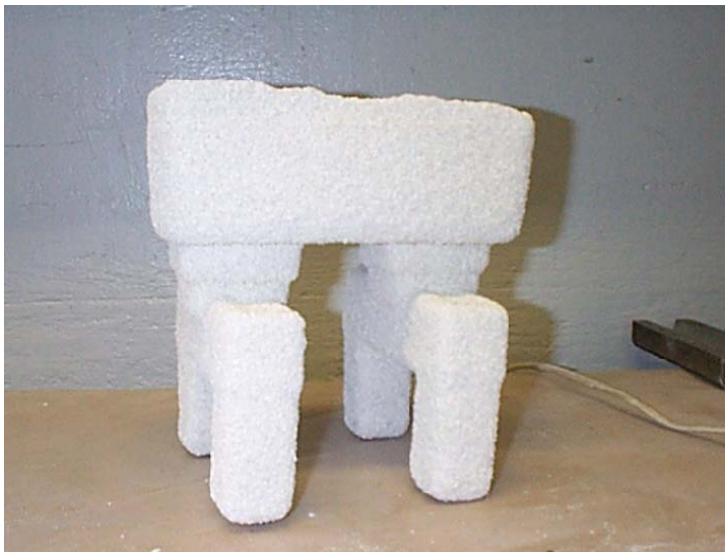

Figure 19. New mold with two ingates. In this design, the gases generated on one side of the mold cannot affect the other side of the mold.

3 RESULTS

3.1 Cooling Curves

A typical cooling curve as measured from the mold at the mold-metal interface is shown in Figure 20.

1. Mold temperature could be controlled with a high accuracy by making small adjustments to the power unit of mold preheating furnace.
2. The temperature drop at the mold-metal interface was small (a few degrees) during the transportation of the mold from the preheating furnace to the casting station and pouring.
3. Although the pouring temperature measured in the crucible was 740^{o}C, the maximum temperature measured at the mold-metal interface was always lower due to the cooling of the melt by mold walls before it reached the thermocouple junction. It was seen that the ceramic filter, which was used in some of the castings, also contributed to this cooling effect by slowing down the entrance speed of the molten magnesium into the mold cavity. However this cooling effect was not as large as the cooling of the melt by the mold walls.
4. The liquidus temperature is about 600^{o}C and the solidus temperature is 430^{o}C. The liquidus temperature of this alloy as measured by DTA was reported to be 602^{o}C (43)
5. Magnesium was “liquid” for more than 30 seconds, and “liquid+solid “ at the mold-metal interface for at least 5 minutes. Prolonged existence of liquid magnesium at the mold-metal interface results in enhanced mold-metal reactions, which will be examined later.

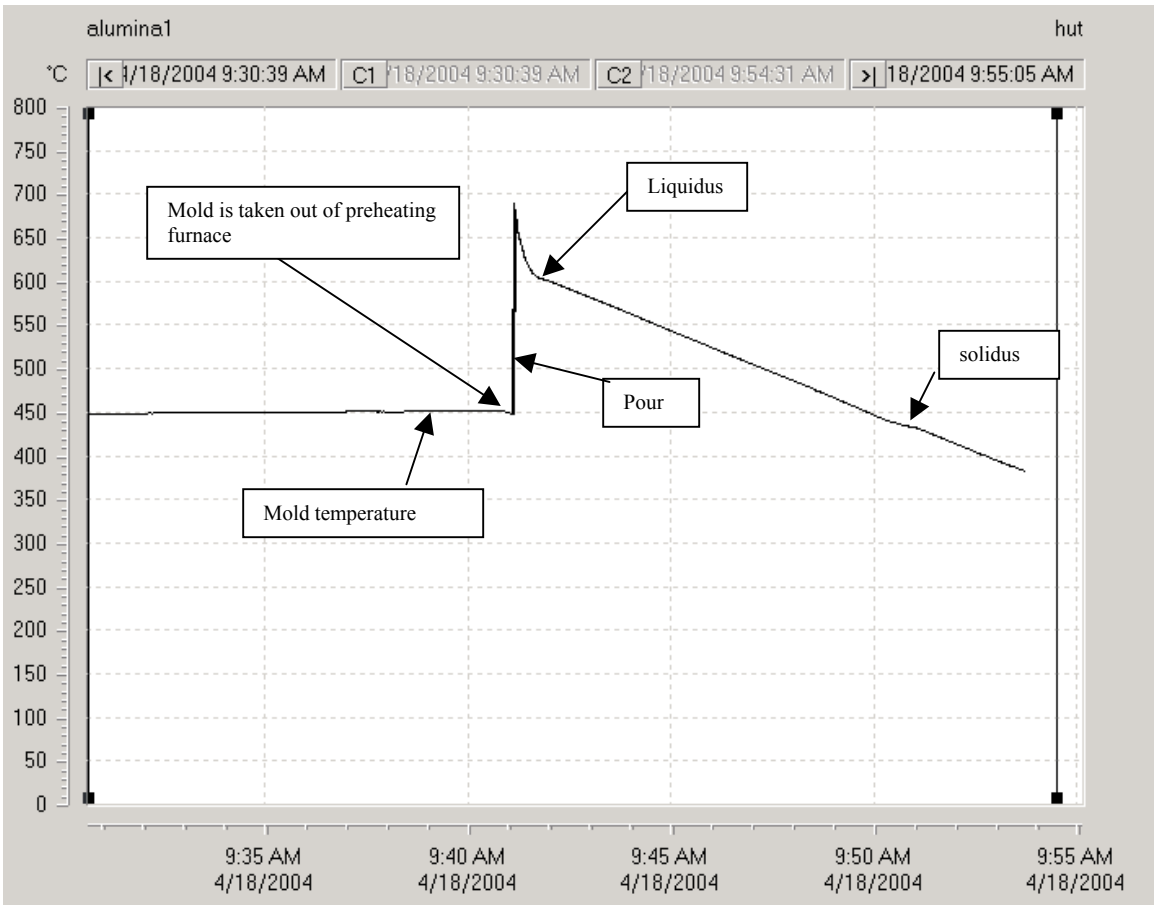

Figure 20. A cooling curve measured at the mold-metal interface. Magnesium is "liquid" for more than 30 seconds, and "liquid+solid " at the mold-metal interface for at least 5 minutes, which may initiate mold-metal reactions.

3.2 Theoretical Calculation of Free Energy of Formation

The free energies of formation for the studied oxide-based refractories were also calculated in the temperature range of 0 to 1000°C using the HSC software[12] and the available database. In these calculations the following simple reactions (each per one mole of oxygen) were assumed:

Silica reaction……..$Si + O_2 = SiO_2$

Zirconia reaction……..$Zr + O_2 = ZrO_2$

Alumina reaction……..$4/3\ Al + O_2 = 2/3\ Al_2O_3$

Magnesia reaction…….$2\ Mg + O_2 = 2\ MgO$

[12] Outokumpu HSC Chemistry for Windows, User's Guide, Version 2.0, 1994

Yttria reaction……..4/3 Y + O_2 = 2/3 Y_2O_3

Molochite[13] reaction…… 4/5 Al + 2/5 Si + O_2 = 2/5 Al_2SiO_5

Zircon reaction…….. ½ Zr + ½ Si + O_2 = ½ $ZrSiO_4$

Results obtained are plotted in Figure 21.

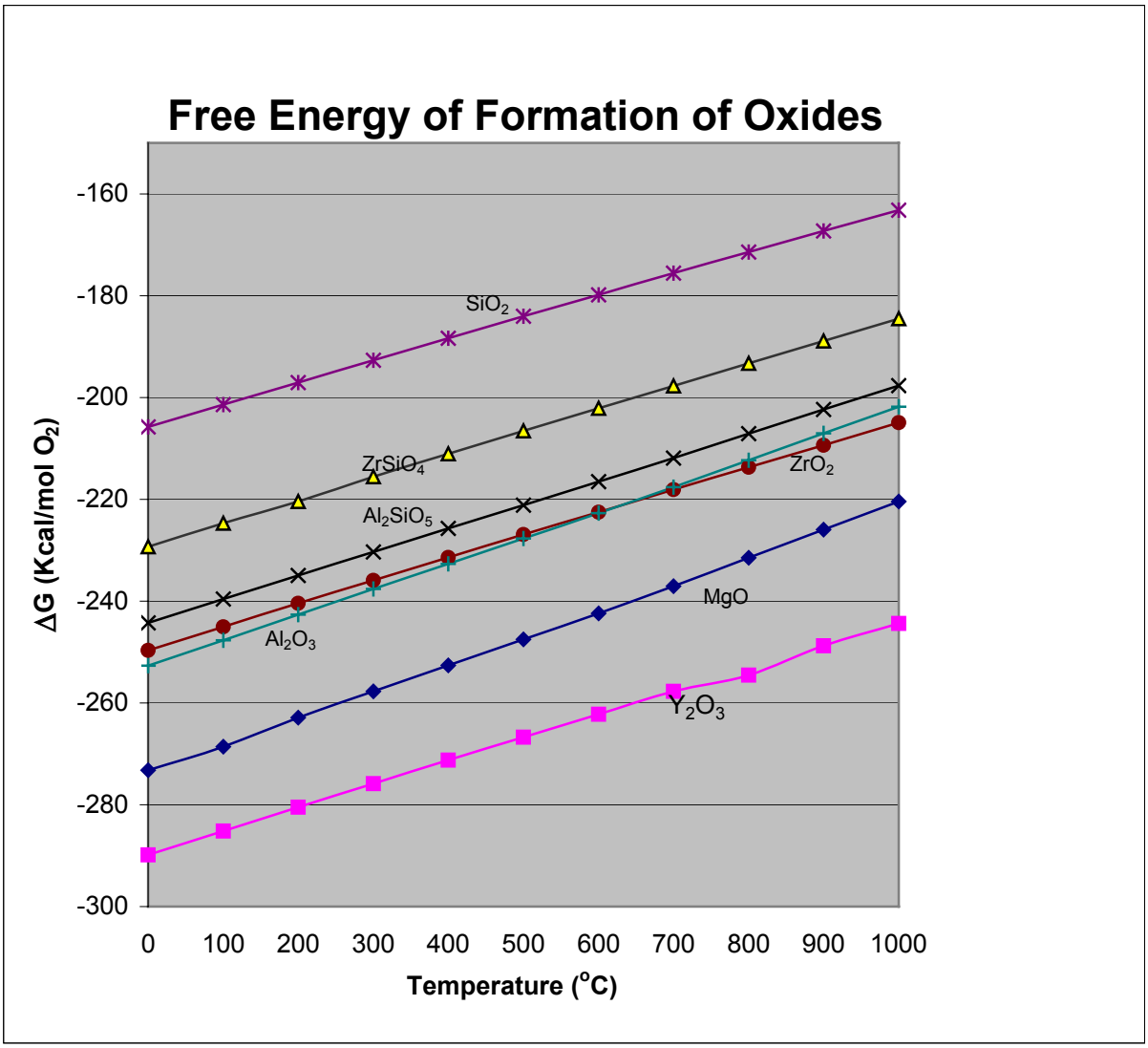

Figure 21. Calculated Free energy of Oxides Investigated, with thermodynamic data available. Calculated values of free energy of formation for oxides are given in Appendix D.

[13] Thermodynamic data for molochite was not available, data given for sillimanite was used in the calculations instead.

3.3 Stability of Slurries

Both magnesia and yttria was observed to produce good alcohol based slurries and application of slurry as a face coat was straightforward. A major problem was with the stability of slurry. Ethyl silicate based magnesia slurries were stable for only 1 day, and ethyl silicate based yttria slurries were stable between 2-7 days. Table 4 shows stability and wax pattern covering properties of slurries.

Table 4. Stability and wax pattern covering properties of slurries prepared in this work

Slurry	**Binder**	**Slurry Life**[14]	**Wax Pattern Covering**[15]
Fused Alumina	Ludox SK-R	Stable, no slurry setting (hardening)	Good/Excellent
Fused Magnesia	Silester XAR	**About 1 Day**, after which setting occurs.	Excellent
Molochite	Ludox SK-R	Stable, no setting observed	Moderate
Fused Silica	Ludox SK-R	Stable, no setting observed	Poor/Moderate
Yttria	Silester XAR	**2-7 Days**. Setting occurs during this time period	Good
Zircon	Ludox SK-R	Stable, no setting observed	Excellent
Zirconia	Ludox SK-R	Stable, no setting observed	Excellent

3.4 Surface quality

No measurements were made in this work for comparing the surface quality of magnesium castings with aluminum castings. On the basis of visual observations it can be said that the aluminum alloy castings tend to be more shiny, whereas the magnesium alloy casting surfaces are more matt. Another obvious difference is the complete absence of mold-metal reactions in aluminum castings.

[14] Prepared slurries were not mixed continuously, settling of powder occurred in all cases. Therefore occasional mixing was necessary.

[15] Comments on wax pattern covering are based on visual judgments, which may differ from one person to another person. No plate covering tests were made.

3.5 Quality Index Values

Four readings for each piece were measured from the four faces of the specimen. Mean value is the arithmetic average of the values in a specific row. Stuccos were applied as described in the mold making program table (Table 2) except for the cases where it is otherwise indicated. Tables 5-12 below show the measured quality index values for four-piece molds. Table 12 shows the measured quality index values for seven-piece molds

Table 5. Quality index values for the mold materials alumina ,zircon, molochite and fused silica

	Casting #1				Casting #2				MEAN
Alumina (Stucco: Alumina 60)	234	241.13	231.6	249.07	152.82	14.99	61.55	50.85	154.50
Zircon	175.5	144.67	195.34	228.1	235.62	223.38	228.6	168.6	214.04
Molochite	166.7	86.06	124.57	102.81	17.73	65.23	74.34	24.64	82.77
F.Silica	4.54	6.99	12.35	1.92	0	0	0	0	6.45

Table 6. Quality index values for the mold materials alumina, zircon, alumina, and zircon

	Casting #1				MEAN
Alumina (Stucco:Alumina 110)	240.07	241.89	249.20	249.91	245.27
Zircon	191.04	207.58	210.89	201.08	202.65
Alumina	218.54	194.30	220.04	210.59	210.87
Zircon	224.47	231.02	238.12	214.38	227

Table 7. Quality index values for the mold materials alumina, zircon, alumina, and zircon

	Casting #1				MEAN
Alumina (Stucco:Alumina 110)	245.6	247.2	232	245.3	242.5
Zircon	238.3	227.9	218.6	239.8	231.15
Alumina (no stucco)	179.6	235.3	220.4	143.8	194.78
Zircon (no stucco)	200.8	172.5	224.2	237.2	200.67

Table 8. Quality index values for the mold materials alumina, molochite, magnesia, and magnesia

	Casting #1				Casting #2				MEAN
Alumina	176.76	74.06	122.74	238.03	236.29	209.19	229.21	213.57	186.36
Molochite	41.13	34.43	66.67	32.26	134.06	179.27	193.45	197.97	109.97
Magnesia	238.41	236.98	241.68	248.38	253.02	253.04	252.93	254.17	247.33
Magnesia	240.90	245.60	223.50	226.40	254.83	253.58	254.55	253.09	244.06

Table 9. Quality index values for the mold materials magnesia, zirconia, zirconia, and fused silica

	Casting #1				Casting #2				MEAN
Magnesia	250.93	254.93	254.77	247.95	252.75	245.42	252.42	250.75	251.19
Zirconia	244.91	249.96	252.22	247.88	202.82	185.50	179.77	203.23	220.74
Zirconia	237.75	211.77	222.76	229.05	174.93	179.48	197.21	175.45	203.55
F.Silica	55.66	37.45	22.88	48.15	25.64	20.56	58.73	23.93	36.63

Table 10. Quality index values for the mold materials alumina, molochite, yttria, and zirconia

	Casting #1				Casting #2				MEAN
Alumina	224.67	230.44	241.88	239.05	211.07	219.67	233.22	224.72	228.09
Molochite	200.67	189.97	214.52	203.49	65.01	148.12	134.45	93.18	156.25
Yttria	241.13	249.54	248.76	250.45	247.42	241.48	240.36	253.08	246.53
Zirconia	204.86	169.68	193.74	175.16	208.94	233.46	237.44	225.37	206.08

Table 11. Quality index values for the mold materials magnesia, molochite, and fused silica

	Casting #1				MEAN
Magnesia	251.5	254	254	254	253.37
Molochite	220.78	221	244	233	229.7
F.Silica	10.22	21	23	21	18.81

Table 12. Quality Index values for the mold materials alumina , magnesia , molochite, silica , yttria, zircon, zirconia as cast in the seven-piece molds

	Casting #1				Casting #2 0 = shell failure				Casting #3				Casting #4 2 molochite test piece, no zirconia				MEAN	RANK
F. Alumina	227.6	222.98	217.45	232.72	235.13	227.30	227.9	228.61	223.96	226.37	198.26	224.02	240.6	171.83	178.69	202.93	217.9	3
F. Magnesia	253.2	255	254.89	253.76	252.59	254.31	253.6	255	254.41	252.92	249.91	251.37	246	251.34	253.67	254.17	252.88	1
Molochite	219.7	219.36	200.28	155.15	125.30	116.4	120.34	151.35	240.37	211.80	237.26	219.35	107.8 34.3	175.97 67.65	178.81 79.77	222.62 204.46	172.02	5
F. Silica	-	-	-	-	0	0	0	0	5.51	31.83	24.07	20.38	24.8	4.13	26.41	28.38	13.79	7
Yttria	226.08	238.32	240.58	234.44	252.28	249.91	251.68	252.71	253.46	249.79	251.11	251.21	240.8	243.74	252.62	245.95	245.92	2
Zircon	222.47	188.1	214.04	192.84	205.36	233.86	233.65	239.21	224.23	222.60	248.41	236.63	120.12	212.41	247.83	187.91	214.35	4
Zirconia	60.18	34.93	41.38	56.27	183.61	162.79	96.5	60.19	67.34	131.94	40.12	129.63	-	-	-	-	88.79	6

MEAN QUALITY INDEX VALUES OBTAINED WITH THE SEVEN-PIECE MOLDS

1.Magnesia 252.88

2.Yttria 245.92

3.Alumina 217.9

4.Zircon 214.35

5.Molochite 172.02

6.Zirconia 88.74

7.Fused silica 13.79

3.6 Permeability of Shells Coated With Various Face Coat Refractories

Permeability of shells produced by using different face coat refractories were measured and the mean results are as given below. During the production of permeability samples, compositions of face coat slurries and mold making program were as in Table 1 and Table 2.

Table 13. Permeability of refractories used in this work

	Permeability (cc N_2/min)
Zircon	168
Molochite	205
Alumina	250
Fused Magnesia	535
Yittria	265
Fused Silica	205
Zirconia	253

3.7 Reaction Layers

3.7.1 EDS Analysis of reaction layers.

Figures 22-28 show typical SEM pictures and analysis spectrum of reacted areas. SEM pictures show mostly distinct boundries between reacted and unreacted areas.

Table 14 shows the detected main elements in weight and atomic percentages and the corresponding most probable oxides.

SEM PICTURES AND ANALYSIS SPECTRUM

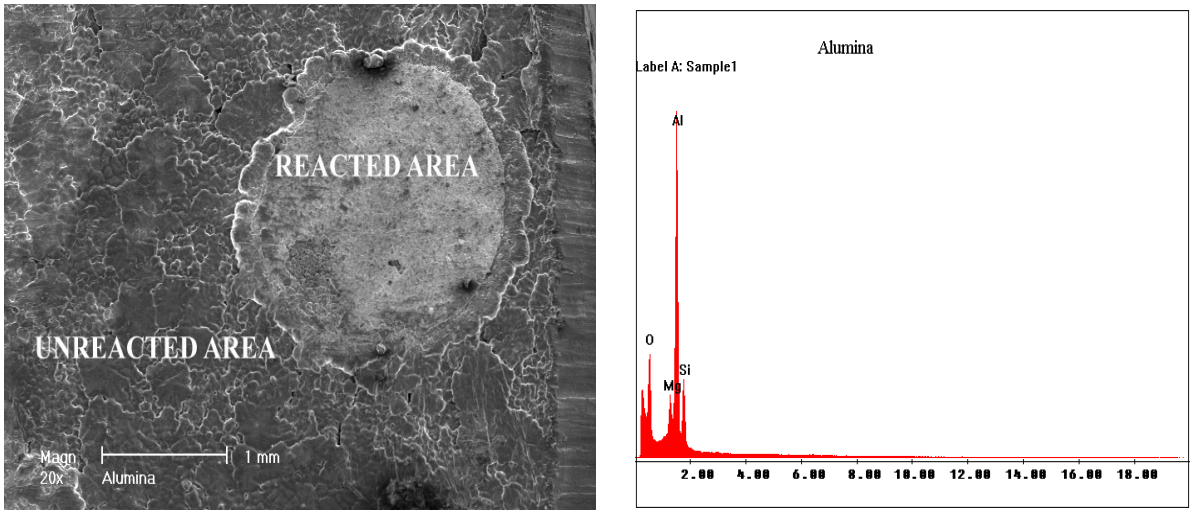

Figure 22. SEM picture showing mold-metal reaction in alumina face-coated sample (left) and typical EDS spectrum of the reacted area (right). Quantitative analysis results are given in Table 14.

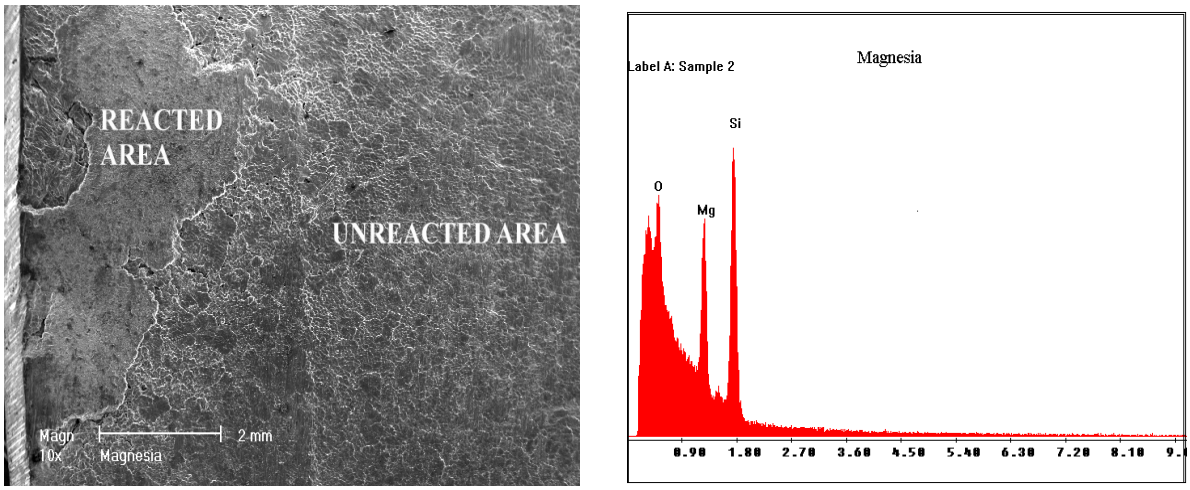

Figure 23. SEM picture showing mold-metal reaction in magnesia face-coated sample (left) and typical analysis spectrum of the reacted area (right). Quantitative analysis results are given in Table 14.

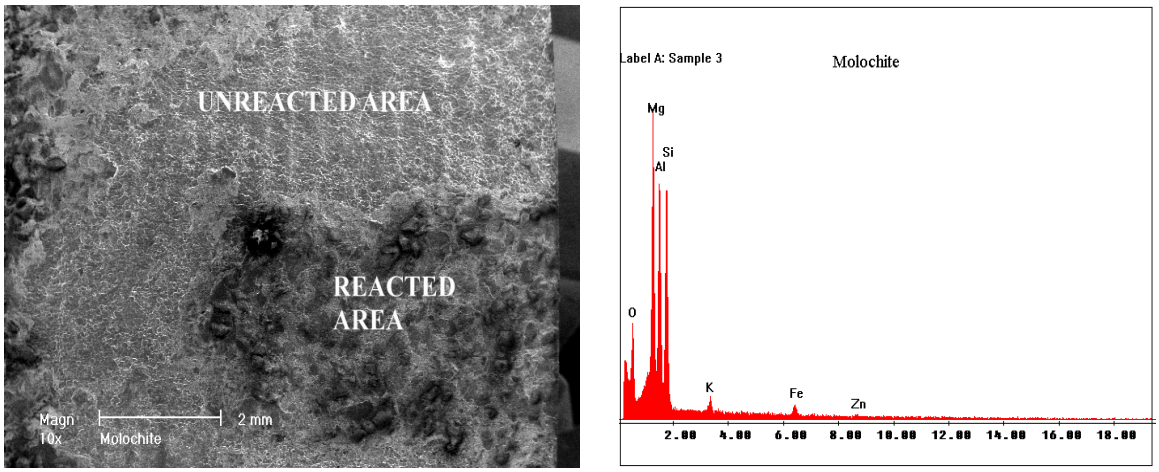

Figure 24. SEM picture showing mold-metal reaction in molochite face-coated sample (left) and typical analysis spectrum of the reacted area (right). Quantitative analysis results are given in Table 14.

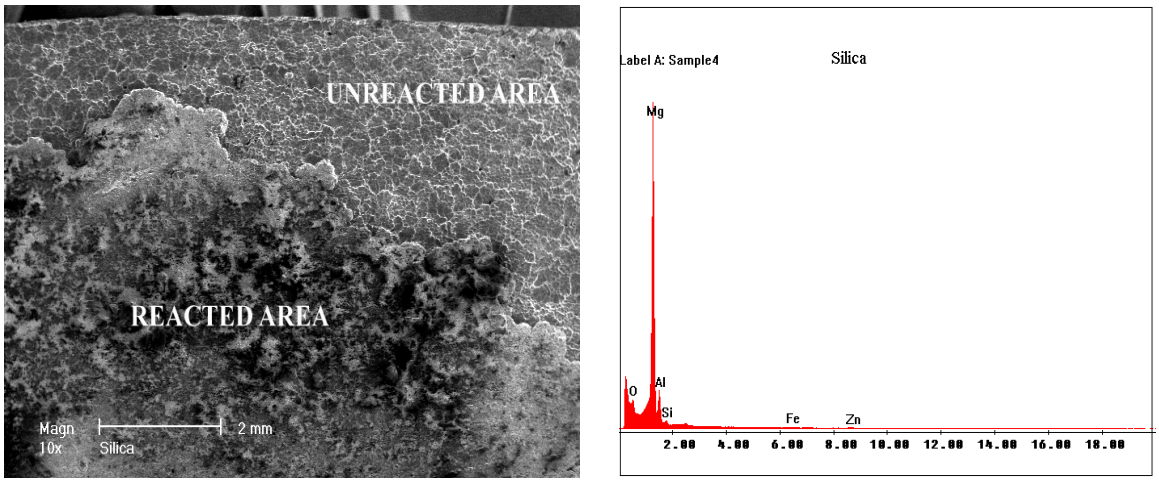

Figure 25. SEM picture showing mold-metal reaction in silica face-coated sample (left) and typical analysis spectrum of the reacted area (right). Quantitative analysis results are given in Table 14.

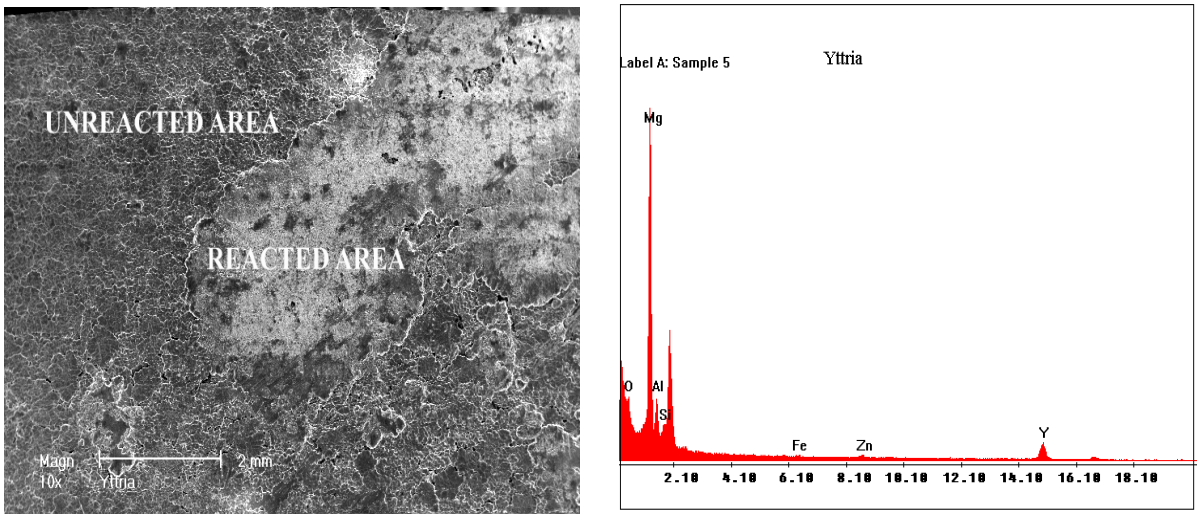

Figure 26. SEM picture showing mold-metal reaction in yttria face-coated sample (left) and typical analysis spectrum (right). Quantitative analysis results are given in Table 14.

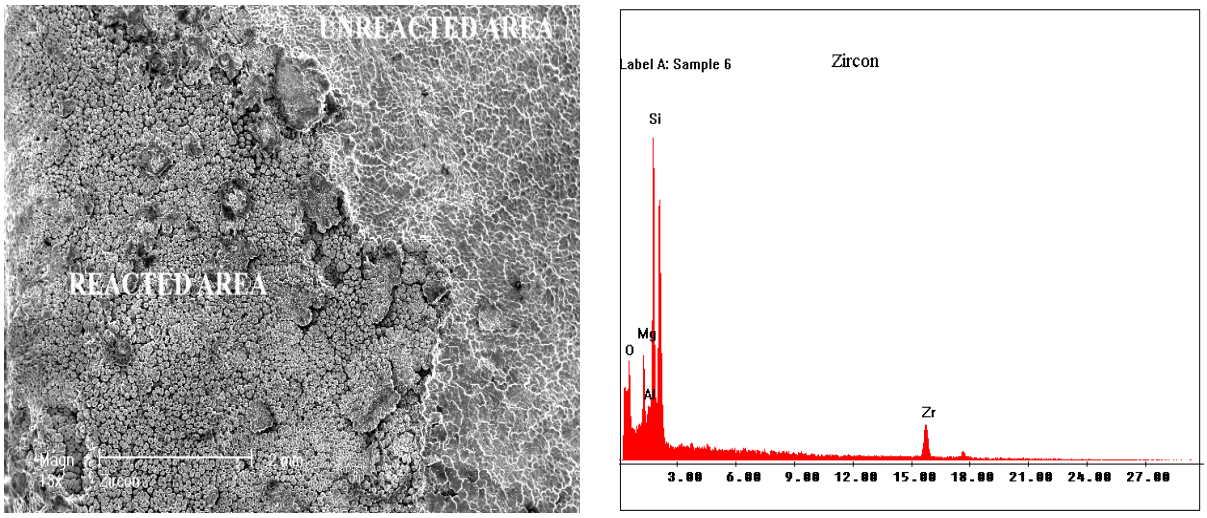

Figure 27. SEM picture showing mold-metal reaction in zircon face-coated sample (left) and typical analysis spectrum of the reacted area (right). Quantitative analysis results are given in Table 14.

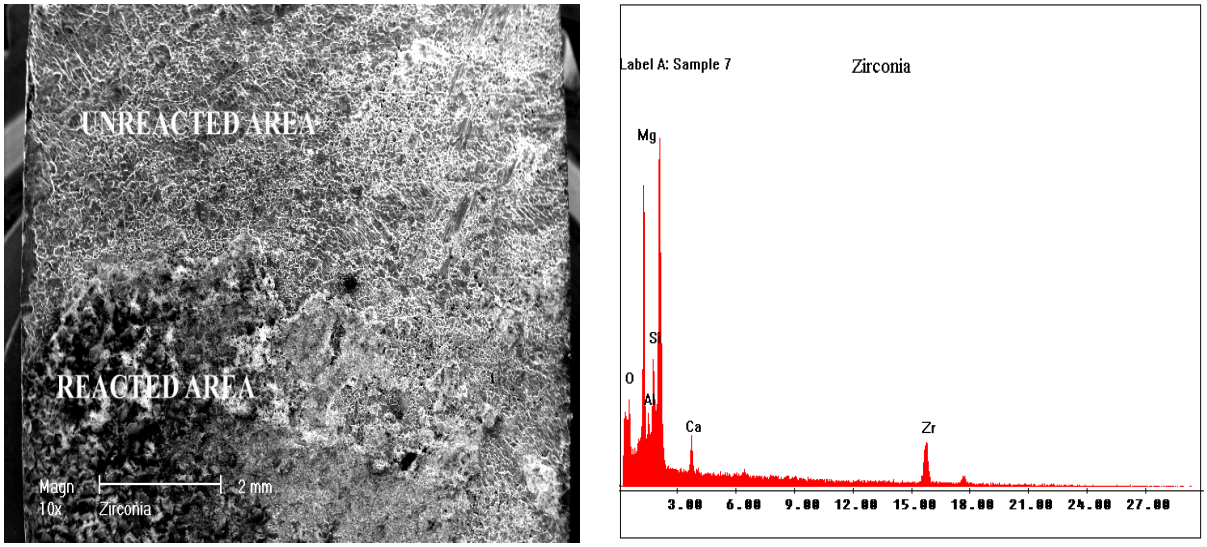

Figure 28. SEM picture showing mold-metal reaction in zirconia face-coated sample (left) and typical analysis spectrum of the reacted area (right). Quantitative analysis results are on Table 14.

Table 14. Detected elements and the corresponding most probable oxides in the reaction layers on the surfaces of cast test pieces.

MOLD FACE COAT	DETECTED ELEMENTS IN WEIGHT AND ATOMIC PERCENTAGES RESPECTIVELY			MOST PROBABLE OXIDES
Fused Alumina	O	43.33	56.23	Al_2O_3, SiO_2, MgO
	Mg	6.27	5.35	
	Al	37.89	29.16	
	Si	12.52	9.26	
Fused Magnesia	O	62.4	73.22	MgO, SiO_2
	Mg	15.88	12.26	
	Si	21.72	14.52	
Molochite	O	32.61	44.77	MgO, SiO_2, Al_2O_3
	Mg	20.45	18.48	
	Al	21.06	17.14	
	Si	23.97	18.74	
	K	0.86	0.48	
	Fe	0.71	0.28	
	Zn	0.33	0.11	
Fused silica	O	21.78	30.41	MgO, Al_2O_3, SiO_2
	Mg	59.28	54.48	
	Al	16.91	14.01	
	Si	0.86	0.68	
	Fe	0.3	0.12	
	Zn	0.87	0.3	
Yttria	O	32.74	47.03	MgO, Y_2O_3, Al_2O_3
	Mg	42.34	40.03	
	Al	8.26	7.03	
	Si	2.75	2.25	
	Fe	0.15	0.06	
	Zn	0.47	0.17	
	Y	13.29	3.44	
Zircon	O	44.06	65.67	$ZrSiO_3$, SiO_2, MgO
	Mg	8.07	7.92	
	Al	2.57	2.27	
	Si	20.92	17.77	
	Zr	24.38	6.37	
Zirconia	O	33.94	53.92	MgO, ZrO_2, SiO_2
	Mg	24.4	25.51	
	Al	4.36	4.11	
	Si	8.76	7.93	
	Ca	1.64	1.04	
	Zr	26.9	7.5	

3.7.2 XRD for silica face coated test pieces

Table 15. XRD results for silica face coated test pieces

Date: 21.4.2006 Time: 18:05:29 File: MgCel070406_2 User: OwnOuti

No.	Visible	Ref. Code	Compound Name	Chemical Formula	Score	SemiQuant [%]
1	☑	00-001-1154	Spinel	Mg Al2 O4	Unmatched Strong	-
2	☑	00-048-0528	Magnesium Alumi...	Mg0.388 Al2.408 ...	Unmatched Strong	-
3	☑	01-077-0729	Magnesium alumin...	Mg0.36 Al2.44 O4	Unmatched Strong	-
4	☑	00-001-1290	Forsterite	Mg2 Si O4	9	-
5	☑	01-089-1625	Dimagnesium silic...	Mg2 (Si O4)	10	-
6	☑	00-016-0602	Aluminum Silicate	Al2 Si O5	Unmatched Strong	-
7	☑	00-001-0613	Mullite	Al6 Si2 O13	Unmatched Strong	-
8	☑	00-003-1162	Magnesium Alumi...	Mg Al2 O4	Unmatched Strong	-
9	☑	00-037-1462	Aluminum Oxide	Al2 O3	Unmatched Strong	-
10	☑	00-047-1770	$GD-alumina	Al2 O3	7	-
11	☑	01-074-2206	Aluminum Oxide	(Al2 O3)5.3333	Unmatched Strong	-
12	☑	01-075-1798	Magnesium dialum...	Mg Al2 O4	7	-
13	☑	01-077-0396	Aluminium oxide - $	(Al2 O3)1.333	Unmatched Strong	-
14	☑	01-089-1627	Dialuminium mag...	Al2 Mg O4	5	-
15	☑	03-065-2869	Aluminum	Al	1	-
16	☑	03-065-6848	Aluminum Magnes...	Al3.16 Mg1.84	53	-
17	☑	00-001-1141	Magnesium	Mg	22	-
18	☑	00-001-0787	Silicon	Si	Unmatched Strong	-

3.8 Direct Reaction of Magnesium Melt With the Mold Refractories

Case 1. When the sample was taken out directly to room atmosphere two things were seen to happen:

a. Within less than a second, surface of the skin of magnesium turned to black

b. Immediately after that, the skin caught fire and burned intensely[16] with a bright light

This burning destroyed the surface of the sample indicating reactions. When the skin burned completely, it changed into a fine white powder. Sample surface turned to mainly black.

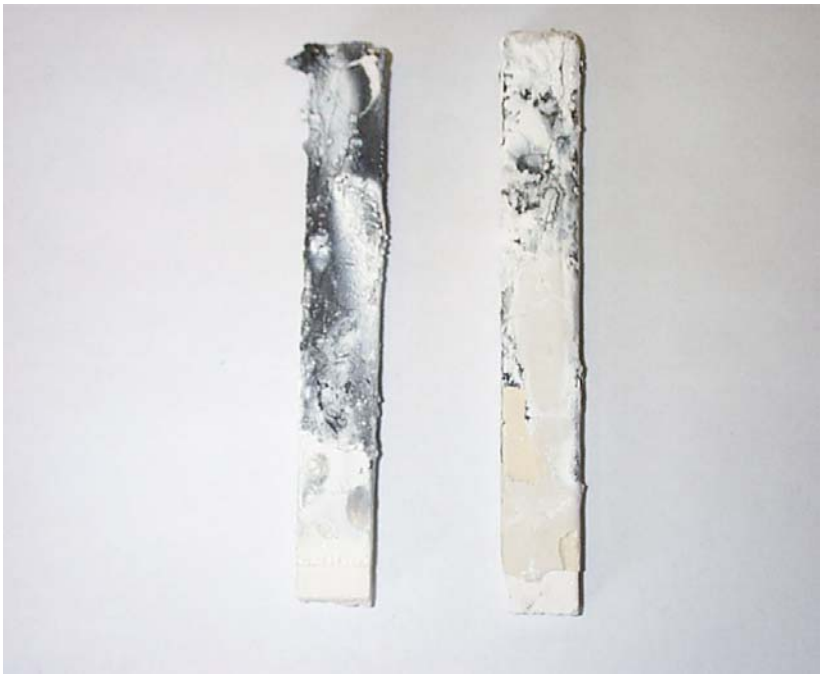

Figure 29. Two samples after dipping in AZ91E melt for 30 seconds at 700^{o} C. Samples were taken directly to directly to room atmosphere after dipping. Burning of magnesium skin destroyed the sample surfaces due to reactions.

Case 2. Samples were taken out to a cooling tube which contained protective gas.

It was seen that the samples after the dipping were the same as before the dipping. No indication of a reaction on any of the sample surfaces. This is shown in Figure 30.

[16] Temperatures during burning of magnesium on shell surface were recorded by a thermocouple attached to the shell surface. It was seen that the temperature exceeds 1000^{o}C during burning.

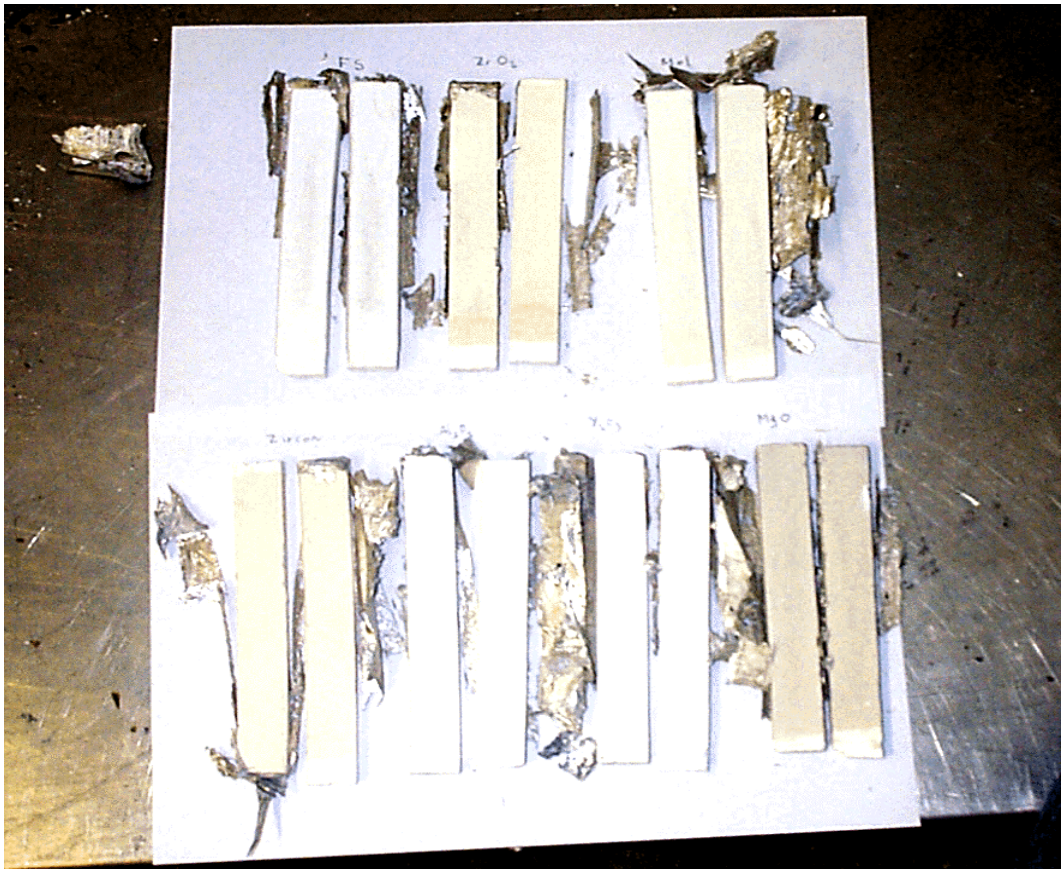

Figure 30. Test bars coated with various refractories after dipping in AZ91E melt for 30 seconds at 700°C.These were cooled in a protective atmosphere. Some of the skin is also seen beside the samples. When the skin was removed, the samples were seen to be the same as before the dipping: No indication of a reaction in any of the samples.

3.9 The Influence of External Oxygen

Quality index values are given in Table 16.

Table 16. Comparison of quality index values showing effect of shell permeability

	Casting #1				Casting #2				MEAN	TOTAL MEAN
Standard Shell	51.39	54.39	120.56	147.81	177.29	129.15	153.11	141.79	121.94	146.62
	145.34	191.37	162.51	173.03	171.50	183.41	155.39	187.82	171.29	
Reduced Permeability Shell	245.10	213.09	198.29	237.40	238.25	233.15	250.98	238.83	231.99	233.62
	231.77	239.53	242.22	243.39	229.20	236.83	240.94	218.03	235.24	

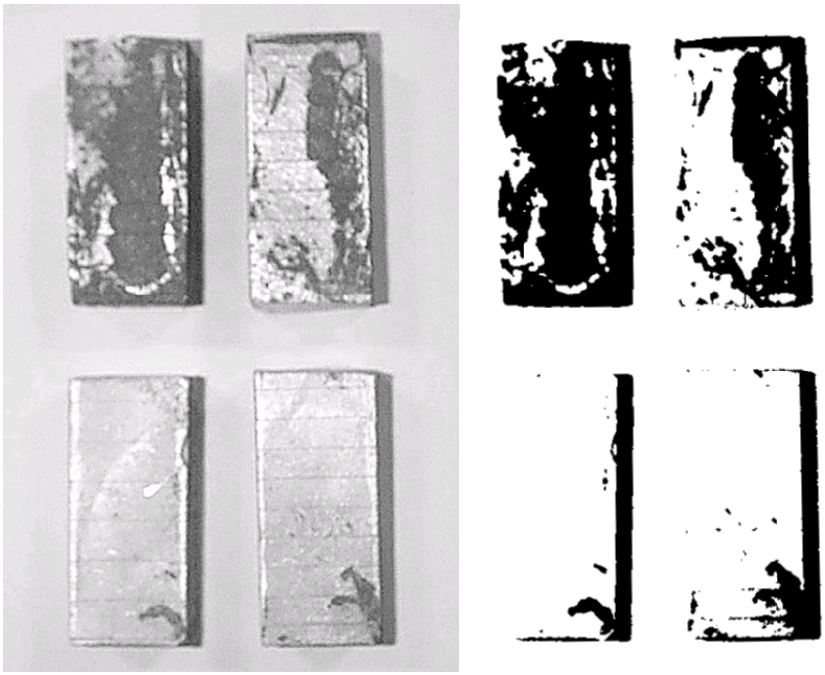

a) b)

Figure 31. Digital images of samples corresponding to first column in Table 16. a) with gray shades in the figure, b) with gray shades removed. Black areas are reacted areas. Numbers given below are the quality index values given by image analyzer.
Upper two pieces in a): Standard mold: 51.39; 145.34
Lower two pieces in a): Cast in a shell of reduced permeability: 245.10; 231.77

It was found that a simple way of reducing gas permeability is the application of a few additional layers of primary zircon slurry on the sintered shell. This results in a low gas permeability mold. Another method, which is used by investment foundries, is the application of a glaze layer on the shell and subsequent sintering.

Shell mold permeability[17] and its reduction due to application of additional zircon layers were measured by the method suggested in reference 52. The results are shown in Figure 32.

[17] Shell permeability depends mainly on the properties of slurry and stucco:
a. A small particle size, high filler percentage and high slurry viscosity result in denser molds and decrease the gas permeability.
b. Another important factor influencing the mold permeability is the shell thickness. At constant test pressures, mold permeability decreases with increasing shell thickness (59).
c. Zircon primary slurry is more viscous than molochite slurry. When used in combination with fine zircon sand as stucco, it was found to be very effective in reducing permeability.

Permeability was decreased from 375 cc/min N_2 to 100 cc/min N_2 after the first dip. The permeability decrease continued progressively due to additional dips and after the 4th dip a shell mold approaching zero permeability was obtained. Thickness gain by 4 dips was about 2mm.

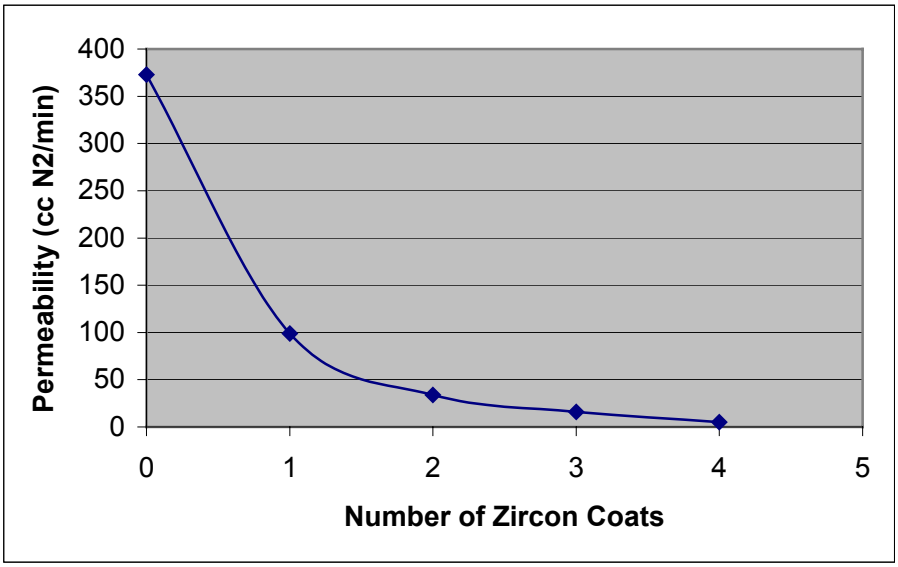

Figure 32. Permeability change obtained by additional dips in zircon slurry

3.10 Heat Release During Mold-Metal Reaction

During mold making, permeability samples from the **same slurries** were prepared and permeability values were measured. Results are given on Table 17.

Table 17. Permeability of magnesia and silica shells

	Permeability (cc N_2/min)
Fused Silica-coated Sample #1	380
Fused Silica-coated Sample #2	325
Fused Silica-coated Sample #3	360
Fused Magnesia-coated Sample #1	750
Fused Magnesia-coated Sample #2	675

Permeability of fused magnesia-coated samples is twice as large as that of fused silica-coated samples. Figure 33 shows the casting after removal of the refractory. Note severe reactions on silica-coated samples and a very small amount of reactions on magnesia-coated samples. Figure 34 shows reactions on one of the silica-coated sample in which reactions had progressed deep into the ceramic shell.

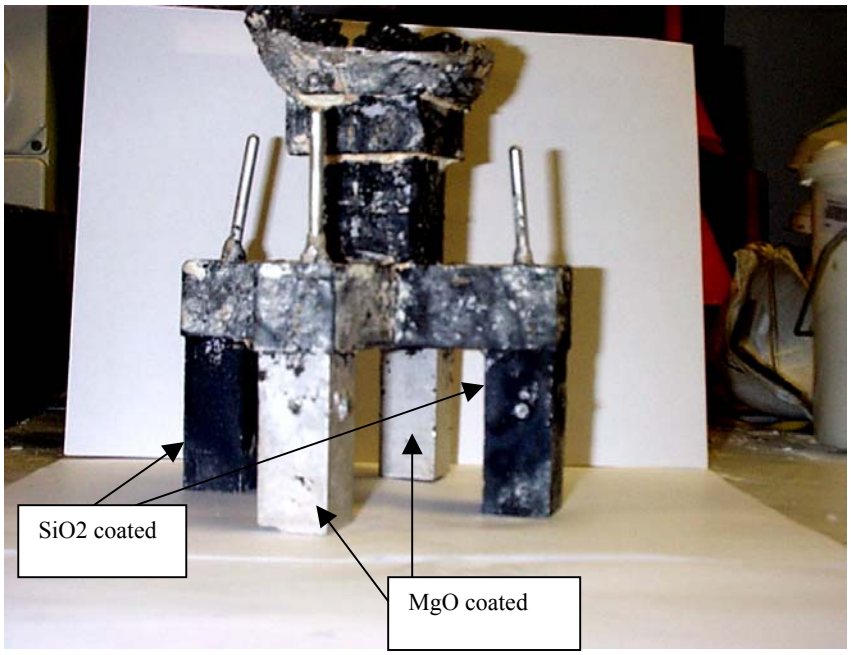

Figure 33. Casting after removal of refractory. Severe reactions on silica-coated samples. Very small amount of reactions on magnesia-coated samples

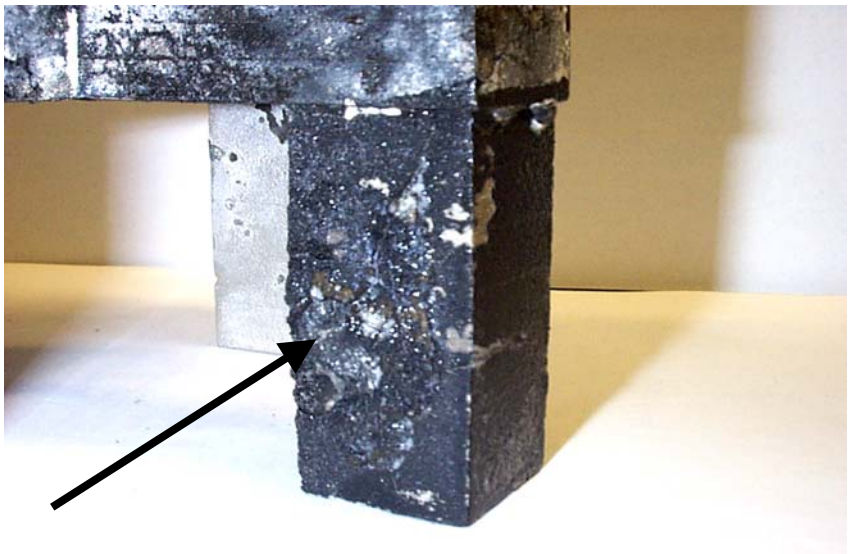

Figure 34. Reactions on this sample face had progressed deep into the ceramic shell. Mold failure was very close.

Cooling Curves for Magnesia and Silica Coated Samples

A) AZ91E Casting

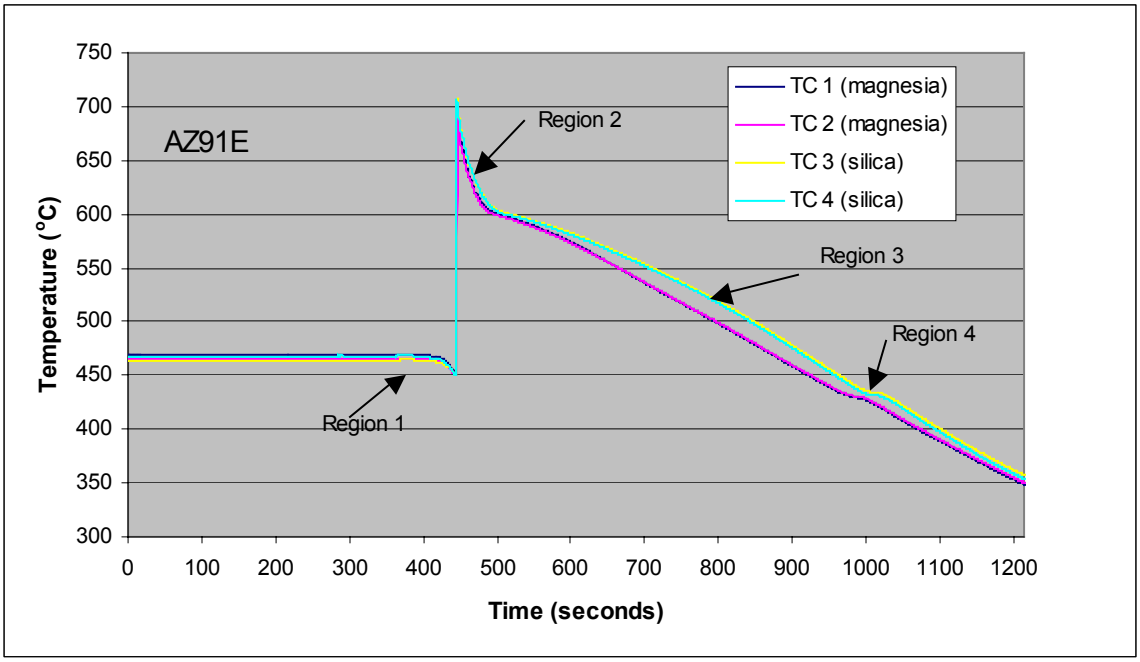

Figure 35. Overall cooling curve for AZ91E.

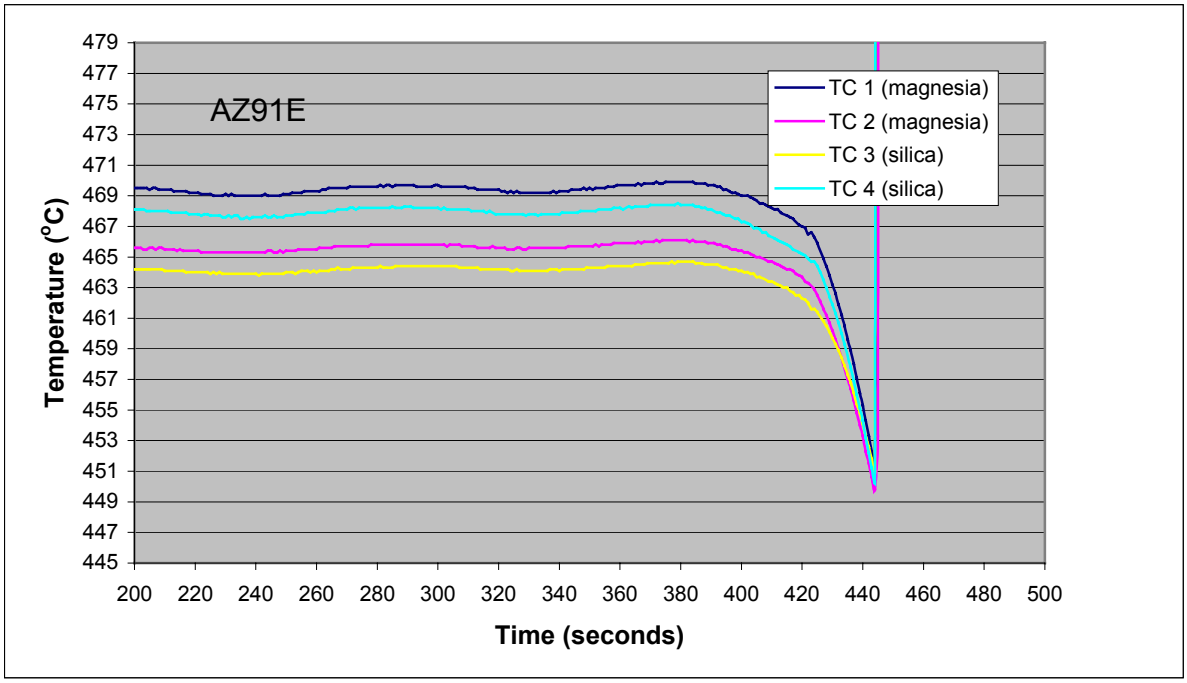

Figure 36. Region 1. Temperatures measured from magnesia- and silica-coated samples are very close to each other

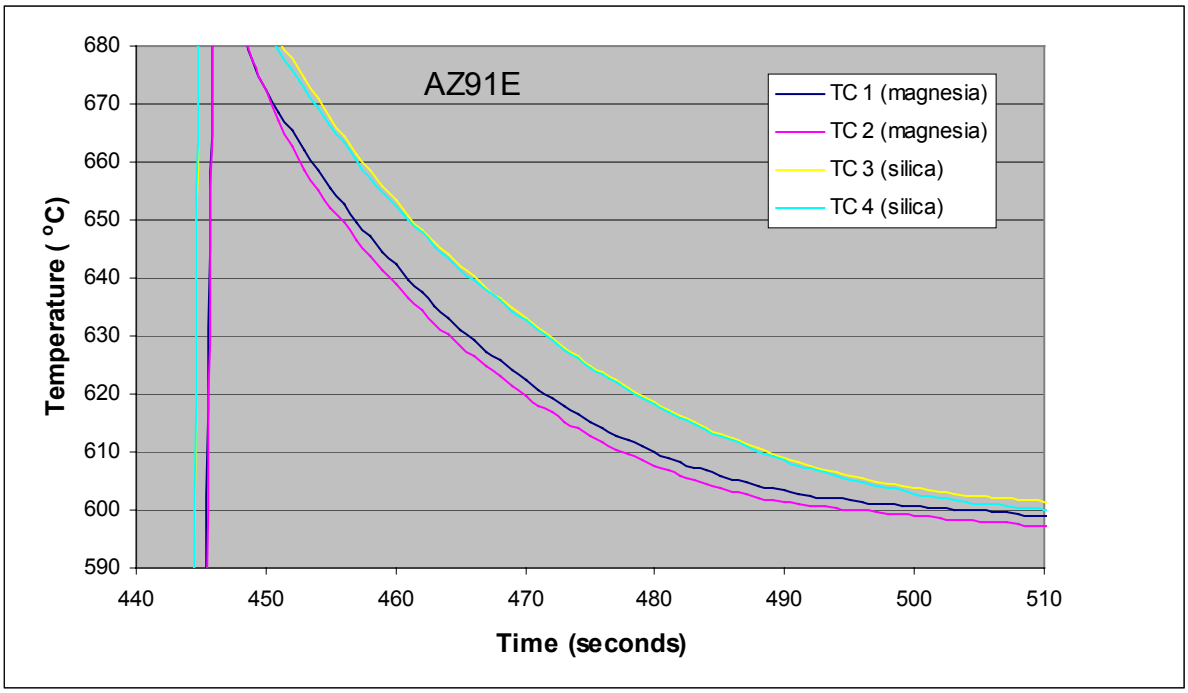

Figure 37. Region 2. Silica-coated sample cools slower than magnesia-coated sample. Time lag to achieve 620°C is 10 seconds.

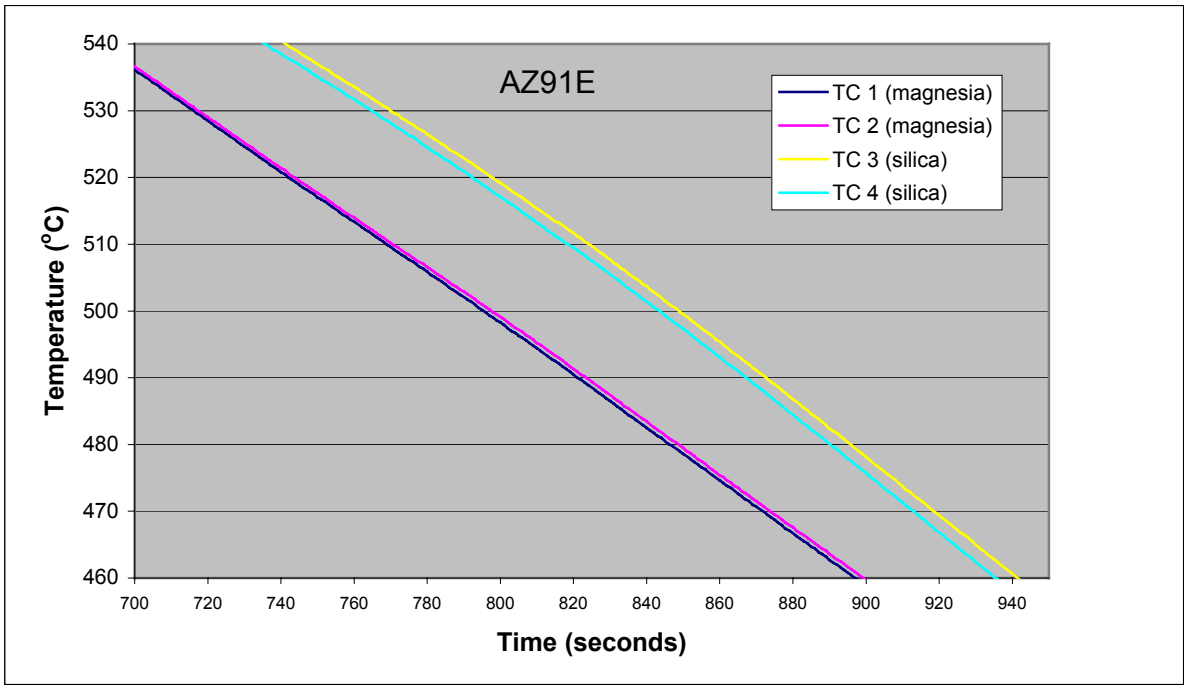

Figure 38. Region 3. Silica-coated sample cools slower than magnesia-coated sample. Time lag to achieve 500°C is 50 seconds. At a given time, temperatures at thermocouples 3 and 4 are about 20°C higher than at thermocouples 1 and 2

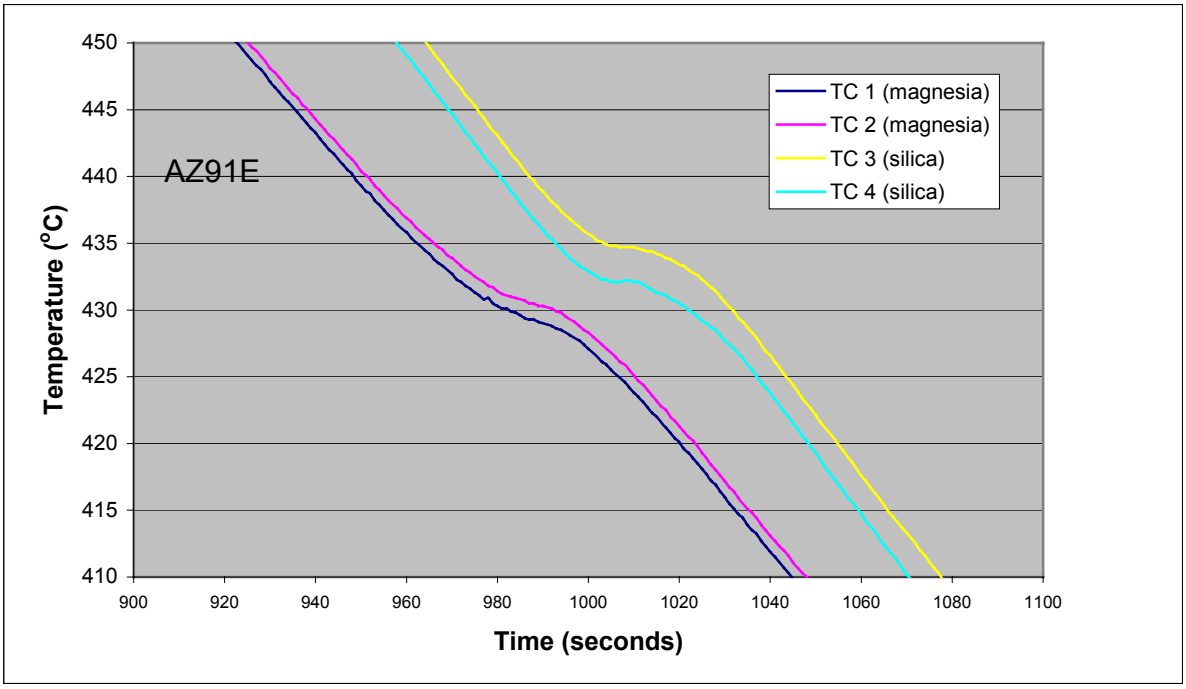

Figure 39. Region 4. *Silica- coated sample cools slower than magnesia-coated sample. Time lag to achieve 425°C is 35 seconds. At a given time, temperatures at thermocouples 3 and 4 are about 13°C higher than at thermocouples 1 and 2*

B) AlSi10Mg Casting

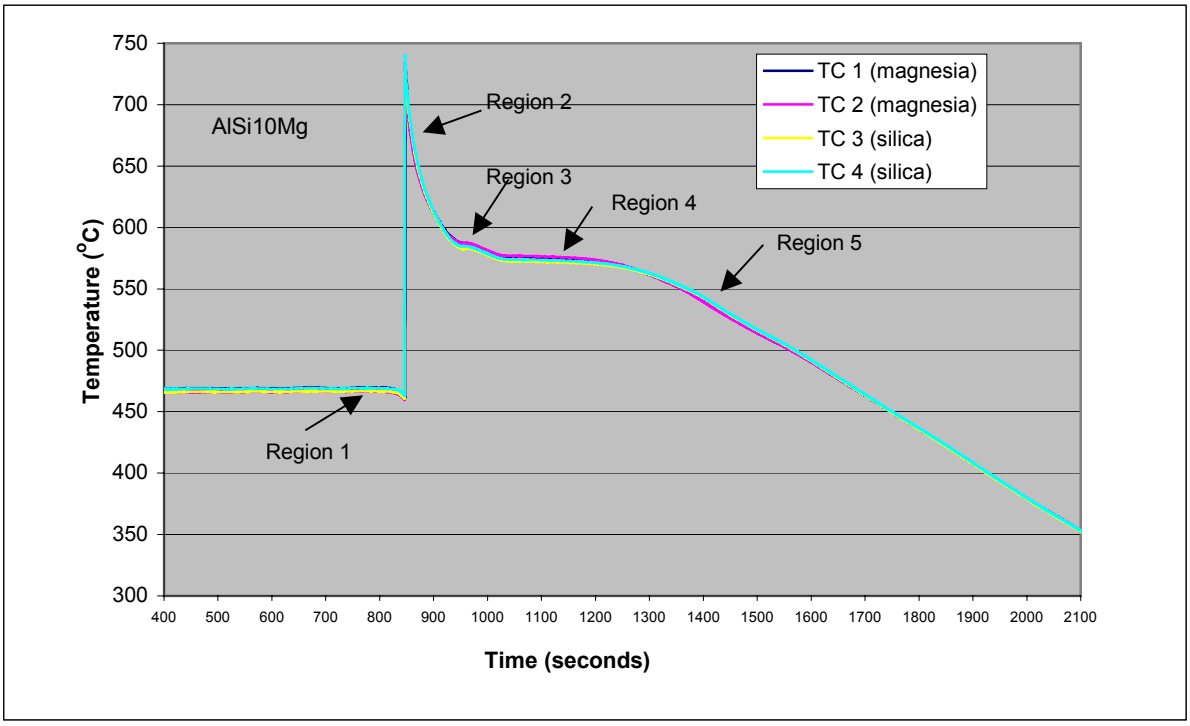

Figure 40. Overall cooling curve for AlSi10Mg.

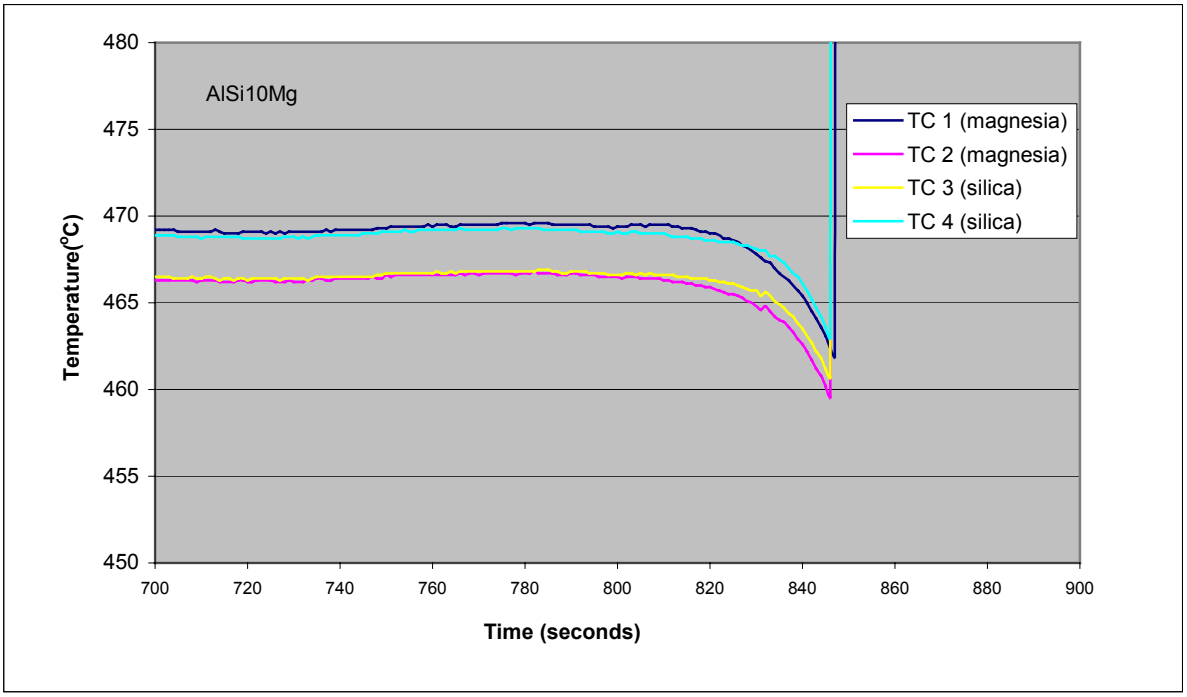

Figure 41. Region 1. Mold entrance temperature measured from magnesia- and silica-coated samples is very close to each other.

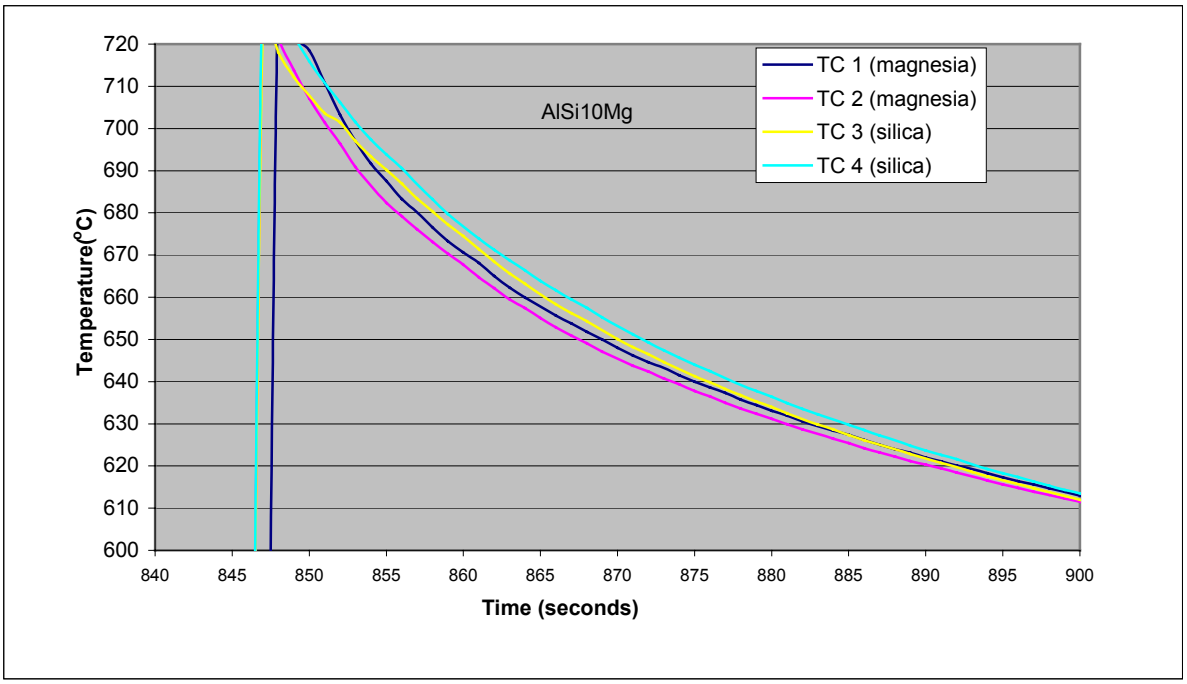

Figure 42. Region 2. Silica-coated sample cools slightly slower than magnesia-coated sample. Time lag to achieve 650°C is about 3 seconds.

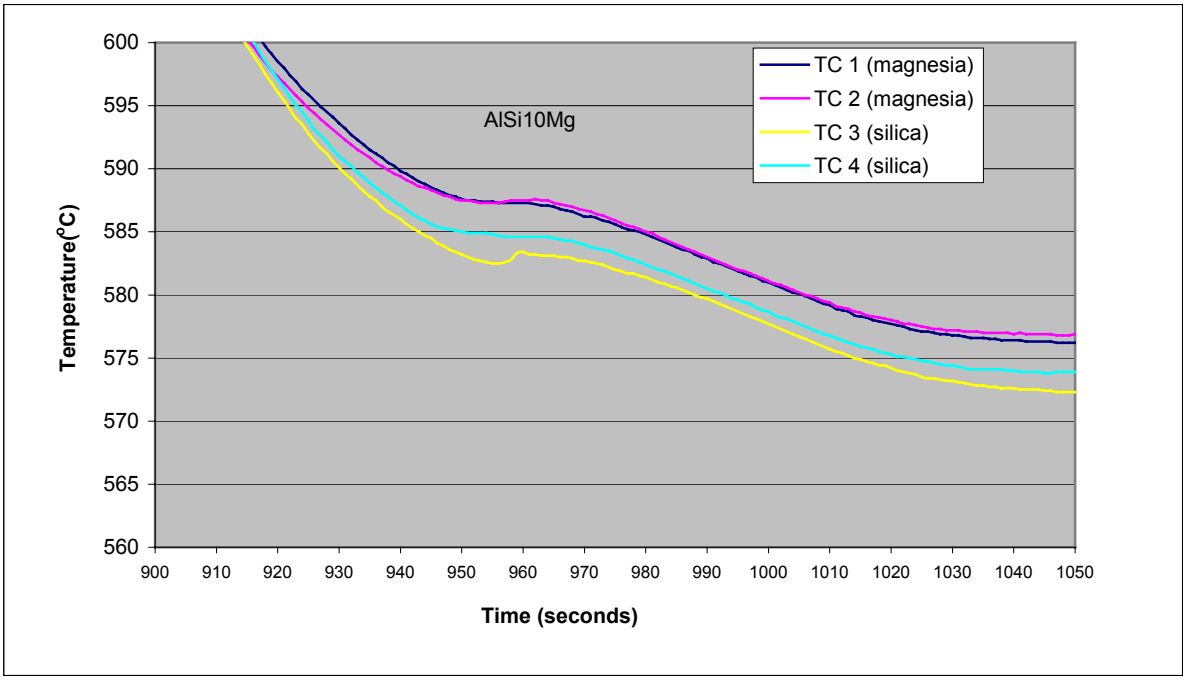

Figure 43. Region 3. Temperature of liquidus undercooling for silica-coated sample (about 584°C) is lower than that for magnesia coated sample (Nucleation is easier for magnesia coated sample). As a result, in the liquid+solid region, temperatures for silica-coated sample are slightly smaller.

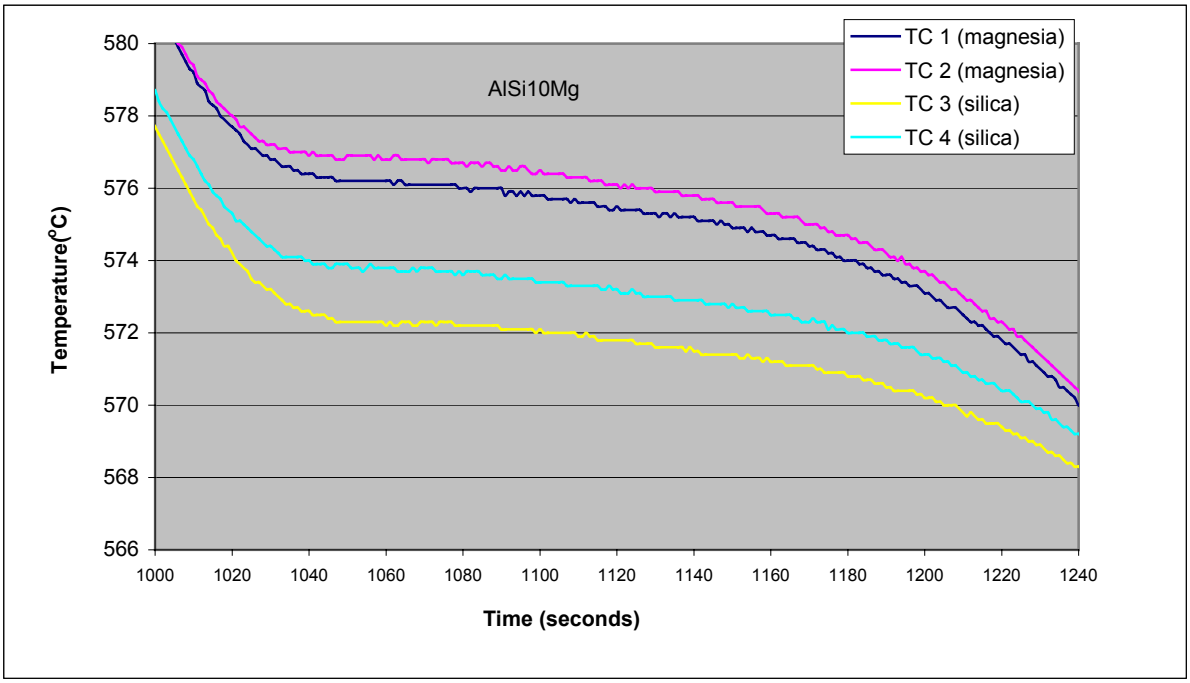

Figure 44. Region 4. Same trend continues at eutectic point. Temperatures for silica-coated sample are slightly smaller.

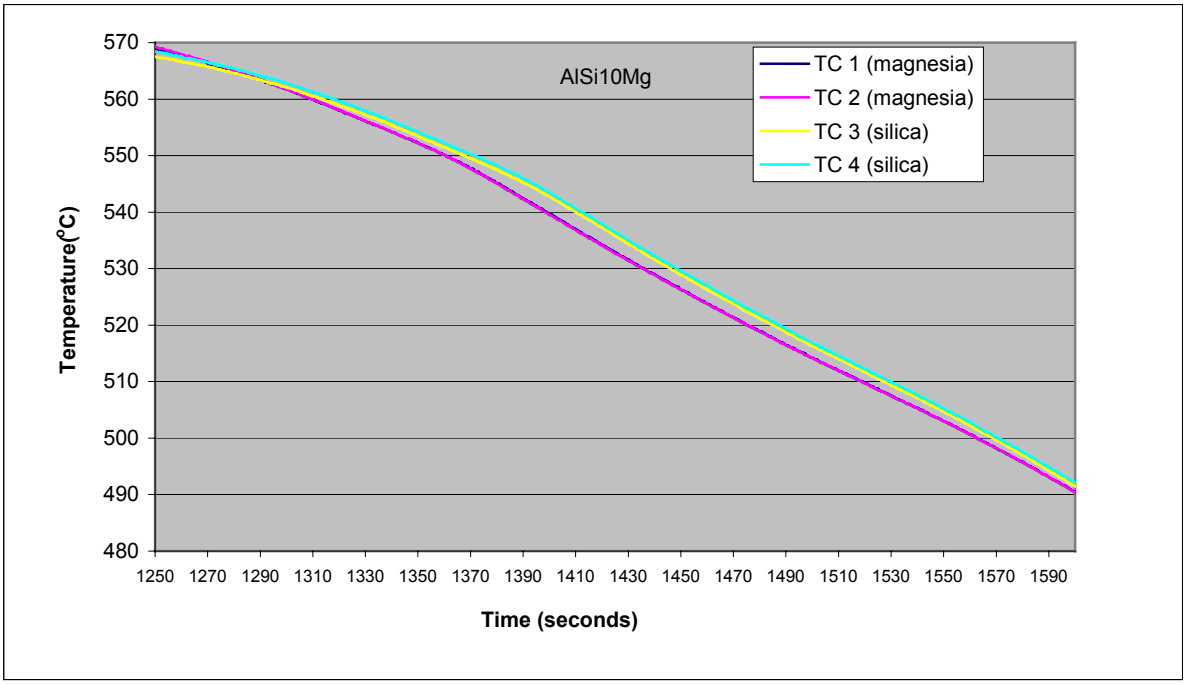

Figure 45. Region 5. At the completion of solidification, probably due to its higher thermal conductivity, magnesia-coated sample cools slightly faster silica-coated sample. Time lag to achieve 530°C is about 10 seconds.

3.11 KBF_4 as an inhibitor

Addition to the mold as a stucco: The mold containing KBF_4 as a stucco produced irregular (rough) cast surfaces. Mold face coat was similarly irregular (Figure 46).

KBF_4 grains were used as first coat and third coat stucco in this experiment. Spalling of first coat was visible.

Figure 46. Face coat stucco in this casting was KBF_4. It produced irregular (rough) cast surfaces. Burning of KBF_4 was also apparent in the shell.

Buried in KBF_4: Quality index values measured from the experiment are given in Table 18. Typical cast surfaces are seen in Figure 47.

Table 18. A comparison of the quality index values for revealing the influence of immersing the mold in KBF_4.

	Casting #1				Casting #2				MEAN	TOTAL MEAN
Nothing around the test pieces	7.72	4.67	4.87	8.06	18.08	6.17	17.89	20.28	10.97	10.05
	1.25	9.75	6.87	15.94	3.74	7.51	11.15	16.93	9.14	
Buried in KBF4	30.86	17.37	11.88	25.15	48.36	40.70	26.81	41.47	29.07	35.64
	44.52	39.65	26.08	62.75	30.43	72.50	34.26	27.53	42.21	

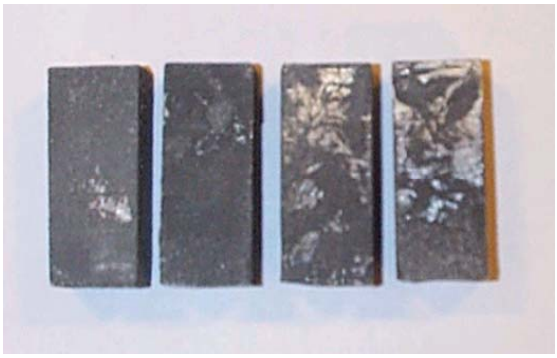

7.72 1.25 30.86 44.52

Figure 47a *Figure 47b*

Figure 47. The influence of KBF_4 inhibitor on the surface quality of the castings. Figure 47a with gray shades in the figure, Figure 47b with gray shades removed. Left two pieces in Figure 47a and Figure 47b: cast in air. Right two pieces in Figure 47a and Figure 47b: cast in a bed of KBF_4. The number under each test piece in Figure 47b is the quality index value measured by the image analyzer.

3.12 Croning sand as an inhibitor

Since the preheated mold was at the temperature of 450^{o}C when it was placed in the sand bed, Croning sand started to harden and resulted in a thick shell around the test pieces (Figure 48). The surface quality of test pieces cast in Croning sand was better than that of the samples cast without this inhibitor (Table 19). Two other observations:

a. In two of the castings, large gas holes were observed in the test pieces (Figure 50).

b. Although the mold-metal reactions were reduced, gases from the Croning sand influenced also the surface color, producing an uneven color pattern.

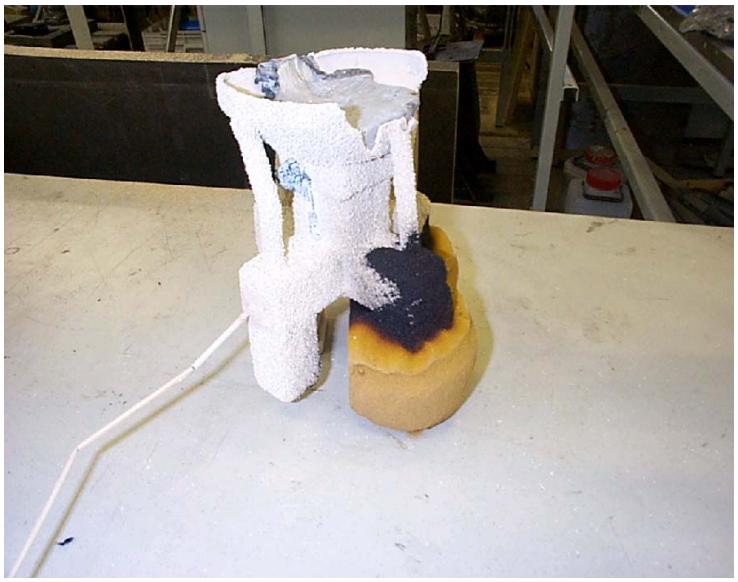

Figure 48. Preheated mold was placed in a bed of croning sand before the casting. With the effect of heat, Croning sand hardened and made a thick shell around the mold.

Table 19. The comparison of quality index values measured for revealing the influence of immersing the preheated mold in a bed of Croning sand before pouring

	Casting #1				Casting #2				Casting #3				MEAN	TOTAL MEAN
Nothing around the mold (2 test pieces)	10.09	10.22	10.18	9.52	46.31	74.74	139.32	114.49	114.1	142.36	192.82	90.41	79.55	59.88
	15.11	4.14	8.86	20.55	12.25	23.62	23.59	84.52	96.16	78.39	62.76	52.61	40.21	
In Croning sand bed (2 test pieces)	157.97	133.90	136.29	165.03	199.98	197.66	212.13	197.17	237.07	251.3	247.9	244.04	198.36	208.95
	161.05	225.14	217.96	164.83	223	156.78	242.32	243.71	243.29	253.83	252.06	250.54	219.54	

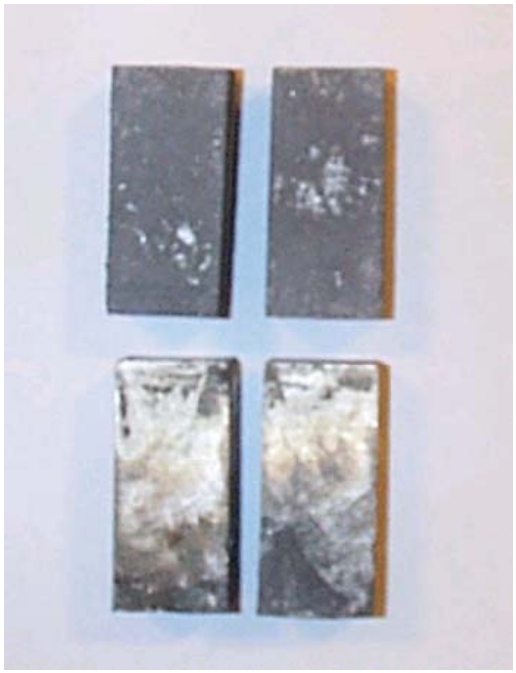

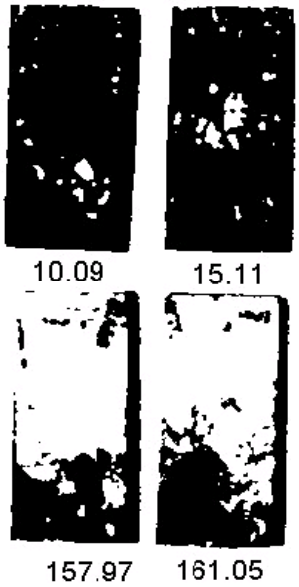

a) b)

Figure 49. The effectiveness of Croning sand as an inhibitor. a) pictures with gray areas b)gray areas removed. Upper two pieces in a): cast in air. Lower two pieces in a): cast in a bed of Croning sand. The number under each test piece in b) is the quality index value measured by the image analyzer.

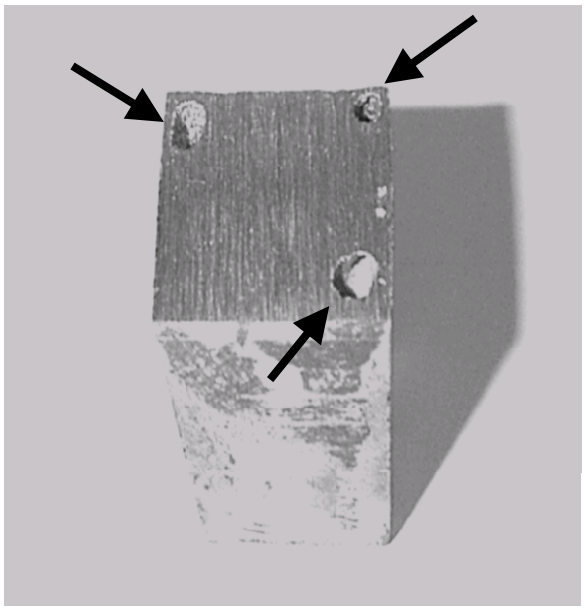

Figure 50. Surface reactions were reduced in the test pieces cast in a bed of Croning sand, but the cast pieces contained large gas holes close to the surfaces.

3.13 $NaBF_4$ as an inhibitor

The quality index values for both standard shells and shells where $NaBF_4$ was used are given in Table 20. Figure 51 shows the casting before the separation of test pieces and Figure 52 shows typical pictures of surfaces.

Table 20. The quality index values measured for cast test pieces with and without $NaBF_4$ inhibitor

	Casting #1				Casting #2				Casting #3				MEAN	TOTAL MEAN
Standard Shell	141.0	154.7	100.88	136.65	107.07	146.03	97.84	41.81	89.78	153.97	216.17	205.04	132.59	
	158.5	237.3	164.95	34.09	142.87	126.84	89.87	92.13	138.38	188.29	207.51	157.01	144.82	138.71
Dipped in $NaBF_4$	250.8	249.9	250.50	250.51	246.41	250.86	251.69	249.33	244.67	244.99	251.81	251.69	249.43	
	247.7	244.9	216.52	239.06	234.52	233.38	253.94	252.09	247.32	246.75	244.82	254.29	242.96	246.2

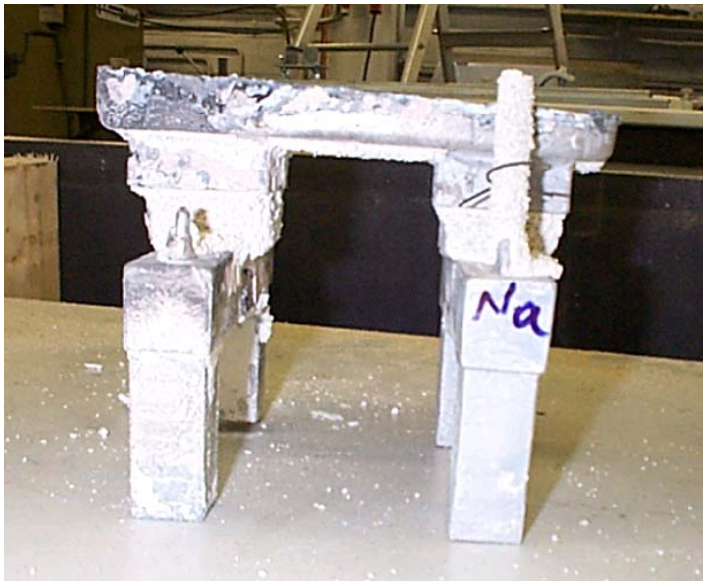

Figure 51. The casting used for studying the influence of $NaBF_4$ as an inhibitor. There is no ceramic material seen on $NaBF_4$-treated pieces (right-hand-side marked Na), whereas left-hand-side pieces show ceramic material stuck on the surface of the casting due to the mold-metal reactions.

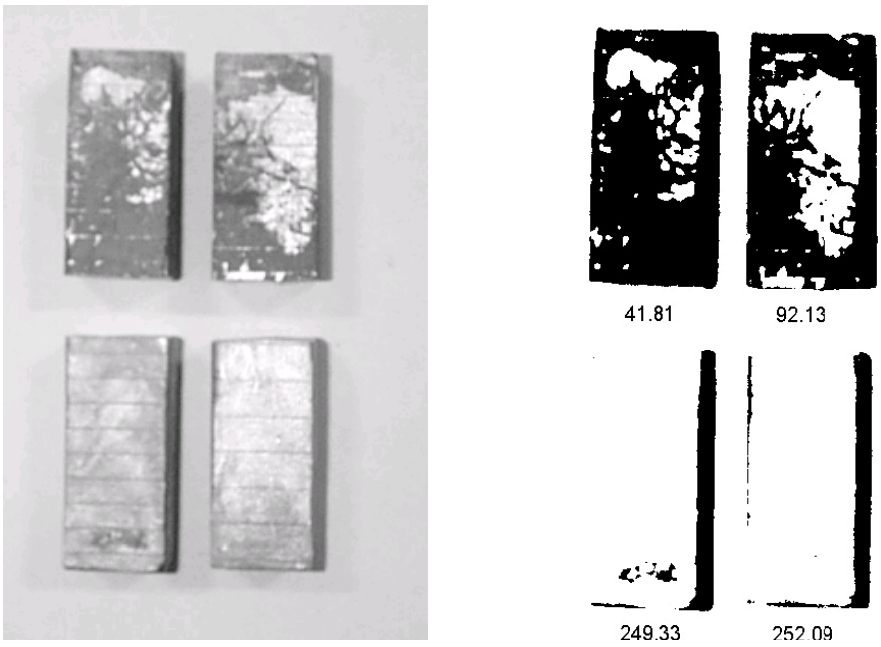

a) b)

Figure 52. The influence of $NaBF_4$ inhibitor on the surface quality of castings. a) pictures with gray areas b)gray areas removed. Upper two pieces in a): no treatment, Lower two pieces in a): Shell was dipped in $NaBF_4$. The number under each test piece in b) is the quality index value measured by the image analyzer.

Effect of Inhibitor on Permeability:

A shell permeability specimen which was dipped in $NaBF_4$ solution was subsequently heated to 200^{o}C to evaporate the free water. After that the gas permeability was measured. No change from the permeability value of the undipped specimen was observed.

4 DISCUSSION

4.1 The Comparison of Mold Refractories

The measured quality index values of all test castings are given in section 3.5. The values given as mean values are the arithmetical averages. Based on the results of seven-piece castings, the mold ceramics can be listed from the least reacted to the most reacted as follows:

1.Fused Magnesia	252.9
2.Yttria	245.9
3.Fused Alumina	217.9
4.Zircon	214.4
5.Molochite	172.0
6.Zirconia	88.7
7.Fused silica	13.8

The values for magnesia and yttria; as well as those for alumina and zircon are very close to each other. Therefore the following arbitrary classification can be considered as more realistic:

Excellent: Fused Magnesia, Yttria
Good: Fused Alumina, Zircon
Moderate to poor: Molochite, zirconia
Extremely poor: Fused silica

There are variations in this order in some castings but the excellent reaction resistance seen for magnesia and yttria and the very poor resistance of the fused silica was obvious for all castings. Fused alumina and zircon also showed good reaction resistance but they did not exceed the values of magnesia and yttria.

Strong mold-metal reactions were observed for fused silica. This sometimes resulted in the fracture of the mold.

The variations in the quality index values from one casting to another can be attributed to:

1. The sensitivity of the mold-metal reactions to small changes in mold and pouring temperatures
2. Small variations in the value of other parameters such as pouring speed.
3. Variations in quality index values were also seen on 4 different faces of the same specimen. This is not unexpected since the burning of magnesium starts already during pouring and filling. The burned layers stick to the part of the surface whereas the unburned mass will come in contact with the rest of the virgin surface area. This contact is obviously not uniform due to turbulences during pouring and filling.

4.2 Free Energy of Formation or Permeability?

The only difference between the shells of the test pieces was the face coat material. Casting parameters such as casting temperature and mold temperature were the same for all test pieces within a particular mold. Therefore, the observed large differences between the reactivities of different ceramics should be explained by either varying face coat or shell permeability change caused by the specific face coat.

Consider the experiment which was carried out to study the heat release (section 3.10). An examination of Table 17 shows that the permeability of magnesia-coated samples was higher than that of the silica-coated samples. In spite of this, there were severe mold-metal reactions in the silica-coated sample and very little reactions in the magnesia-coated sample. Therefore the difference in reaction severity cannot be explained by the permeability change and the consequent change in the availability of oxygen. One plausible explanation can be given by considering the free energy of formation of these materials: Magnesia having a very high free energy of formation is much more stable than silica.

In fact, comparison of permeability measurements of other refractories[18] tested in this work (Table 13) implies that the differences in the relative reactivities cannot be explained by permeability differences, but can only be explained by considering the free energies of formation of these substances. The permeability of molochite and silica shells, (which were found to be the most reactive refractories), are comparable in magnitude to the permeability of alumina and zircon shells. Magnesia, which was found to be most resistant to reactions, gives more permeable shells than the others[19].

4.3 Theoretical Calculation of Free Energy of Formation

Section 3. 2 gives the assumptions made for theoretical calculation of free energies of formation of studied refractories as well as calculated free energies of formation versus temperature in graphical presentation (Figure 21).

1. The excellent reaction resistance of magnesia and yttria observed during the experiments is in agreement with the calculations. Strongly negative free energy of formation makes these oxides very stable.
2. In practice, zirconia showed smaller resistance to reactions as compared to the theoretical predictions.
3. Fused silica has the least negative free energy of formation at any temperature, which makes it very susceptible to reactions. This is in agreement with the experimental observation, which showed that this refractory reacted most strongly with magnesium melt.

The tendency of magnesium melt to react with the studied refractories can be also theoretically predicted as follows:

The direct reactions of magnesium with the studied refractories can be written as

$x\ Mg + u$ Refractory oxide$(MO) \rightarrow y\ MgO + z\ M$ (Metal)

$\Delta G^{o}_{T} = \Sigma \Delta G^{o}$ (products) - $\Sigma \Delta G^{o}$ (reactants)

[18] Density of back-up slurry was not the same in two series, therefore a difference in the values of the same ceramic in two series. In each series, however same back-up slurry was used for all the samples.

[19] The reason why magnesia shells are more permeable is not clear. Apparently, the combined effect of specific powder and stucco applied should be considered. Microcracks which may be present in the shells may also influence the readings.

The magnitude and the sign of ΔG^{o}_{T} depend on the free energies of formation of oxides, as free energies of formation for pure elements are zero. Therefore, if no reaction is desired, the ΔG^{o} for the MO must be less negative than that for MgO.

Referring to the Figure 21 calculated in this work and also to Figures 1, 2 and 3 it can be predicted theoretically that in magnesium melting only the refractories Y_2O_3 (yttria), BeO and ThO_2 will not react with the magnesium melt (positive free energy change).

The dipping experiments in this work showed that oxygen is required for the reactions to start. Therefore the above magnesium melt reaction with refractories should be altered as follows:
x Mg + O_2 + u Refractory oxide(MO) $\rightarrow$ y MgO + z M (Metal)
(See sections 4.5 and 4.6)

4.4 Reaction Layers

Referring to Table 14, it can be seen that oxygen is the most predominant element in the reaction layers, which shows that the reaction layers are basically a mixtures of oxides. MgO seems to be present in all cases. Other elements such as Al and Si can be originating from the products of reaction of magnesium melt with the refractory oxide, or they can come from the unreacted oxides of the shell.

Note also that analysis of silica-coated sample shows 0.86% as the silicon concentration. This is too low. Therefore in order to search for ternary compounds, X-ray diffraction analysis was carried out for the silica-coated sample. Results are given in Table 15. The numbered compounds are the most likely compounds present in the reaction layer. Among these, Mg_2SiO_4 and $Mg_2(SiO_4)$ can be considered the same compound.

4.5 Direct Reaction of Magnesium Melt with the Mold Refractories

All samples were dipped in the AZ91E melt at 700^{o}C. Although the casting temperature in the investment casting of this magnesium alloy is higher, normally between 740-750^{o}C, the metal

stream is rapidly cooled by the mould walls during pouring. (Figure 20 cooling curve) Therefore dipping the refractory into the melt at 700^{o}C for 30 seconds should reveal realistic information about the possible direct reactions between the magnesium melt and the investment casting mold in the absence of oxygen.

No indication of a reaction could be observed as a result of the dippings. All surfaces were seen to be unaffected.

It can be concluded that for the studied refractories at the parameters given, oxygen must be present for refractory-magnesium reaction to occur. Higher melt temperatures might result in the direct reactions but this was not investigated systematically.

These experiments also explain the result obtained with molochite (section 3. 9). When the mold permeability is reduced, the passage of oxygen through the shell is blocked and the reactions are also drastically reduced.

It also implies that if ceramic shell molds are completely sealed before pouring (either by glazing or by additional zircon coatings), and the oxidation during filling is prevented by the use of a preventive gas (such as SF_6), all studied ceramics are expected to show similar performance i.e. no reaction.

Therefore, based on this evidence, it can be concluded that mold-metal reactions are initiated by the help of oxygen.

4.6 The Influence of External Oxygen

Table 16 and Figure 31 shows large improvements in the surface quality of the castings produced in reduced permeability shells. This shows that in magnesium investment castings, mold-metal reactions can be reduced effectively by reducing the gas permeability of the ceramic mold.

This result can also be combined with the result obtained with magnesium direct reactions experiments. It is suggested that the reactions between the molten magnesium and the mold occurs in two stages:

1. During pouring and filling, oxygen reacts with magnesium melt and makes MgO. This oxide skin sticks to the cast surface and resembles a mold-metal reaction. Mold-metal reaction also starts in this stage. Use of SF_6 will reduce or eliminate oxidation and mold-metal reactions during the pour and fill.
2. External oxygen reacts with magnesium melt after filling and initiates mold-metal reactions. Dipping experiments show that magnesium melt does not immediately react with any of the refractories in the absence of oxygen. This is in spite of the fact that ΔG is negative in sign and a spontaneous reaction is indicated! In other words, the following reaction (which represent a direct reaction) does not happen without oxygen

   $Mg + MO \rightarrow MgO + M$, where MO is the refractory oxide

   When oxygen is present:

   $Mg + O_2 + xMO \rightarrow MgO + yM + zMO$

When the permeability of the shell is adequate[20], stability of MO (i.e. free energy of formation) seems to be the most important factor determining the extent of this reaction.

An example of the above reactions can be given as follows in silica-coated shells.

Case 1. Direct reaction

$2Mg + 2SiO_2 \rightarrow Mg_2SiO_4 + Si$ (dissolved in the Mg)……..…..I

Free energy change[21]= -298.534 kJ

Case 2. Free oxygen is available

$2Mg + O_2 + SiO_2 \rightarrow Mg_2SiO_4$, ……..…II

Free energy change= -1054.681 kJ

Therefore, Reaction II is favorable over Reaction I.

Reaction II can be thought of occurring in two stages (sum of the two gives Reaction II):

$2Mg + O_2 \rightarrow 2MgO$ .....……....III

Free energy change= -991.865 kJ

$2MgO + SiO_2 \rightarrow Mg_2SiO_4$……..IV

[20] It has been found (52) that for gravity casting mold designs where a fair amount of the air must go through the mold, a permeability of 80-120 cc N_2/min is generally adequate. A permeability of 100 cc N_2/min corresponds to the flow rate achieved by a 1/64" diameter hole under the pressure conditions of the shell permeability test.

[21] Free Energy Change for the reactions of silica with magnesium melt is given as Appendix E.

Free energy change= -62,817 kJ

Free energy change for Reaction III is very large compared to that for Reaction IV. It is also known to be exothermic (30). $Mg + O \rightarrow MgO$ reaction can therefore be thought of an energy supplier for Reaction IV to take place.

Once the above reaction II starts, heat is produced, solidification is delayed and the reaction may continue leading to a mold failure. Here obviously, rate of heat loss from the solidifying mold should also be taken into account in order to predict whether the continuing reaction would lead to a mold failure.

Let us consider an investment-casting mold cast at 740^{o}C. Cooling curve shows that mold-metal interface temperature rises up to a maximum of 700^{o}C (Figure 20). What happens if the supply of oxygen is cut off soon after the mold-metal reaction started? It is obvious that if III does not take place, IV will not take place either. Even if the temperature of the mold-metal interface may have initially increased due to reaction, as soon as the oxygen supply is cut off, the exothermic $Mg + O \rightarrow MgO$ reaction will not take place and the temperature of the mold-metal interface will drop quickly back to 700^{o}C level. At that level, it was already shown that direct reaction represented by I does not take place. The reactions will stop. Therefore, oxygen is necessary not only for the initiation of the mold-metal reactions but also for the continuation of the reactions.

In fact, even at higher temperatures, the tendency of the direct reaction I between magnesium and silica is not theoretically enhanced. Referring to Appendix E for the direct reaction

$2Mg + 2SiO_2 \rightarrow Mg_2SiO_4 + Si$ (dissolved in the Mg),

Free energy change= -298.534 kJ, at 700^{o}C

Free energy change= -295.569 kJ, at 800^{o}C

Free energy change= -288.534 kJ, at 1000^{o}C

Reactions with other mold ceramics can be treated in the same way. However the total free energy change becomes smaller as more stable refractories (larger free energy of formation) reacts with magnesium melt. In other words, consider the reaction:

$Mg + O_2 + MO \rightarrow MgO + M$

As the free energy of formation of refractory MO on the left hand side becomes larger, the total free energy change becomes smaller which means that the degree of reaction is reduced.

In the above reaction, it is also possible[22] that M forms ternary compounds with MgO as in the case of silica reactions.

Mold failures (breakage), which was were sometimes observed for fused silica, occurred long after (15 seconds or more) the mold filling was complete. Here obviously rate of heat loss from the solidifying mold was not large enough, so that the continuing reactions, additional heat supplied by the reactions and consequent solidification delays lead to the mold failure.

Section 4.7 gives details of an experiment, which suggests that heat is evolved during the reactions.

In this work, the protective gas SF_6 + CO_2 was used only during the pouring. In a separate experiment, no gas at all was used during pouring. Visual observations and examination of cast surfaces indicated that excessive burning occurred already during the pouring and filling. The difference in the extent of reactions between the permeable and impermeable shells remained also in this experiment.

A similar observation was made by Idris and Clegg (40) but with a different explanation: *When the ceramic molds were flushed directly with CO_2/SF_6 gas, reactions were observed. When the mold was flushed within an enclosure (container), a clean metallic surface was obtained.* The authors considered that the method of putting the ceramic mold inside an enclosure and flushing the whole system (inside the mold and inside the enclosure) was more "reliable". It "ensured that the flushing gas remains both within the enclosure and the mold". No comments on the permeability of the mold and the influence of oxygen around the mold was given in their work. It is obvious that in their case, the presence of SF_6 in the container eliminated the influence of external oxygen.

[22] More chemical analysis may be required for each refractory to find out whether M stays as pure metal or it makes a compound. EDS analysis indicated only the presence of these elements, not their specific compound form. XRD analysis in the case of silica-coated shells indicates also the presence of ternary compounds such as Mg_2SiO_4. This may be the case for other studied refractories as well: In addition to binary compounds, ternary or quadri compounds may form during the reactions.

We have already stated that when the ceramic shell molds are made impermeable to gases, the mold-metal reactions are reduced. After the filling is complete, the reactions will tend to slow down or to stop due to the lack of oxygen. This certainly is a benefit in magnesium investment casting. However the reduction in gas permeability may result in filling problems. Gas permeability is an important intrinsic property of a ceramic shell mold. During filling, the entrapped air is removed through the mold walls due to the porous structure of the shell. Separately introduced air vents help in the removal of air, but it is difficult to incorporate air vents at every potential spot, particularly if the mold contains several small parts with thin sections.

If mold filling becomes a problem, a solution can be found as follows: First the molds are made with normal mold making process, and then additional thickness (e.g. with a brush) can be applied only on the problematic areas, e.g. thick sections of the casting. This would stop the passage of the air into the mold and prevent excessive burning. At the same time the permeability of shell in thin sections, which is essential for complete filling, would not be affected. No experiments were carried out in this work to check the applicability of this suggestion.

Another way of preventing mold-metal reactions would be to employ a protective atmosphere also outside the shell. Reactions would be prevented in spite of the presence of oxygen, as the investigators in reference 40 have suggested. An investment foundry in the UK already investigated this aspect further, during which a series of test castings, employing various concentrations of SF_6 in the atmosphere around the shell, were cast (39).

A comparison of the influence of oxygen in melting and casting titanium and magnesium can also be carried out as follows:
As suggested by Piwonka (5), the sources of oxygen during the melting of titanium are as follows:

b. Initial oxygen content of the melt.
c. The oxygen picked up by the metal as it travels through the gating system.
d. Oxygen picked up from the furnace atmosphere. This is negligible in vacuum melting.
e. The oxygen dissolved from the mold when the metal comes to rest in the casting.

Piwonka indicated that only the last factor is of significance in titanium melting. In magnesium melting and casting, the situation is different:

a. Initial oxygen content of the melt can be assumed to be zero[23].
b. Reactions between the oxygen and the melt, when the melt is poured into the pouring cup and when it travels through the gating system, are important and they constitute a part of the observed reactions. Use of protective gas reduces or eliminates the reactions.
c. If a protective gas is continuously used on the melt, the oxygen pick up from the furnace atmosphere is negligible.
d. Oxidation from the mold atmosphere during the filling. This is unavoidable unless the mold cavity is flushed with a protective gas at a proper gas concentration and for an appropriate period.
e. Diffusion of oxygen from the external atmosphere into the mold cavity is important in the casting of magnesium.

Unlike titanium melting, there is no dissolution of oxygen in the casting. Instead, oxygen seems to be consumed continuously during the reactions of the melt with the mold, and it accumulates in the reaction products forming on the surface of the casting.

4.7 Heat Release During Mold-Metal Reaction

Figures 35 to 39 are show the cooling curves for AZ91E alloy. In Region 1, which is the region before the casting is poured, the recorded temperatures are about the same, *on the average* silica - coated sample is 1 degree colder than magnesia-coated sample.

In Region 2, we have higher temperature readings from silica-coated shells. Difference is 10 degrees (Figure 37). In Region 3, the difference becomes 20 degrees. Time lag to achieve 500^{o}C is 50 seconds (Figure 38). As a result, solidification of sample in silica-coated shell is delayed by about 35 seconds in Region 4 (Figure 39). A growing difference in temperatures from 10 degrees

[23] Gaseous oxygen is not soluble in Mg melts, whenever oxygen is present, it is in the form of MgO. Hydrogen on the contrary is soluble in Mg melts. (60)

to 20 degrees can be interpreted as follows: Reactions started in Region 2 (liquid region) and it continued in Region 3 (liquid+solid) with additional reactions and consequent heat generated.

This implies that heat is generated by the reactions in the silica-coated sample. Temperature difference is actually rather small, maximum 20^{o}C. Figure 17 shows the location of the thermocouple. After the sintering of the shell mold, a hole was drilled through the mold wall and the thermocouple was placed. Thermocouple junction is very close to the mold face coat. However the tip is in contact with the melt. In this arrangement, heat generated by the reactions at the mold-metal interface will be quickly dissipated to the melt. Therefore, it is more correct to say that, we are measuring the melt temperature in the very vicinity of the face coat rather than the reaction temperature. The actual reaction temperature is expected to be higher than the measured temperature. In practice, it is difficult to place the tip right at the face coat. It requires a mold, which is open on both sides so that after drilling the hole and placing the thermocouple at exactly the same level as the mold wall, the tip can be coated with the same refractory.

Heat conductivity of MgO is larger than that of SiO_2. It was therefore decided to check the effect of heat conductivity on the cooling curves.

An identical mold was cast with AlSi10Mg alloy. Figure 40 shows the overall cooling curve for AlSi10Mg alloy, and Figures 41 to 45 shows the detailed views of 5 regions in the cooling curve.

The overall cooling curve of AlSi10Mg alloy reveals that the cooling rate of magnesia-coated sample is very similar to that of silica-coated sample. At the completion of solidification (Region 5) a very small difference between the cooling rates appears. This is probably a result of the heat conductivity difference between the magnesia and silica.

Relatively higher temperature readings observed in AZ91E casting for silica-coated samples in Region 2 and particularly in Region 3 is **absent** in AlSi10Mg casting.

It can therefore be concluded that the influence of heat conductivity difference between magnesia and silica is negligible on the cooling curves. Higher temperature readings in Region 2 and

particularly in Region 3 in AZ91E casting can only be explained by a heat release due to mold-metal reactions.

Since we have two thermocouples for each sample giving approximately the same readings, the measurements should be considered reliable.

4.8 Possibility of Replacing Zircon with Magnesia or Yttria Face Coat

Replacing zircon face coat with magnesia or yttria face coat would increase the mold making costs if production work is attempted by using these refractories.

Yttria is exceptionally expensive and it cannot hence be considered for production or prototype work. Fused magnesia is inexpensive (£1360 per ton); its price is comparable to that of zircon. However, the slurry life of fused magnesia is very short. Repeated renewal of the slurry in the production would undoubtedly increase the total production costs.

According to the information obtained from the supplier of magnesia (53), "there may be a number of patents for primary coats in casting certain metals where magnesia was used in the slurry". The patents mentioned in this information are US Patent No. 4,415,673; 4,504,591; 4,740,246 and 5,944,088. These patents describe the use of zirconia sols and yttria sols with different ceramics including magnesia. Sample quantities from these patented binders were obtained from the manufacturers and the binders were tested with the aim to obtain stable slurries with magnesia as the filler. The initial experiments were not successful. Additional work is required.

4.9 Possible Dimensional Problems as a Result of Replacing Zircon with Another Refractory

In order to avoid or to reduce the mold-metal reactions it is sufficient to change only the face coat material because the face coat is in contact with the molten magnesium during the casting. Face coat is only a very thin part of the shell. Therefore it is unlikely that a change from, for instance, a zircon face coat to magnesia face coat would result in dimensional changes in the castings. There

are numerous variables influencing the dimensions of investment castings (54). Rosenthal showed that the largest contributions to dimensional changes are coming from metal shrinkage, pattern wax shrinkage, and shell materials changes, in order of importance (55).

Even if the refractory material for the whole shell were changed, the dimensional changes would probably be very small. Snow and Scott (56,57) compared the fused silica and alumino-silicate shells and showed that when both types of shells were held for 2hr in a preheat furnace, the same dimensions were obtained in the castings. Production foundries have also found that they can switch from an alumino-silicate shell to a fused silica shell without any dimentional problems, except for some jobs with very tight dimensional tolerances.

4.10 Use of Different Binders

It has been claimed that silica binders are not ideal binders for magnesium casting. Silica binders produce a silica bond between the ceramic particles upon setting. The mold-metal reactions seen in magnesium investment castings could be enhanced by the reactions between the silica bond and the molten metal. Therefore some commercial foundries prefer to use a silica-free binder such as zirconia sol (see 1.1.7), but it is a more expensive solution.

In all ceramic shells in this work silica binders were used. Results show that magnesium reacts strongly with some mold materials yet it does not react with some other mold materials, although for all mold materials silica binders were used. If the contribution of the binder to the reactions were considerable, we would have observed strong reactions in magnesia and yttria coated samples as well. But this was not the case. So it can be concluded that reaction between the molten magnesium and silica bond is negligible[24] at investment casting temperatures compared to the reaction which occurs between molten magnesium and the major mold constituents i.e. refractory powder and stucco material.

[24] This does not mean that silica bond does not react with magnesium at all. During dipping experiments, a silica-coated test bar was let to burn in air freely after dipping. After the intense burning ended, the strength of the test bar was seen to decrease drastically, it disintegrated easily. This shows that the bond was destroyed. The temperature however during the free burning of magnesium is considerably higher; it was measured to go over 1000^{o}C.

For this reason, silica binder was not replaced with another binder in this work. In addition, silica binder is the universal binder in the investment casting world, it was considered that the results obtained with it would be more useful to the industry than the ones obtained with a special binder.

4.11 KBF_4 as an Inhibitor

Addition to the mold as a stucco

Irregular cast surfaces suggests that the KBF_4 may have melted and destroyed the face coat during the sintering stage. The high temperatures used for sintering (800-950^oC) is not compatible with this chemical. Normal cast surfaces may be obtained if the inhibitor is used in the backup coats (outer layers). This was not tried in this work. It is however clear that irrespective of the location of inhibitor; its disintegration at sintering temperatures would reduce the strength of the mold considerably, which may lead to mold failures.

Buried in KBF_4

There was only a small increase in the quality index values (from 10.05 to 35.64) when KBF_4 was used. This result shows that this technique is not suitable for effectively reducing the mold-metal reactions. The obtained results are consistent with the work of Idris and Clegg (40) who could not get satisfactory results with KBF_4 as an inhibitor. However they found also some reductions in the reactions (section 1.1.8).

4.12 Croning Sand as an Inhibitor

It is difficult to explain why the reactions were reduced when the ceramic mold was placed in the resin sand just before the casting. An explanation could be that the oxygen is consumed during the hardening and burning of Croning sand binder[25]. It was shown in section 3.8 that degree of mold-metal reactions in magnesium casting also depends on the permeability of the mold and on the eventual reaction of magnesium melt with oxygen available around the mold. If external

[25] This is very likely, since it is known that the mold gases evolving during the burning of Croning sands consist of primarily hydrocarbons, hydrogen and carbon monoxide. Varying amounts of water vapor and carbon dioxide will also be present depending on the availability of oxygen in the atmosphere (58). This results in the presence of a reducing atmosphere.

oxygen is consumed during the hardening and subsequent burning of the Croning sand binder, there will be less oxygen available for the reaction with magnesium. This may explain the reduced level of reactions when the molds were placed before pouring in a bed of Croning sand. Another explanation might be that the Croning sand, forming a barrier, reduces the passage of external oxygen through the mold walls. The net result is again a reduction in the amount of oxygen and consequent reactions.

Large gas holes observed in the samples can be explained by the release and reaction of gases forming during the setting and burning of the Croning resin sand by the diffusion of these gases through the shell mold into the melt. Croning sand binder first hardens and then partly burns during the casting process. Since the hardening starts and continues during the pouring of the melt, the amount of evolved gases must be higher than in the normal practice where pre-hardened shell molds are used.

The time of placing the sand around the mold (before or after the pouring) might have had an influence on the formation of the gas defects. This was not investigated in this work.

4.13 $NaBF_4$ as an Inhibitor

There is a large improvement in quality obtained with the use of $NaBF_4$ inhibitor (see section 3.12). All test pieces cast in shells, which had been dipped in a $NaBF_4$ solution, showed very little or no mold-metal reactions.

The reductions in the mold-metal reactions due to the use of $NaBF_4$can be attributed to one or both of the following factors:

1. Liberation of BF_3 gas upon mold preheating and/or casting:

   $NaBF_4 \longrightarrow BF_3$ (gas)+ NaF

   The temperature at which dissociation of $NaBF_4$ starts is 384^oC. This is well below 450^oC which is the mold preheating temperature employed in this work. Consequently it can be assumed that some BF_3 gas evolves during mold preheating and it is present in the mold cavity. BF_3 gas can also start evolving during the pouring stage when the liquid metal hits the

mold walls. No gas liberation, however, was visible during the heating of the mold or during the casting.

2. Modified surface energy of the mold walls due to the inhibitor ($NaBF_4$) in the mold structure: The presence of the inhibitor salt may increase the surface energy of the refractory so that the solid/liquid contact angle becomes greater than 90^o. This has the net effect that the mold is not "wetted" by the magnesium alloy, which in turn explains reduced reactions. The non-wetting behavior in the case of $NaBF_4$ treatment was apparent immediately after the casting. No sticking of the face coat onto the cast surface could be seen (see Figure 51)

It was also observed that some edges of $NaBF_4$-treated castings were not as sharp as those in untreated pieces. This may be due to a gas evolution, which influences the filling of the mold. The backpressure of the evolving gas may prevent the complete filling of the edges[26]. No experiments were carried out for studying this effect further. It is, however, known that a similar inhibitor KBF_4 may cause misruns in sand castings (49).

In this work, the casting was poured, as soon as the mold reached the casting temperature (450^oC). In practical casting, this is not always the case. Molds are sometimes kept in the preheating furnace for long periods of time during which the inhibitor may be completely lost.

Further experiments were recently carried out with $NaBF_4$ inhibitor. In these experiments, molds were **filled up** with the inhibitor solution. After a waiting period of about 4 minutes for the inhibitor to be absorbed by the ceramic mold, the mold was emptied of the solution. This method is obviously easier than dipping the mold in the solution, particularly when large molds are treated in production. Results can be summarized as follows:

a. The amount of the $NaBF_4$ inhibitor which is given in section 2.12.3, can be considered as the optimum amount to be used.

b. Isolation wool which had been originally used on the pouring sprue has no influence on the results.

[26] This is analogous to the case in sand casting where various sand additives have been claimed to enhance the resistance of the mold to penetration. Additives include cereals and carbonaceous materials. The beneficial effect of these additives was attributed either to increased pressure in the mold due to the gases resulting from the combustion process of the additives, or due to the reducing atmosphere resulting from their combustion (19).

c. Molds can be kept in the preheating furnace for at least 4 hours without a change in the effectiveness of the inhibitor.

If the reduction in the mold-metal reactions is attributed to the liberation of BF_3 gas, b and c suggest that the dissociation of the $NaBF_4$ inhibitor at mold preheating temperatures is very slow and/or BF_3 is liberated mainly when the liquid metal hits the mold walls.

The Influence of Inhibitor on Permeability:

The dipping treatment of the shell in $NaBF_4$ solution did not influence the shell permeability (see section 3.13). The possibility that the mold-metal reactions are reduced simply due to reduced shell permeability can be ruled out.

5 CONCLUSIONS AND FINAL REMARKS

1. Mold-metal reactions between investment cast magnesium alloy AZ91E and different refractories used as face-coats in the molds were investigated. Excellent reaction resistance was noticed in the case of fused magnesia and yttria face-coated shells. Fused alumina and zircon face-coats also showed good resistance. Molochite and zirconia provided moderate to poor reaction resistance. Strong mold-metal reactions were observed in the case of fused silica.
2. Dipping experiments show that oxygen is required for the mold-metal reactions to be initiated in the investment casting of magnesium.
3. Oxidation and mold-metal reactions start already during pouring and filling of the ceramic mold. This appears as defects on the surface of the casting. After the filling is complete, further mold-metal reactions are initiated by the diffusion of the free oxygen surrounding the mold through the mold walls.
4. Shell permeability measurements suggest that the severity of mold-metal reactions cannot be correlated to shell permeability. The severity of mold-metal reactions is related to the free energy of formation of the refractory. Refractories with a high free energy of formation are more stable and they react least. The free energies of the formation of the studied refractories were calculated. The predicted order of stability agrees fairly with the experimental observations given in 1.
5. As a consequence of the above conclusions, the followings can be recommended for producing castings free of mold-metal reactions:
    a. Before pouring, the shell mold should be flushed with a protective gas such as SF_6 to eliminate oxidation during the fist stage of the reactions.
    b. Shell molds should be sealed by either a glaze layer or by applying additional layers of zircon on the sintered mold. If a complete sealing is achieved, all studied refractories in this work show the same performance, i.e. no mold-metal reaction occurs with the magnesium melt. If a complete sealing cannot be achieved and partial passage of oxygen through the mold walls is likely to occur, then a refractory with a high free energy of formation should be selected as the face coat refractory.

6. SEM analysis of reaction layers indicated presence of oxides mainly in the form of MgO and other refractory oxides as mold-metal reaction products. XRD analysis suggested presence of a ternary compound Mg_2SiO_4 as the reaction product in the silica face-coated molds. Free energy changes were calculated for the mold-metal reactions in the silica face-coated mold. Calculations suggest that the reaction involving free oxygen is strongly favored over the direct reaction of silica with the magnesium melt. This is consistent with the main result of dipping experiments that the presence of oxygen is required for the mold-metal reactions to be initiated. It was also argued that at normal investment casting temperatures, the presence of oxygen is required also for the continuation of the reactions.
7. Calculations show that the free energy change for the direct reaction slightly decreases with increasing temperatures. Therefore, even at higher casting temperatures, the tendency of a direct reaction between magnesium and silica is not theoretically enhanced.
8. Calculations in the other refractory systems require further chemical analysis, with the aim to find out reaction products more precisely and quantitatively including the ternary reaction compounds. This can be suggested as a future work.
9. Cooling curves of AZ91E and AlSi10Mg were compared in a casting, which contained magnesia and silica face-coated samples. Results suggest that heat is released during mold-metal reactions in silica face-coated sample. Further measurements are required if the degree of heat release is to be related to the specific refractory used as a face coat. This can also be suggested as a future work.
10. Neither the use of KBF_4 as stucco material in the shell or casting the shell in a bed of KBF_4 inhibitor proved successful in inhibiting mold-metal reactions.
11. Mold-metal reactions was reduced in ceramic shell molds which were cast in a bed of Croning sand. However, large gas holes in the castings were found.
12. Mold-metal reactions were reduced effectively by dipping the ceramic shell in a solution of $NaBF_4$ before casting. Possible industrial use of the suggested method requires further tests and refinements in the method in a commercial foundry.

REFERENCES

1. Pettersen, G., Øvrelid, E., Tranell, G.,Fenstad, J., Gjestland, H., "Characterization of the surface films formed on molten magnesium in different protective atmospheres", Material Science and Engineering A332 (2002) p. 285-294.
2. Cashion, S.P., Ricketts, N.J., Hayes, P.C., "Characterization of protective surface films formed on molten magnesium protected by air/SF_6 atmospheres", Journal of Light Metals 2 (2002) p. 37-42.
3. Cashion, S.P., Ricketts, N.J., Hayes, P.C., "The mechanism of protection of molten magnesium by cover gas mixtures containing sulphur hexafluoride", Journal of Light Metals 2 (2002) p. 43-47
4. Aarstad, K. Tranell, G., Pettersen, G., Engh, T.A., "Various techniques to study the surface of magnesium protected by SF6", Magnesium Technology 2003 Edited by Howard I. Kaplan TMS (The Minerals, Metals & Materials Society), 2003, p. 5-10
5. Piwonka, T.S., "Reactions at the mold/metal interface in investment castings," Investment Casting Institute, 42nd annual technical meeting ,1994.
6. Frye, H., Yasrebi, M., Sturgis, D.H., " Basic Ceramic Considerations for Lost Wax Processing of High Melting Alloys", http://www.pgi-platinum-tech.com/pdf/V8N1.pdf , June 12, 2006.
7. Handbook of Industrial Refractories Technology, Principles, Types, Properties and Applications, Carniglia, S.C.; Barna, G.L., William Andrew Publishing, 1992.
8. Stull, D.R. and Prophet, H. ed., JANAF THERMODYNAMIC TABLES, 2nd Ed., 1971, U.S. Dept. of Commerce, Nat. Bur. of Standards, Washington, D.C. Supplements: J. Phys. Chem. Ref. Data 3 (2) (1974); 4 (1) (1975); 7 (3) (1978); 11 (3) (1982).
9. CRC HANDBOOK OF CHEMISTRY AND PHYSICS, 71st Ed., CRC Press, Boca Raton, FL ,1990.
10. Huseby, I.C., Klug, F.J., "Chemical compatibility of ceramics for directionally solidifying Ni-base eutectic alloys" Am. Ceram. Soc., Vol 58, No.5, 1979, p. 527-35
11. Ingo, G.M., Chiozzini, G., Faccenda, V., Bemporad, E., and Riccucci, C., "Thermal and microchemical characterizations of CaSO4-SiO2 investment materials for casting jewellery alloys", Thermochimica Acta 321, 1998, 173-83

12. Wagman, D.D., Evans, W.H., Parker, V.B., Schum, R.H., Halow, I., Bailley, S.M., Churney, K.L., and Nuttall, R.L., "The NBS tables of chemical thermodynamic properties", Am. Chem. Soc.,1982.
13. Levin, et alia, Phase Diagrams for Ceramists, American Ceramic Society, 1964, p. 68
14. Bates, C.E. and Monroe, R.W., "Eliminating Sand and Ceroxide Defects in Steel Castings", Proc. 39th Technical and Operating Conf., Nov. 1984, Steel Founders Society of America.
15. Griffen, J.S., Bates, C.E., Monroe, R.W., Svoboda, J., "Appearance and Composition of Oxide Macro-Inclusions in Steel Castings", AFS Transactions, Vol. 93 ,1985, p. 185
16. Campbell, J., Runjoro, J., Boutorabi, S.M.A., "Critical Gate Velocities for Film-Forming Casting Alloys", AFS Transactions, Vol. 100 ,1992, p.225
17. Stefanescu, D.M., Delannoy, P., Piwonka, T.S., Kacar, S., "An Investigation on the Role of Sand-Metal Contact Angle in the Formation of Casting Penetration Defects", AFS Transactions, Vol. 99, 1991, p. 761.
18. Giese, S., Stefanescu, D.M., Piwonka, T.S., Sen, S., and Dhindaw, B.K., "An Investigation on the Role of Sand-Metal Contact Angle in the Formation of Casting Penetration Defects: Phase II" AFS Transactions, Vol. 100, p.785
19. Stefanescu, D.M., Giese, S.R., Piwonka, T.S., and Lane, A.M., "Cast Iron Penetration in Sand Molds, Part I: Physics of Penetration Defects and Penetration Model", AFSD Transactions, Vol. 104, p.1233
20. Hudson, J.B., "Surface Science, An Introduction," John Wiley & Sons, Inc.,1998, p. 55
21. Engineered Materials Handbook, Volume 4, Ceramics and Glasses, ASM International, 1991, p. 483
22. New Energy and Industrial Technology Projects, Internet: http://www.nedo.go.jp/english/archives/170117/pdf/H-17G_E.pdf , June 12, 2006.
23. Cosneanu, C., Metalurgia (Romania), No.10, 1966, p. 563-567
24. Keene, B.J., International Materials Reviews, 33:1, 1988, p. 2-37
25. Ravaglioli, A., Vincenzini, P., Krajewski, A., "Ceramic Coating: An Ancient Art with a Bright Future", Surface Engineering Volume I, p.303, Published by the Royal Society of Chemistry, 1993.
26. Richards, R.W., Clarke, H., and Goodwin, F.E., "The Relationship Between Steel Surface Chemistry and Galvanising Reactivity", Surface Engineering Volume I, p.265, Published by the Royal Society of Chemistry, 1993.

27. Thorpe, J.P., The British Foundryman, Vol. 10, 1950, p. 380-482
28. Svoboda, J.M., Geiger, G.H., AFS Transactions, Vol.77, 1969, p. 281
29. Chakraborty, M., Dhindaw, B.K., Kher, R., The British Foundryman, June 1986, p. 230
30. "Safety in Magnesium Die Casting", Hydro Magnesium Data Sheet., 2002
31. Metals Handbook, Ninth Edition, 1988, Vol. 15, ASM International, p. 800
32. Magnesium Die Casting Handbook, NADCA Publication, 1998, p.24
33. "Melting and Handling Magnesium for Die Casting", Hydro Magnesium Data Sheet, 1996.
34. "Non-Ferrous Foundryman's Handbook", Foseco , 1999, Chapter 15, p. 222
35. Ricketts, N.J., Cashion, S.P., " Hydrofluorocarbons as a Replacement for sulphur hexafluoride in magnesium processing", in J.N. Hryn (ed.), Magnesium Technology 2001, The Minerals, Metals and Materials Society, 2001, p. 31-36
36. http://www.hatch.ca/Light_Metals/Articles/Replacement_SF6_%20Magshield.pdf , 12 June, 2006
37. http://www.kballoys.com/Products/Chemicals___Fluxes/Potassium_Fluoborate/potassium_fluoborate.html , 12 June, 2006
38. Private communication with Bob Brown, Remet UK, Ltd., 8 June 2004
39. Private communication with John W. Townsend, Stone Foundries Ltd, 2 June 2005
40. Idris, M.H., Clegg, A.J., "Processing and Evaluation of Investment Cast Magnesium- Base Alloy", AFS Transactions, 96-80, 1996, p. 237-244
41. Kim, S., Kim, M., Hong, T., Kim, H., and Kim, Y. "Investment Casting of AZ91HP Magnesium Alloy", Metals and Materials, Vol.6, No.3 ,2000, p. 275-279
42. Kim, S., Kim, T., Kim, Y. "Evaluation of Thermal Stability of Mold Materials for Magnesium Investment Casting", Materials Transactions, Vol. 42, No.3, 2001, p. 539-542
43. Kim, S.K. and Kim, Y. "Process Improvement and Mold Development for Mg Investment Casting", Proceedings of the 65th World Foundry Congress, Gyeongyu, Korea, 2002
44. Kim, S.K., Kim, J.I. and Kim, Y. "Rotating Cylinder Manufacturing Method and Investment Casting of SiC/AZ91HP Magnesium Composites", Materials Science and Technology, July-August 2000, Vol. 16, p. 769
45. "Refractory Ceramics" in Ullmann's Encyclopedia of Industrial Chemistry, John Wiley & Sons, Inc. 2004.
46. Zhang, Z., Morin, G., "Effect of Inhibitor Gas on Mold-Magnesium Reactions in Investment Castings", Magnesium Technology 2004, TMS, p. 197-202.

47. Zhang, Z., Turcotte, C, and Morin, G.,"Magnesium Investment Casting and Mould-Magnesium Reactions", Proc. Materials Week, September 30-2 October 2002, Munich, Germany,
48. Clegg, A.J., "Precision Casting Processes", 1991, Pergamon Press, 293p.
49. Metals Handbook, 8th Edition, 1970, Vol. 5, ASM International, p. 437
50. Private communication with Dr. Konrad Weiss and Dr. Achim Wendt, RWP GmbH, 3 September 2004.
51. http://www.morita-kagaku.co.jp/products/Fluoroborate/KBF4.htm ,12 June, 2006
52. "Ceramic Test Procedures", A Publication by Investment Casting Institute, Dallas, TX, USA, 1979.
53. Private communication with Malcolm Brown, Minco Ltd, 27 May 2004 and 3 June 2004
54. Peters, F., Voigt, R., Blair, M., "Dimensional Repeatability of Investment Castings", Incast, July 1977, No. 7, p. 7-11
55. Rosenthal, H. "Shrink Allowance for Pattern Dies in Investment Casting", 27th Annual Meeting of the Investment Casting Institute ,1979.
56. Snow, J., Scott, D.H., "Comparing Fused Silica and Alumino-Silicate Investment Refractories", Incast, April 2001, p. 24-27
57. Snow, J.D.; " How the Shell Affects Casting Dimensions", 43rd Annual Technical Meeting of the Investment Casting Institute", 1995
58. Metals Handbook, 8th Edition, 1970, Vol. 5, ASM International, p. 192.
59. Cingi, C., Vuorinen, J.J., "Countergravity Casting in Flexible Casting Bags", Proceedings of 9th World Conference on Investment Casting ,1996, 14:1- 14:9
60. Phase Diagrams for Binary Alloys, ASM International, 2000, p. 551 and p. 430.
61. Lyon, P., Jeal, N., "Magnesium Prototyping-Investing in a Lightweight Solution", 13th Magnesium Automative and End User Seminar, September 22-23, 2005, Germany.

APPENDIX A 1/15. FIGURES FOR THE COMPARISON OF REFRACTORIES

Figure 53. Digital pictures for Table 5, Casting#1. Alumina-Zircon-Molochite-F.Silica. Left: Pictures with gray shades, Right: Grey shades removed. Each row represents one face of the rectangular samples. Numbers under each picture are quality index value measured by the image analyzer.

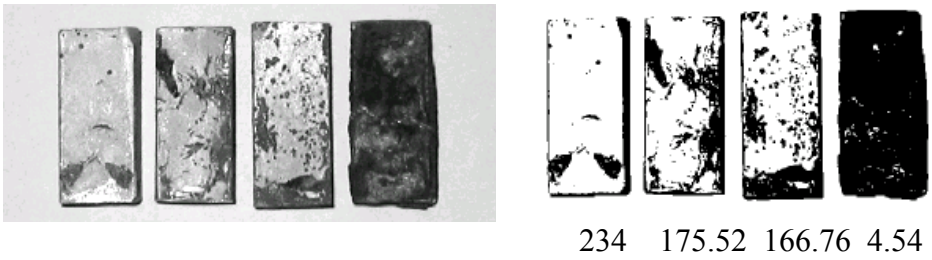

234 175.52 166.76 4.54

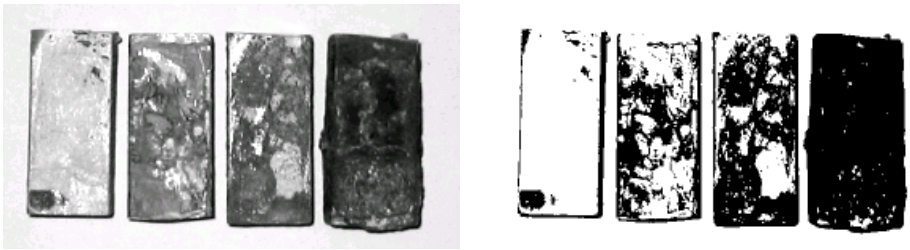

241.13 144.67 86.05 6.99

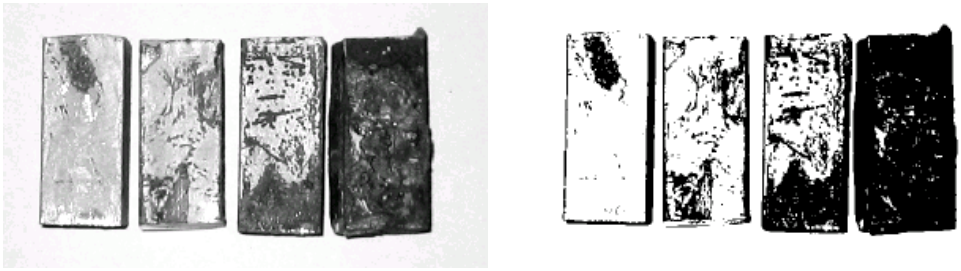

231.6 195.34 124.57 12.35

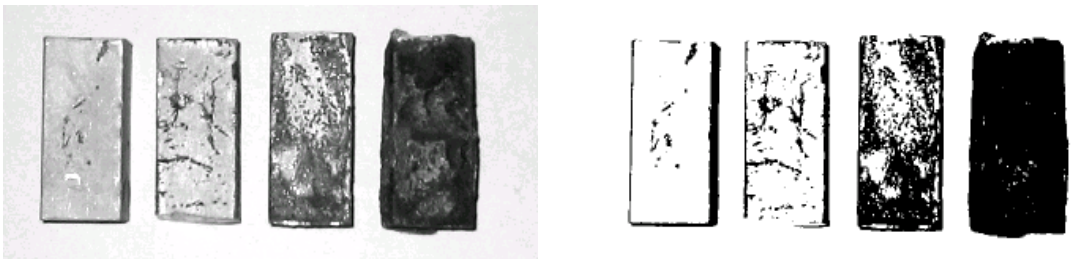

249.07 228.1 102.81 1.92

APPENDIX A 2/15. FIGURES FOR THE COMPARISON OF REFRACTORIES

Figure 54. Digital pictures for Table 5, Casting#2. Alumina-Zircon-Molochite-F.Silica. Left: Pictures with gray shades, Right: Grey shades removed. Each row represents one face of the rectangular samples. Numbers under each picture are quality index value measured by the image analyzer.

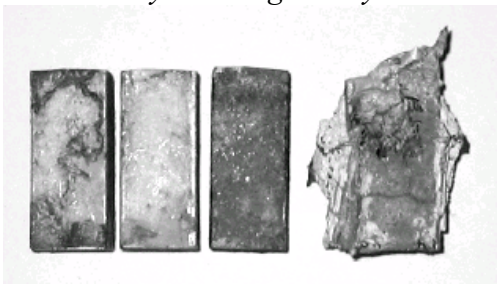

152.83 235.62 17.73 0

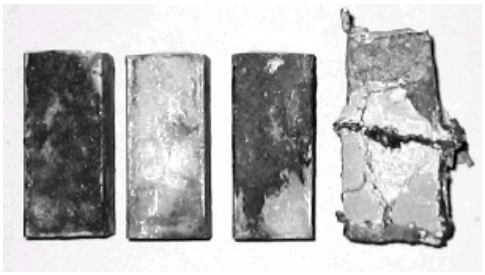

14.99 223.28 65.23 0

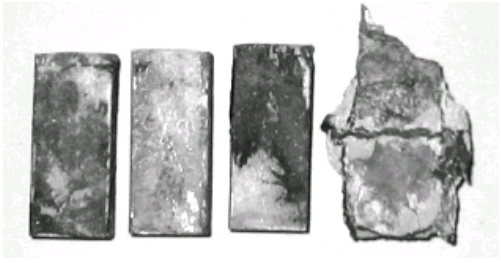

61.55 228.6 74.34 0

50.85 168.6 24.64 0

APPENDIX A 3/15. FIGURES FOR THE COMPARISON OF REFRACTORIES

Figure 55. Digital pictures for Table 6, Casting#1. Alumina-Zircon-Alumina-Zircon. Left: Pictures with gray shades, Right: Grey shades removed. Each row represents one face of the rectangular samples. Numbers under each picture are quality index value measured by the image analyzer.

240.07 191.04 218.54 224.47

241.89 207.58 194.30 231.02

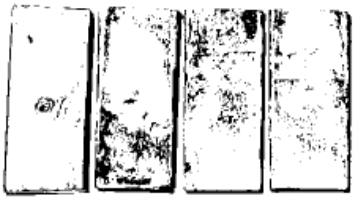

249.20 210.89 220.04 238.12

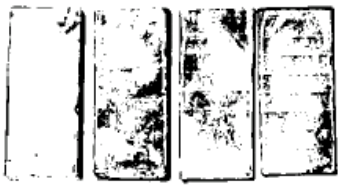

249.91 201.08 210.59 214.38

APPENDIX A 4/15. FIGURES FOR THE COMPARISON OF REFRACTORIES

Figure 56. Digital pictures for Table 7, Casting#1. Alumina-Zircon-Alumina-Zircon Left: Pictures with gray shades, Right: Grey shades removed. Each row represents one face of the rectangular samples. Numbers under each picture are quality index value measured by the image analyzer.

245.6 238.3 179.6 200.8

247.2 227.9 235.3 172.5

232 218.6 220.4 224.2

245.3 239.8 143.8 237.2

APPENDIX A 5/15. FIGURES FOR THE COMPARISON OF REFRACTORIES

Figure 57. Digital pictures for Table 8, Casting#1. Alumina-Molochit-Magnesia-Magnesia. Left: Pictures with gray shades, Right: Grey shades removed. Each row represents one face of the rectangular samples. Numbers under each picture are quality index value measured by the image analyzer.

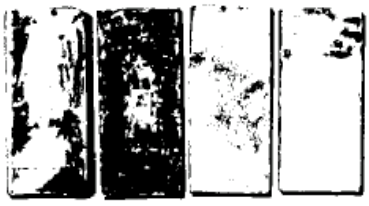

176.76 41.13 238.41 240.90

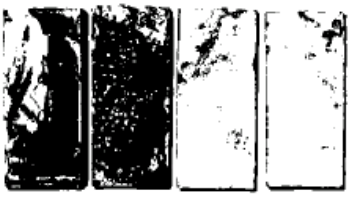

74.06 34.43 236.98 245.60

122.74 66.67 241.68 223.50

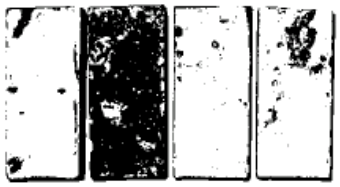

238.03 32.26 248.38 226.40

APPENDIX A 6/15. FIGURES FOR THE COMPARISON OF REFRACTORIES

Figure 58. Digital pictures for Table 8, Casting#2. Magnesia-Magnesia-Alumina-Molochite. Left: Pictures with gray shades, Right: Grey shades removed. Each row represents one face of the rectangular samples. Numbers under each picture are quality index value measured by the image analyzer.

253.02 254.83 236.29 134.06

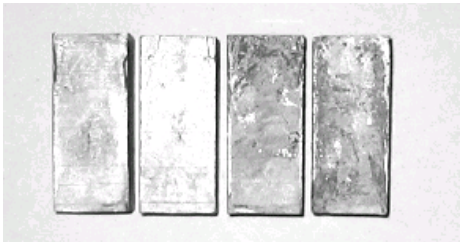

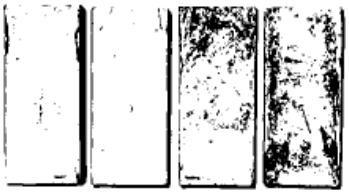

253.04 253.58 209.19 179.27

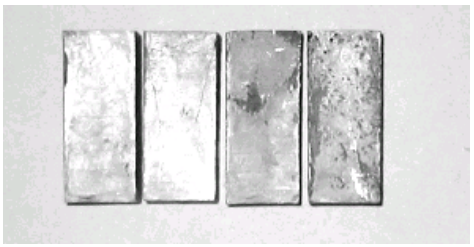

252.93 254.55 229.21 193.54

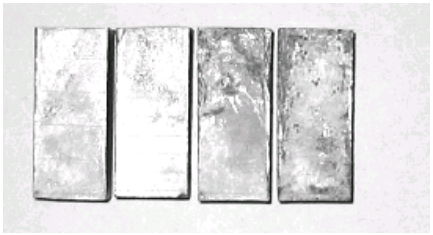

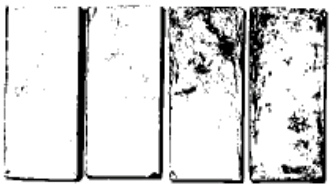

254.17 253.09 213.57 197.97

APPENDIX A 7/15. FIGURES FOR THE COMPARISON OF REFRACTORIES

Figure 59. Digital pictures for Table 9, Casting#1. Magnesia-Zirconia-Zirconia-F.Silica. Left: Pictures with gray shades, Right: Grey shades removed. Each row represents one face of the rectangular samples. Numbers under each picture are quality index value measured by the image analyzer.

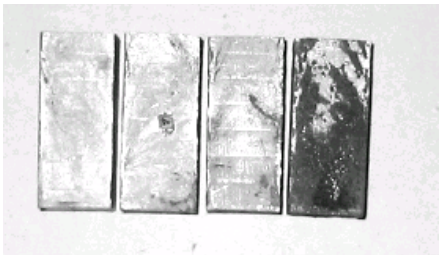

250.93 244.91 237.75 55.66

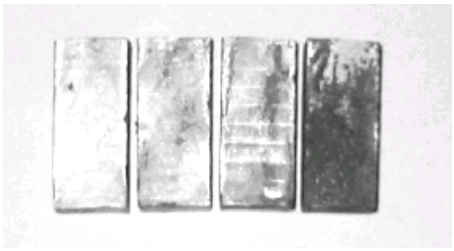

254.33 249.56 211.77 37.45

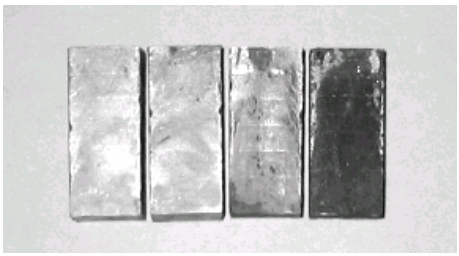

254.77 252.22 222.76 22.88

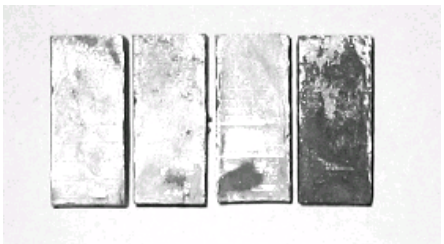

247.95 247.88 229.05 48.15

APPENDIX A 8/15. FIGURES FOR THE COMPARISON OF REFRACTORIES

Figure 60. Digital pictures for Table 9, Casting#2. Magnesia-Zirconia-Zirconia-F.Silica. Left: Pictures with gray shades, Right: Grey shades removed. Each row represents one face of the rectangular samples. Numbers under each picture are quality index value measured by the image analyzer.

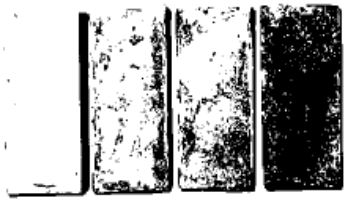

252.75 202.82 174.93 25.64

245.42 185.50 179.48 20.56

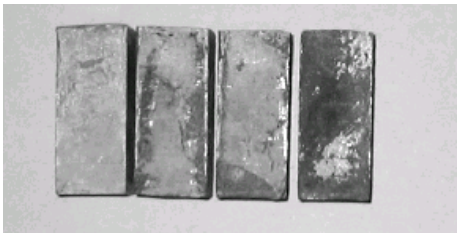

252.42 179.77 197.21 58.73

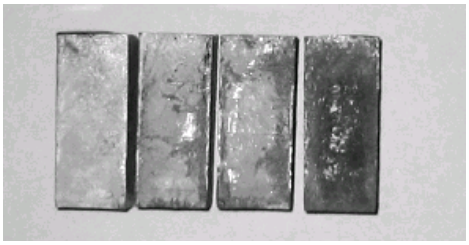

250.75 203.23 175.45 23.93

APPENDIX A 9/15. FIGURES FOR THE COMPARISON OF REFRACTORIES

Figure 61. Digital pictures for Table 10, Casting#1. Alumina-Molochite-Yttria-Zirconia. Left: Pictures with gray shades, Right: Grey shades removed. Each row represents one face of the rectangular samples. Numbers under each picture are quality index value measured by the image analyzer.

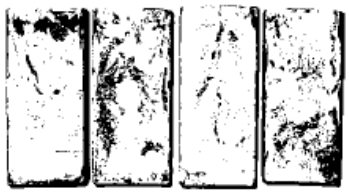

224.67 200.67 241.13 204.86

230.44 189.97 249.54 169.68

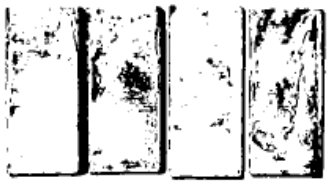

241.88 214.52 248.76 193.74

239.05 203.49 250.45 175.16

APPENDIX A 10/15. FIGURES FOR THE COMPARISON OF REFRACTORIES

Figure 62. Digital pictures for Table 10, Casting#2. Alumina-Molochite-Yttria-Zirconia. Left: Pictures with gray shades, Right: Grey shades removed. Each row represents one face of the rectangular samples. Numbers under each picture are quality index value measured by the image analyzer.

211.07 65.01 247.42 208.94

219.67 148.12 241.48 233.46

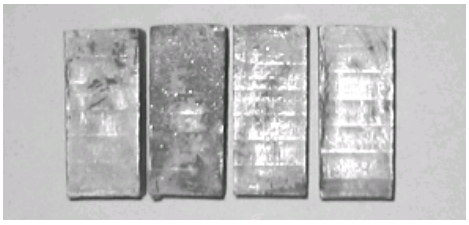

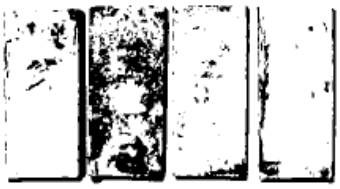

233.22 134.45 240.36 237.44

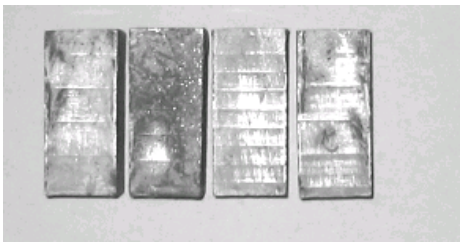

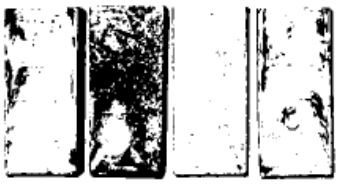

224.72 93.18 252.08 225.37

APPENDIX A 11/15. FIGURES FOR THE COMPARISON OF REFRACTORIES

Figure 63. Digital pictures for Table 11, Casting#1. Magnesia-Molochite-F.Silica. Left: Pictures with gray shades, Right: Grey shades removed. Each row represents one face of the rectangular samples. Numbers under each picture are quality index value measured by the image analyzer.

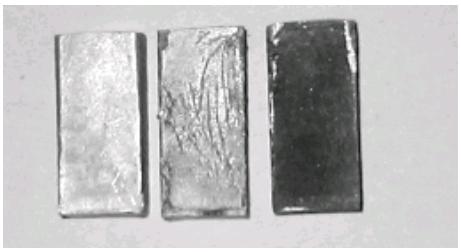

251.5 220.78 10.22

254 221 21

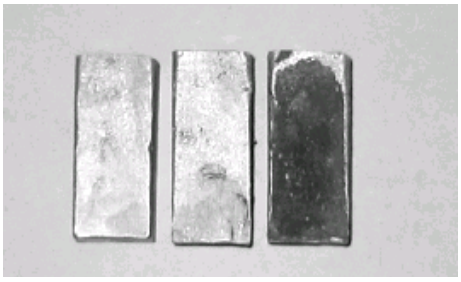

254 244 23

254 233 21

APPENDIX A 12/15. FIGURES FOR THE COMPARISON OF REFRACTORIES

Figure 64. Digital pictures for Table 12, Casting#1. Alumina-Magnesia-Molochite-F.Silica-Yttria-Zircon-Zirconia. Left: Pictures with gray shades, Right: Grey shades removed. Each row represents one face of the rectangular samples. Numbers under each picture are quality index value measured by the image analyzer.

227.6 253.2 219.7

226.08 222.47 60.18

222.98 255 219.36

238.32 188.1 34.93

217.45 254.89 200.28

240.58 214.07 41.38

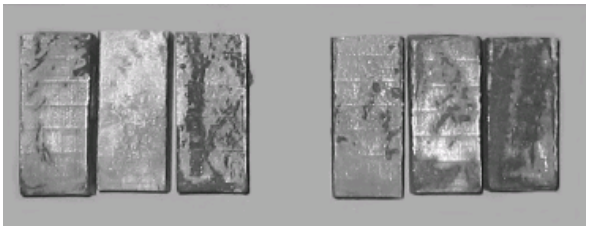

232.72 253.76 155.15

234.44 192.84 56.27

APPENDIX A 13/15. FIGURES FOR THE COMPARISON OF REFRACTORIES

Figure 65. Digital pictures for Table 12, Casting#2. Alumina-Magnesia-Molochite-F.Silica-Yttria-Zircon-Zirconia. Left: Pictures with gray shades, Right: Grey shades removed. Each row represents one face of the rectangular samples. Numbers under each picture are quality index value measured by the image analyzer.

235.13 252.59 125.30 0 252.28 205.36 183.61

227.30 254.31 116.40 0 249.91 233.86 162.79

227.9 253.6 120.34 0 250.68 233.65 96.5

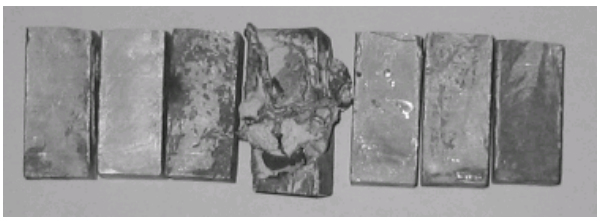

228.61 255 151.35 0 252.73 239.21 60.19

APPENDIX A 14/15. FIGURES FOR THE COMPARISON OF REFRACTORIES

Figure 66. Digital pictures for Table 12, Casting#3. Alumina-Magnesia-Molochite-F.Silica-Yttria-Zircon-Zirconia. Left: Pictures with gray shades, Right: Grey shades removed. Each row represents one face of the rectangular samples. Numbers under each picture are quality index value measured by the image analyzer.

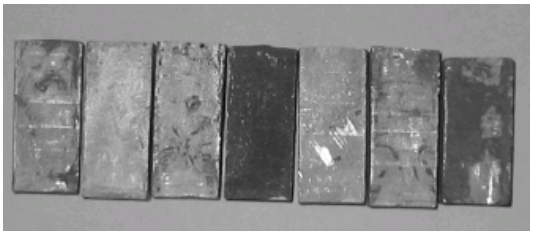

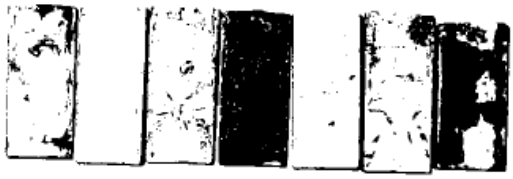

223.96 254.41 240.37 5.51 253.46 224.23 67.34

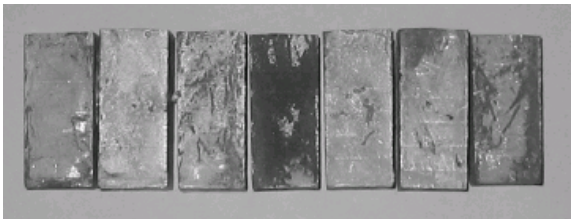

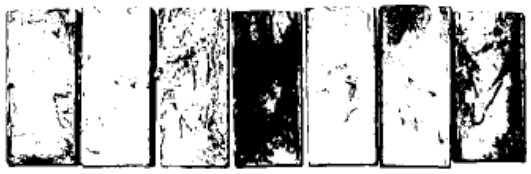

226.37 252.92 211.80 31.83 249.79 222.6 131.94

198.26 249.91 237.26 24.07 251.11 248.41 40.12

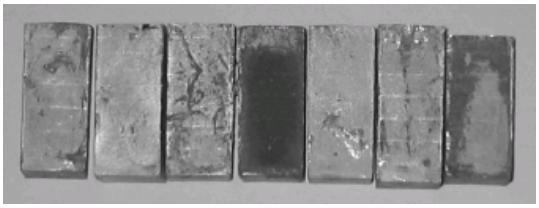

224.02 251.37 219.35 20.38 251.21 236.63 129.63

APPENDIX A 15/15. FIGURES FOR THE COMPARISON OF REFRACTORIES

Figure 67. Digital pictures for Table 12, Casting#4. Alumina-Magnesia-Molochite-F.Silica-Yttria-Molochite-Zircon. Left: Pictures with gray shades, Right: Grey shades removed. Each row represents one face of the rectangular samples. Numbers under each picture are quality index value measured by the image analyzer.

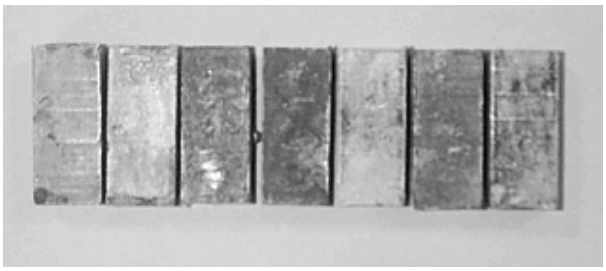

240.6 246 107.8 24.08 240.8 34.3 120.12

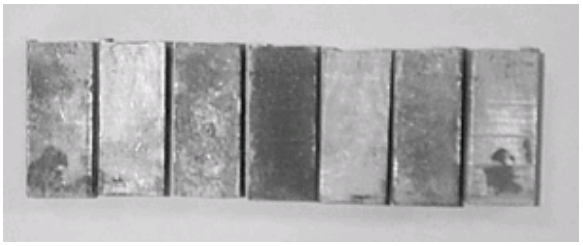

171.83 251.34 175.97 4.13 243.74 67.65 212.41

178.69 253.67 178.81 26.41 252.62 79.77 247.83

202.93 254.17 222.62 28.38 245.95 204.46 187.91

APPENDIX B 1/18. FIGURES FOR REVEALING THE INFLUENCE OF INHIBITORS AND THE INFLUENCE OF EXTERNAL OXYGEN

Figure 68. Digital pictures for Table 18, Casting#1. Influence of KBF_4. Left: Pictures with grey shades, Right: Grey shades removed. Each row represents one face of the rectangular samples. Numbers under each picture are quality index value measured by the image analyzer.

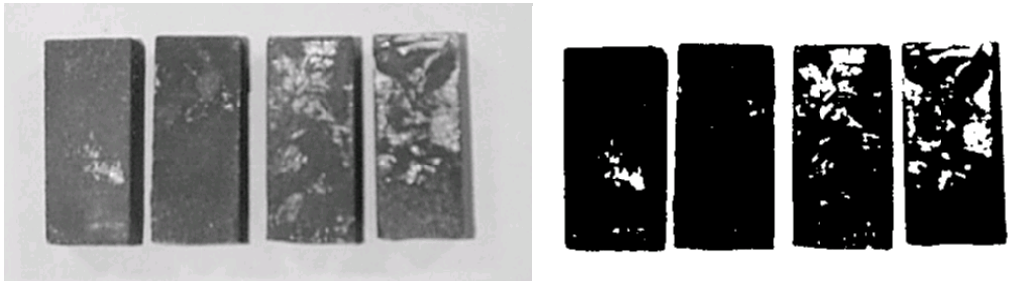

Left two: Without KBF_4: 7.72; 1.25
Right two: Buried in KBF_4: 30.86; 44.52

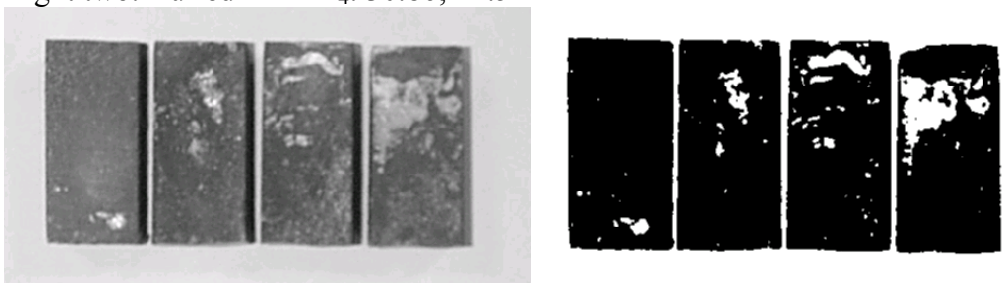

Left two: Without KBF_4: 4.67; 9.75
Right two: Buried in KBF_4: 17.37; 39.65

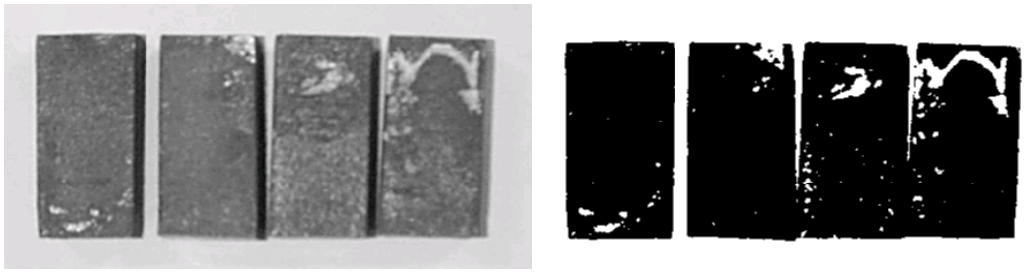

Left two without KBF_4: 4.87; 6.87
Right two: Buried in KBF_{44}: 11.88; 26.08

Left two: Without KBF_4: 8.06; 15.94
Right two: Buried in KBF_4: 25.15; 62.75

APPENDIX B 2/18. FIGURES FOR REVEALING THE INFLUENCE OF INHIBITORS AND THE INFLUENCE OF EXTERNAL OXYGEN

Figure 69. Digital pictures for Table 18, Casting#2. Influence of KBF_4. Left:Pictures with grey shades, Right: Grey shades removed. Each row represents one face of the rectangular samples. Numbers under each picture are quality index value measured by the image analyzer.

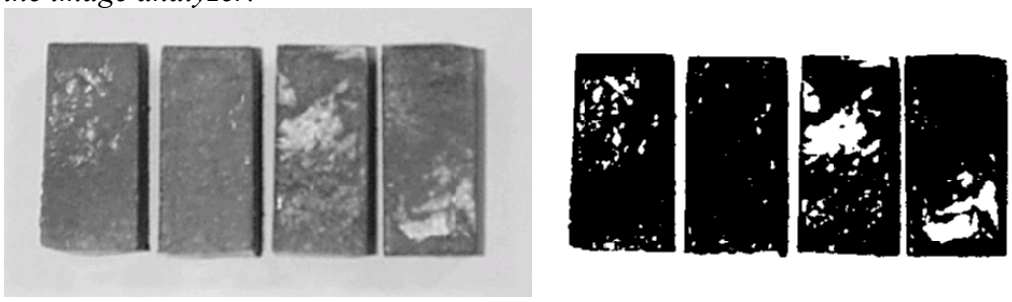

Left two: Without KBF_4: 18.08; 3.74
Right two: Buried in KBF_4: 48.36; 30.43

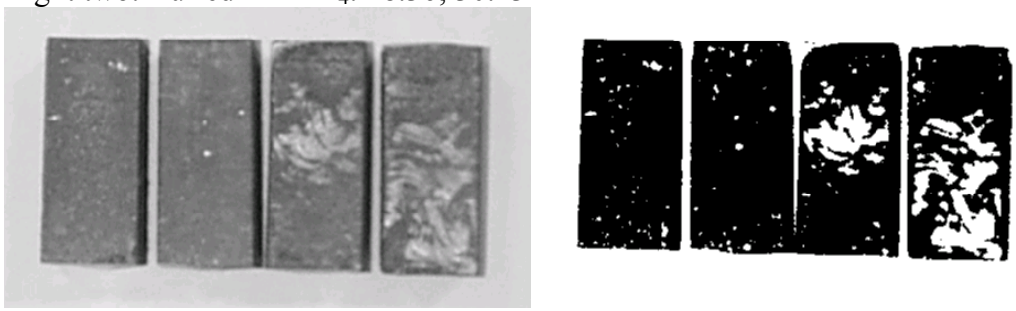

Left two: Without KBF_4: 6.17; 7.51
Right two: Buried in KBF_4: 40.70; 72.50

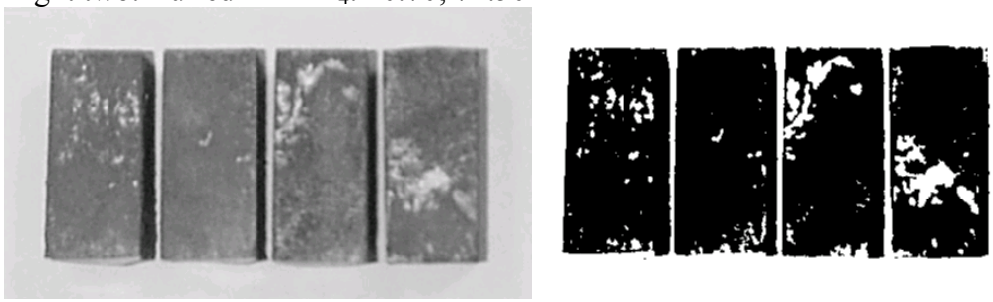

Left two: Without KBF_4: 17.89; 11.15
Right two: Buried in KBF_4: 26.81; 34.26

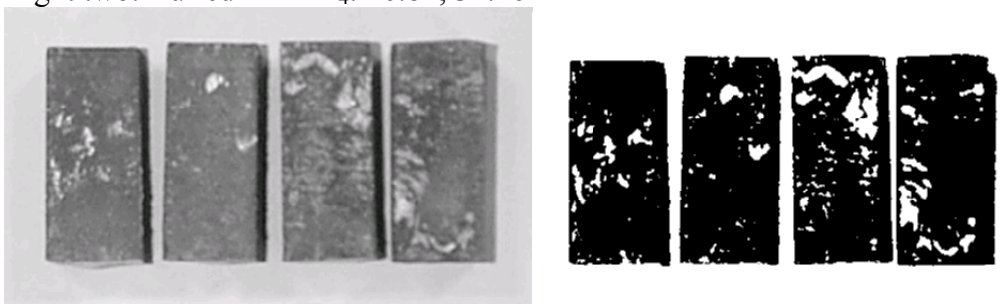

Left two: Without KBF_4: 20.28; 16.93
Right two: Buried in KBF_4: 41.47; 27.53

APPENDIX B 3/18. FIGURES FOR REVEALING THE INFLUENCE OF INHIBITORS AND THE INFLUENCE OF EXTERNAL OXYGEN

Figure 70. Digital pictures for Table 19, Casting#1. Influence of Croning sand. Left:Pictures with grey shades, Right: Grey shades removed. Each set of pictures represents one face of the rectangular samples. Numbers under each picture are quality index value measured by the image analyzer.

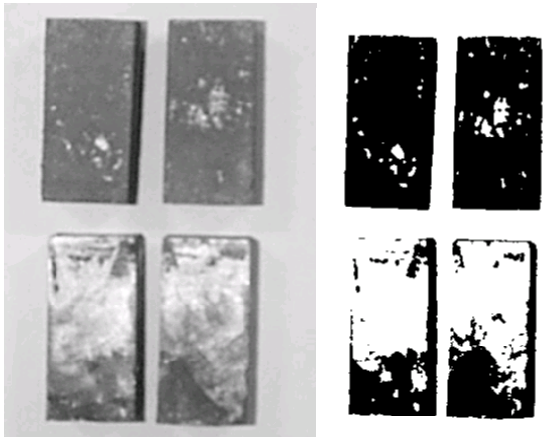

Upper two: Nothing around the shell: 10.09 ; 15.11
Lower two: Buried in Croning sand: 157.97; 161.05

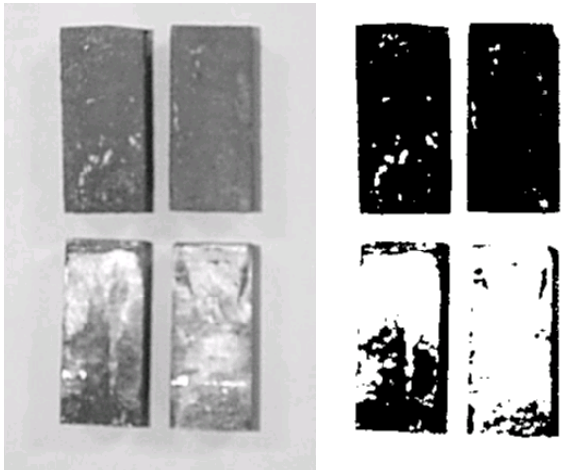

Upper two: Nothing around the shell: 10.22; 4.14
Lower two: Buried in Croning sand: 133.90; 225.1

APPENDIX B 4/18. FIGURES FOR REVEALING THE INFLUENCE OF INHIBITORS AND THE INFLUENCE OF EXTERNAL OXYGEN

Figure 70(continues). Digital pictures for Table 19, Casting#1. Influence of Croning sand. Left:Pictures with grey shades, Right: Grey shades removed. Each set of pictures represents one face of the rectangular samples. Numbers under each picture are quality index value measured by the image analyzer.

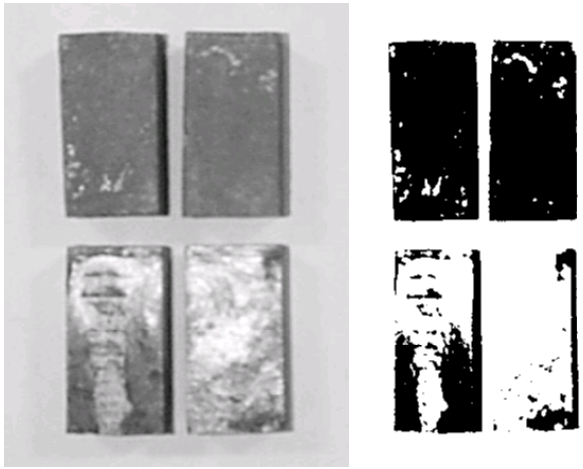

Upper two: Nothing around the shell: 10.18; 8.86
Lower two: Buried in Croning sand: 136.29; 217.96

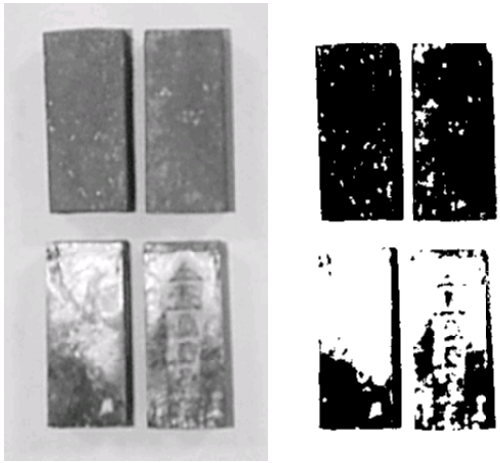

Upper two: Nothing around the shell: 9.52; 20.55
Lower two: Buried in Croning sand: 165.03; 164.83

APPENDIX B 5/18. FIGURES FOR REVEALING THE INFLUENCE OF INHIBITORS AND THE INFLUENCE OF EXTERNAL OXYGEN

Figure 71. Digital pictures for Table 19, Casting#2. Influence of Croning sand. Each set of pictures represents one face of the rectangular samples. Left:Pictures with grey shades, Right: Grey shades removed.Numbers under each picture are quality index value measured by the image analyzer.

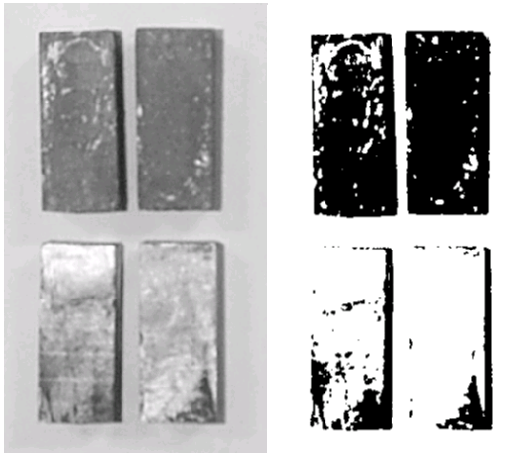

Upper two: Nothing around the shell: 46.31; 12.25
Lower two: Buried in Croning sand: 199.98; 223

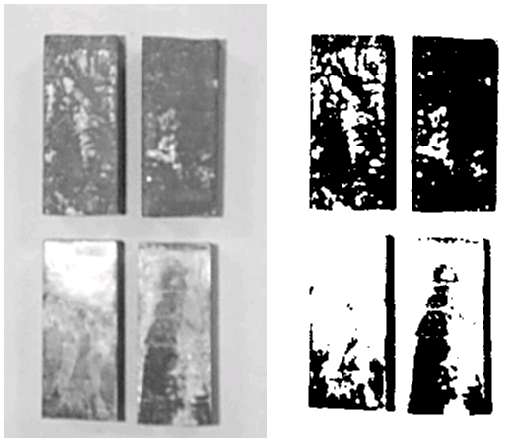

Upper two: Nothing around the shell: 74.74; 23.62
Lower two: Buried in Croning sand: 197.66; 156.78

APPENDIX B 6/18. FIGURES FOR REVEALING THE INFLUENCE OF INHIBITORS AND THE INFLUENCE OF EXTERNAL OXYGEN

Figure 71(continues). Digital pictures for Table 19, Casting#2. Influence of Croning sand. Each set of pictures represents one face of the rectangular samples. Left:Pictures with grey shades, Right: Grey shades removed.Numbers under each picture are quality index value measured by the image analyzer.

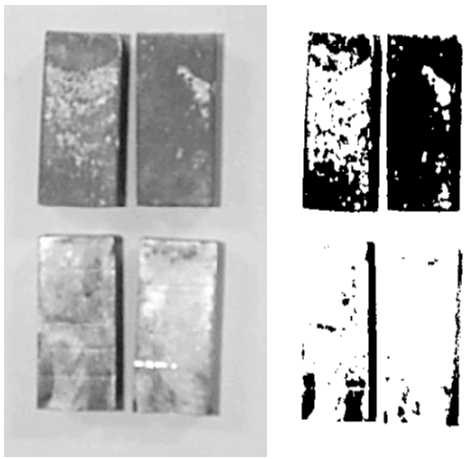

Upper two: Nothing around the shell: 139.32; 23.49
Lower two: Buried in Croning sand: 212.13; 242.32

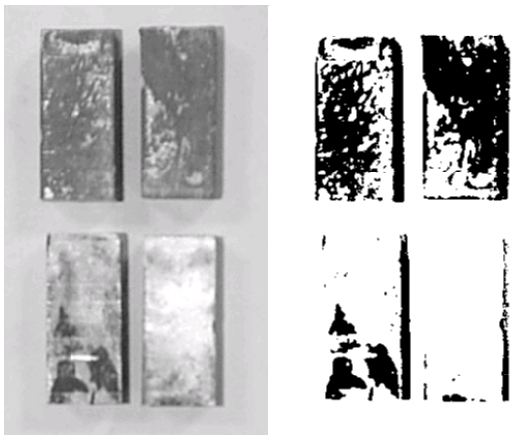

Upper two: Nothing around the shell: 114.49; 84.52
Lower two: Buried in Croning sand: 197.17; 243.71

APPENDIX B 7/18. FIGURES FOR REVEALING THE INFLUENCE OF INHIBITORS AND THE INFLUENCE OF EXTERNAL OXYGEN

Figure 72. Digital pictures for Table 19, Casting#3. Influence of Croning sand. Each set of pictures represents one face of the rectangular samples. Left:Pictures with grey shades, Right: Grey shades removed. Numbers under each picture are quality index value measured by the image analyzer.

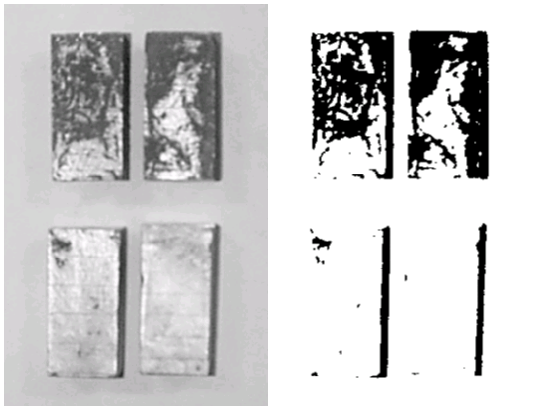

Upper two: Nothing around the shell: 114.1; 96.16
Lower two: Buried in Croning sand: 237.07; 243.29

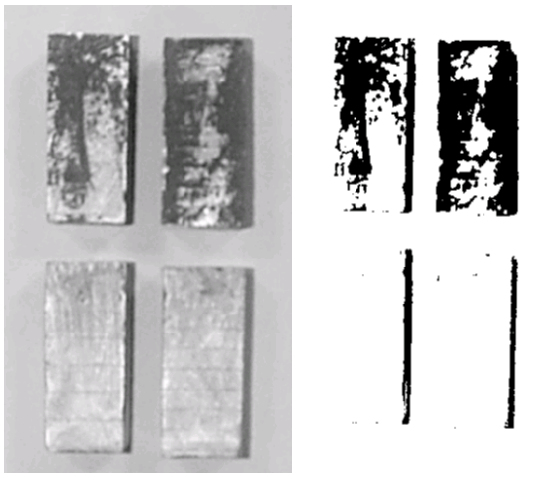

Upper two: Nothing around the shell: 142.36; 78.39
Lower two: Buried in Croning sand: 251.3; 253.83

APPENDIX B 8/18. FIGURES FOR REVEALING THE INFLUENCE OF INHIBITORS AND THE INFLUENCE OF EXTERNAL OXYGEN

Figure 72(continues). Digital pictures for Table 19, Casting#3. Influence of Croning sand. Each set of pictures represents one face of the rectangular samples. Left:Pictures with grey shades, Right: Grey shades removed.Numbers under each picture are quality index value measured by the image analyzer.

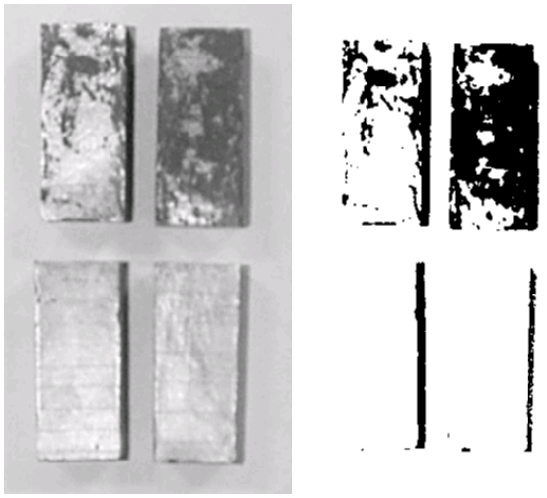

Upper two: Nothing around the shell: 192.82; 62.76
Lower two: Buried in Croning sand: 247.9; 252.06

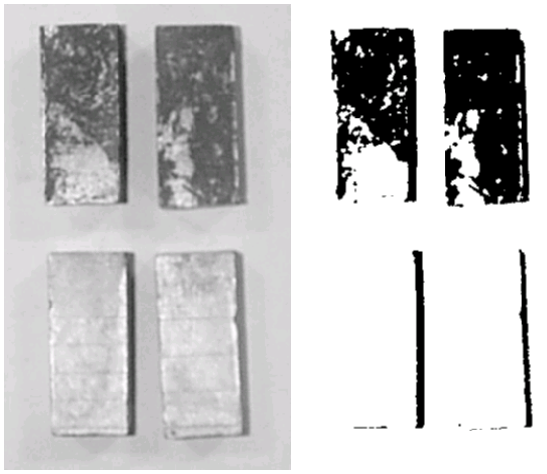

Upper two: Nothing around the shell: 90.41; 52.61
Lower two: Buried in Croning sand: 244.04; 250.54

APPENDIX B 9/18. FIGURES FOR REVEALING THE INFLUENCE OF INHIBITORS AND THE INFLUENCE OF EXTERNAL OXYGEN

Figure 73. Digital pictures for Table 20, Casting#1. Influence of $NaBF_4$. Each set of pictures represents one face of the rectangular samples. Left:Pictures with grey shades, Right: Grey shades removed.Numbers under each picture are quality index value measured by the image analyzer.

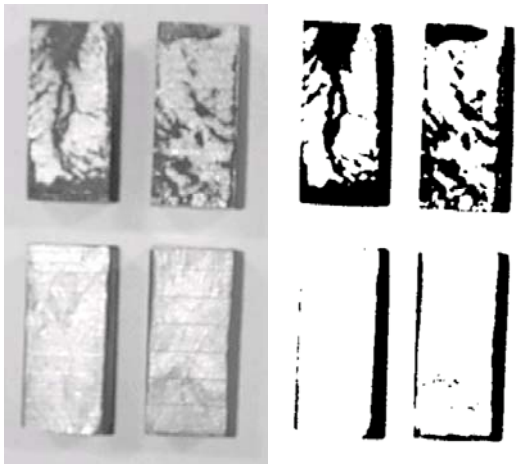

Upper two: Not dipped: 141.08; 158.55
Lower two: Dipped in $NaBF_4$: 250.81; 247.75

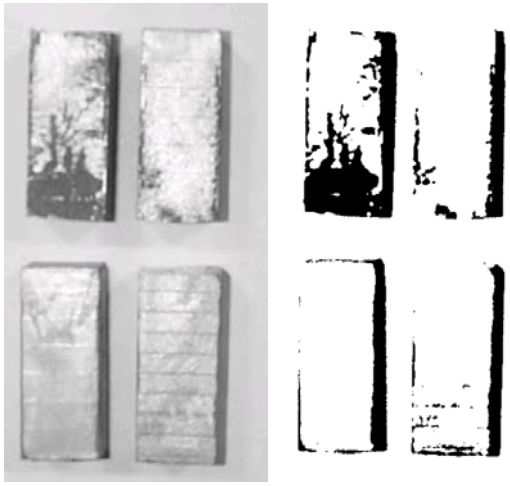

Upper two: Not dipped: 154.72; 237.33
Lower two: Dipped in $NaBF_4$: 249.91; 244.95

APPENDIX B 10/18. FIGURES FOR REVEALING THE INFLUENCE OF INHIBITORS AND THE INFLUENCE OF EXTERNAL OXYGEN

Figure 73(continues). Digital pictures for Table 20, Casting#1. Influence of $NaBF_4$. Each set of pictures represents one face of the rectangular samples. Left:Pictures with grey shades, Right: Grey shades removed.Numbers under each picture are quality index value measured by the image analyzer.

Upper two: Not dipped: 100.88; 164.95
Lower two: Dipped in $NaBF_4$: 250.50; 216.52

Upper two: Not dipped: 136.65; 34.09
Lower two: Dipped in $NaBF_4$: 250.51; 239.06

APPENDIX B 11/18. FIGURES FOR REVEALING THE INFLUENCE OF INHIBITORS AND THE INFLUENCE OF EXTERNAL OXYGEN

Figure 74. Digital pictures for Table 20, Casting#2. Influence of $NaBF_4$. Each set of pictures represents one face of the rectangular samples. Left:Pictures with grey shades, Right: Grey shades removed.Numbers under each picture are quality index value measured by the image analyzer.

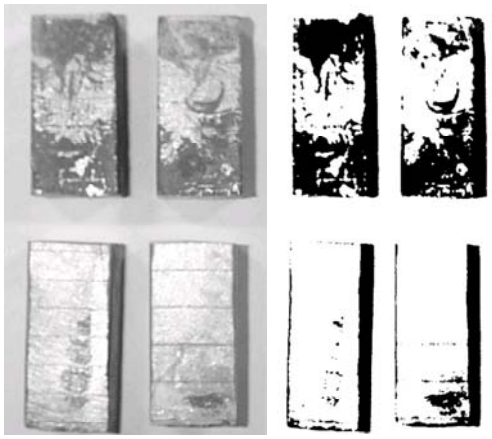

Upper two: Not dipped: 107.07; 142.87
Lower two: Dipped in $NaBF_4$: 246.41; 234.52

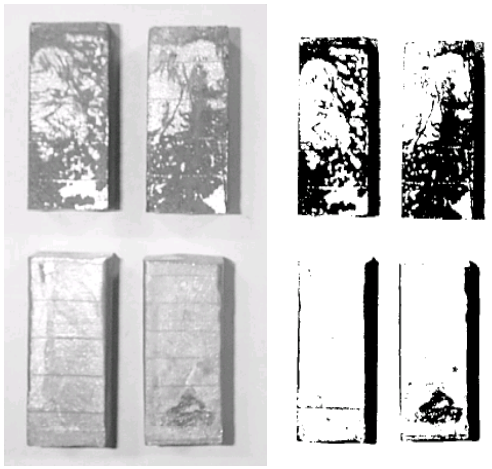

Upper two: Not dipped: 146.03; 126.84
Lower two: Dipped in $NaBF_4$: 250.86; 233.38

APPENDIX B 12/18. FIGURES FOR REVEALING THE INFLUENCE OF INHIBITORS AND THE INFLUENCE OF EXTERNAL OXYGEN

Figure 74(continues). Digital pictures for Table 20, Casting#2. Influence of $NaBF_4$. Each set of pictures represents one face of the rectangular samples. Left:Pictures with grey shades, Right: Grey shades removed.Numbers under each picture are quality index value measured by the image analyzer.

Upper two: Not dipped: 97.84; 89.87
Lower two: Dipped in $NaBF_4$: 251.69; 253.94

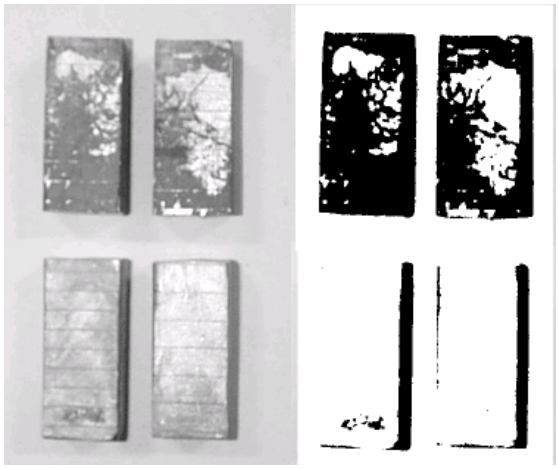

Upper two: Not dipped: 41.81; 92.13
Lower two: Dipped in $NaBF_4$: 249.33; 252.09

APPENDIX B 13/18. FIGURES FOR REVEALING THE INFLUENCE OF INHIBITORS AND THE INFLUENCE OF EXTERNAL OXYGEN

Figure 75. Digital pictures for Table 20, Casting#3. Influence of $NaBF_4$. Each set of pictures represents one face of the rectangular samples. Left:Pictures with grey shades, Right: Grey shades removed. Numbers under each picture are quality index value measured by the image analyzer.

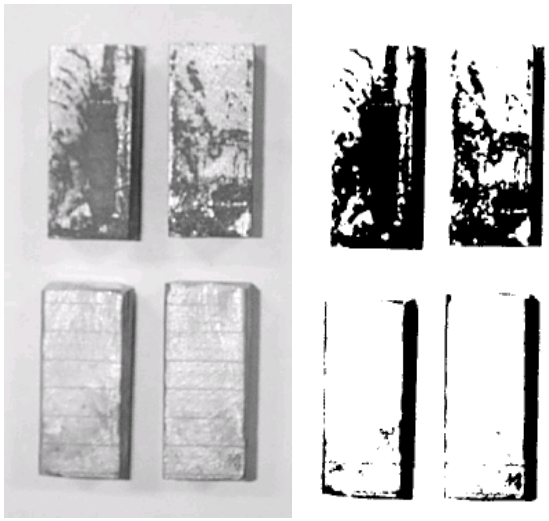

Upper two: Not dipped: 89.78; 138.38
Lower two: Dipped in $NaBF_4$: 244.67; 247.32

Upper two: Not dipped: 153.97; 188.29
Lower two: Dipped in $NaBF_4$: 244.99; 246.75

APPENDIX B 14/18. FIGURES FOR REVEALING THE INFLUENCE OF INHIBITORS AND THE INFLUENCE OF EXTERNAL OXYGEN

Figure 75(continues). Digital pictures for Table 20, Casting#3. Influence of $NaBF_4$. Each set of pictures represents one face of the rectangular samples. Left:Pictures with grey shades, Right: Grey shades removed. Numbers under each picture are quality index value measured by the image analyzer.

Upper two: Not dipped: 216.17; 207.51
Lower two: Dipped in $NaBF_4$: 251.81; 244.82

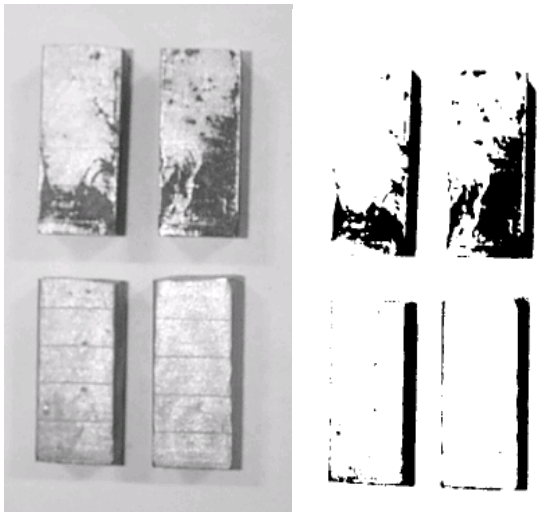

Upper two: Not dipped: 205.04; 157.01
Lower two: Dipped in $NaBF_4$: 251.69; 254.29

APPENDIX B 15/18. FIGURES FOR REVEALING THE INFLUENCE OF INHIBITORS AND THE INFLUENCE OF EXTERNAL OXYGEN

Figure 76. Digital pictures for Table 16, Casting#1. Influence of external oxygen. Each set of pictures represents one face of the rectangular samples. Left:Pictures with grey shades, Right: Grey shades removed. Numbers under each picture are quality index value measured by the image analyzer.

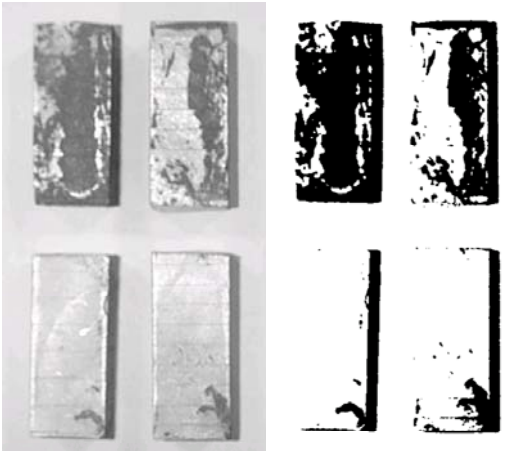

Upper two pieces: Nothing around the mold: 51.39; 145.34
Lower two pieces: Cast in a shell of reduced permeability: 245.10; 231.77

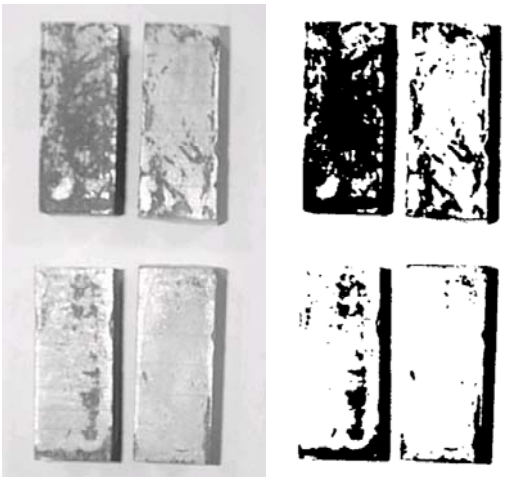

Upper two pieces: Nothing around the mold: 54.39; 191.37
Lower two pieces: Cast in a shell of reduced permeability: 213.09; 239.53

APPENDIX B 16/18. FIGURES FOR REVEALING THE INFLUENCE OF INHIBITORS AND THE INFLUENCE OF EXTERNAL OXYGEN

Figure 76(continues). Digital pictures for Table 16, Casting#1. Influence of external oxygen. Each set of pictures represents one face of the rectangular samples. Left:Pictures with grey shades, Right: Grey shades removed. Numbers under each picture are quality index value measured by the image analyzer.

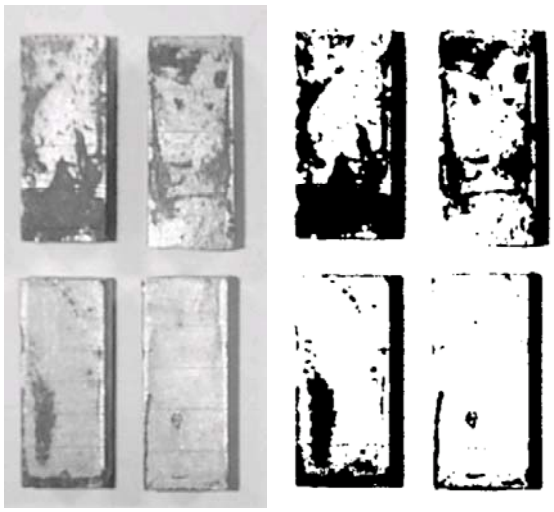

Upper two pieces: Nothing around the mold: 120.56; 162.51
Lower two pieces: Cast in a shell of reduced permeability: 198.29; 242.22

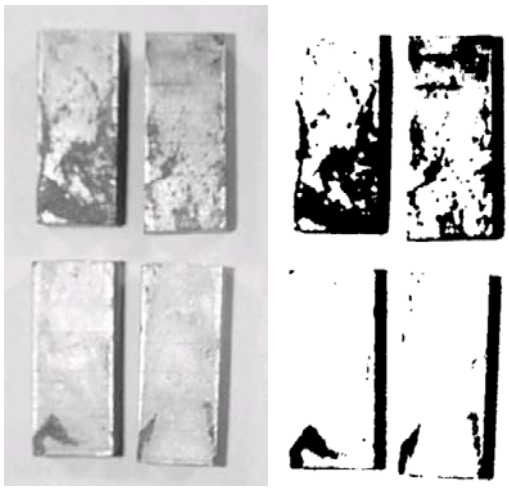

Upper two pieces: Nothing around the mold: 147.81; 173.03
Lower two pieces: Cast in a shell of reduced permeability: 237.40; 243.39

APPENDIX B 17/18. FIGURES FOR REVEALING THE INFLUENCE OF INHIBITORS AND THE INFLUENCE OF EXTERNAL OXYGEN

Figure 77. Digital pictures for Table 16, Casting#2. Influence of external oxygen. Each set of pictures represents one face of the rectangular samples. Left:Pictures with grey shades, Right: Grey shades removed. Numbers under each picture are quality index value measured by the image analyzer.

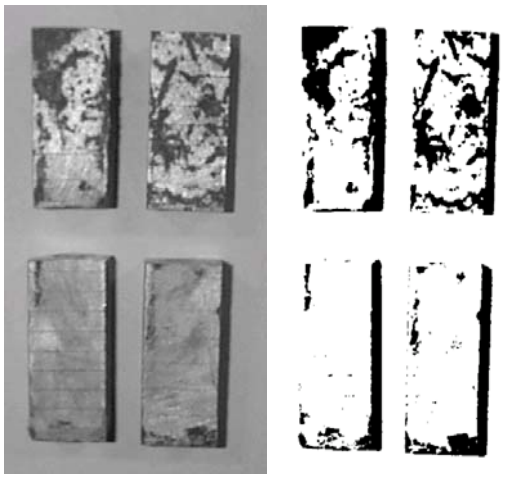

Upper two pieces: Nothing around the mold: 177.29; 171.50
Lower two pieces: Cast in a shell of reduced permeability: 238.25; 229.20

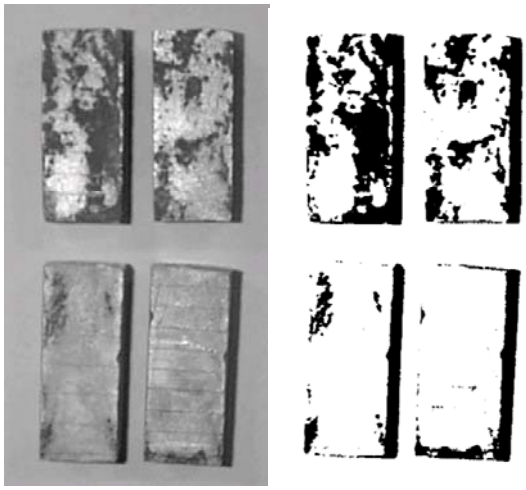

Upper two pieces: Nothing around the mold: 129.15; 183.41
Lower two pieces: Cast in a shell of reduced permeability: 233.16; 236.83

APPENDIX B 18/18. FIGURES FOR REVEALING THE INFLUENCE OF INHIBITORS AND THE INFLUENCE OF EXTERNAL OXYGEN

Figure 77(continues). Digital pictures for Table 16, Casting#2. Influence of external oxygen. Each set of pictures represents one face of the rectangular samples. Left:Pictures with grey shades, Right: Grey shades removed. Numbers under each picture are quality index value measured by the image analyzer

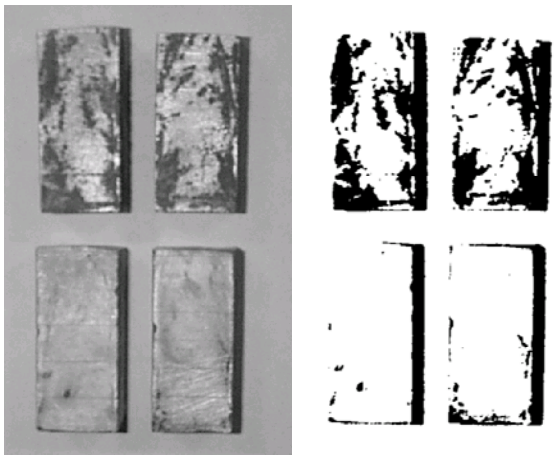

Upper two pieces: Nothing around the mold: 153.11; 155.39
Lower two pieces: Cast in a shell of reduced permeability: 250.98; 240.94

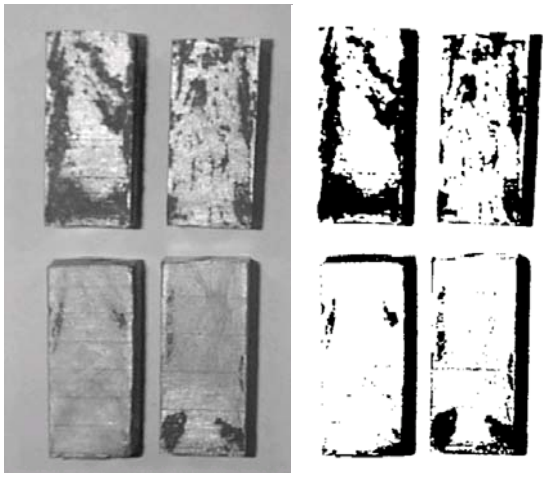

Upper two pieces: Nothing around the mold: 141.79; 187.82
Lower two pieces: Cast in a shell of reduced permeability: 238.83; 218.03

APPENDIX C 1/4. QUALITY INDEX MEASUREMENT BY USING IMAGE ANALYZER

1. All loose refractory material on cast pieces must be removed. For the removal of refractory material, light rubbing with wire brush/knife/sand paper and/or high pressure water jet can be used.
Sand blasting should be avoided as this damages the surface.

2. Digital pictures of the cast surfaces are taken. Surfaces to be compared must be flat and they must be photographed side by side together. The illumination should be about the same on all sides of the picture.

3. Then, in order to reduce errors, grey areas in each picture are removed.
For this purpose, Adobe Photoshop 5.0 Limited Edition was used in IDEA project as follows:

a. First remove the colors
Image→Mode→Grayscale →discard color information? OK→ Save.

b. Image→Adjust→Brightness/Contrast

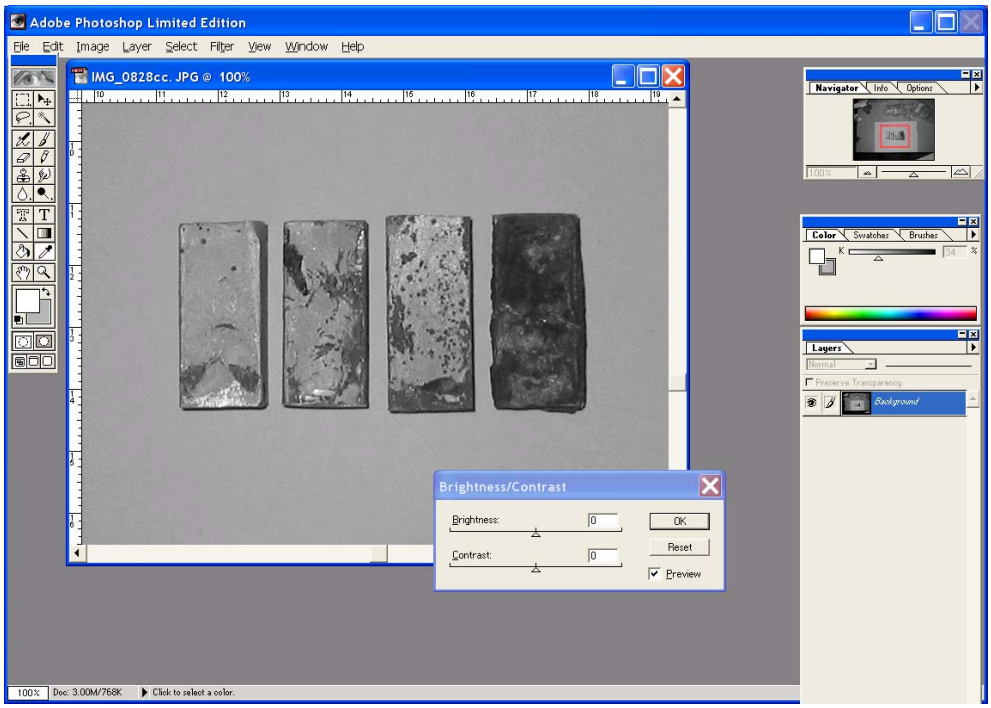

APPENDIX C 2/4. QUALITY INDEX MEASUREMENT BY USING IMAGE ANALYZER

c. Increase Contrast to +100%

d. Increase/Decrease Brightness slowly (preview on) until the picture obtained on the monitor screen is exactly the same as the actual cast piece. While doing this step, the cast pieces can be beside the monitor for comparison. All grey areas in the test pieces must be removed. Check also by comparison with the actual piece that the dark areas in the picture really are the reaction areas. Save.

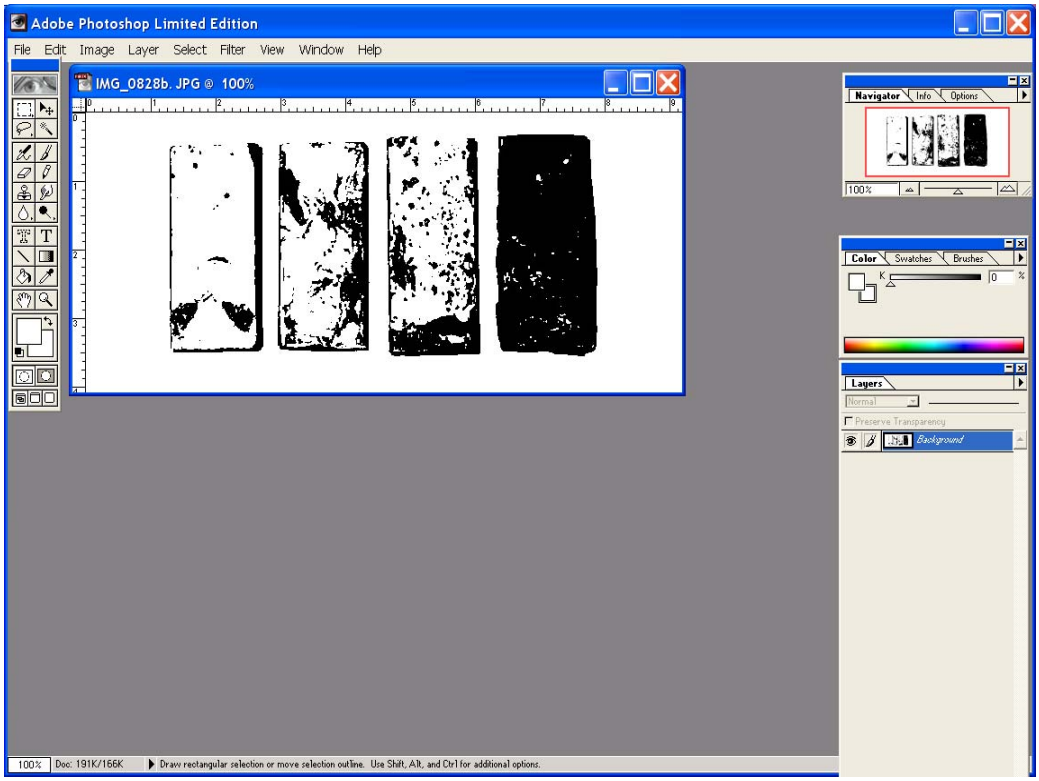

4. An image analyzer[1] can now be used to measure the cumulative size of white areas and black areas.

a. Open the picture saved in the previous step with Image Analyzer.

[1] Image Analyzer 1.22.2. Internet http://meesoft.logicnet.dk/Analyzer/

APPENDIX C 3/4. QUALITY INDEX MEASUREMENT BY USING IMAGE ANALYZER

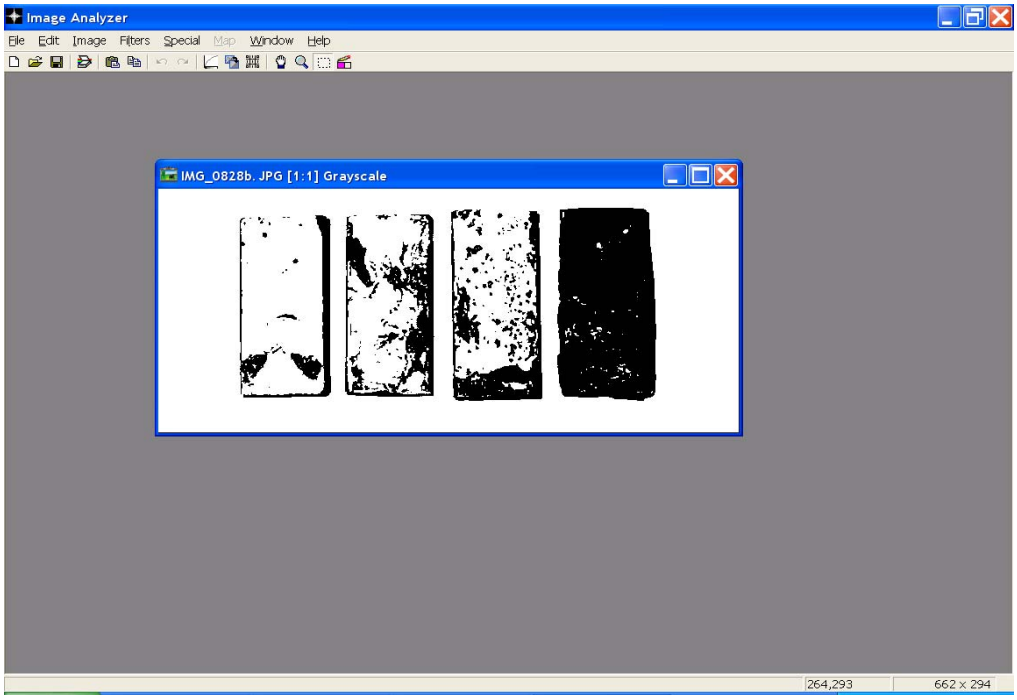

b. Use rectangle select tool to take a portion of the first piece and crop. (Crop an area as close to the edges as possible)
Rectangle select tool
Image→Crop

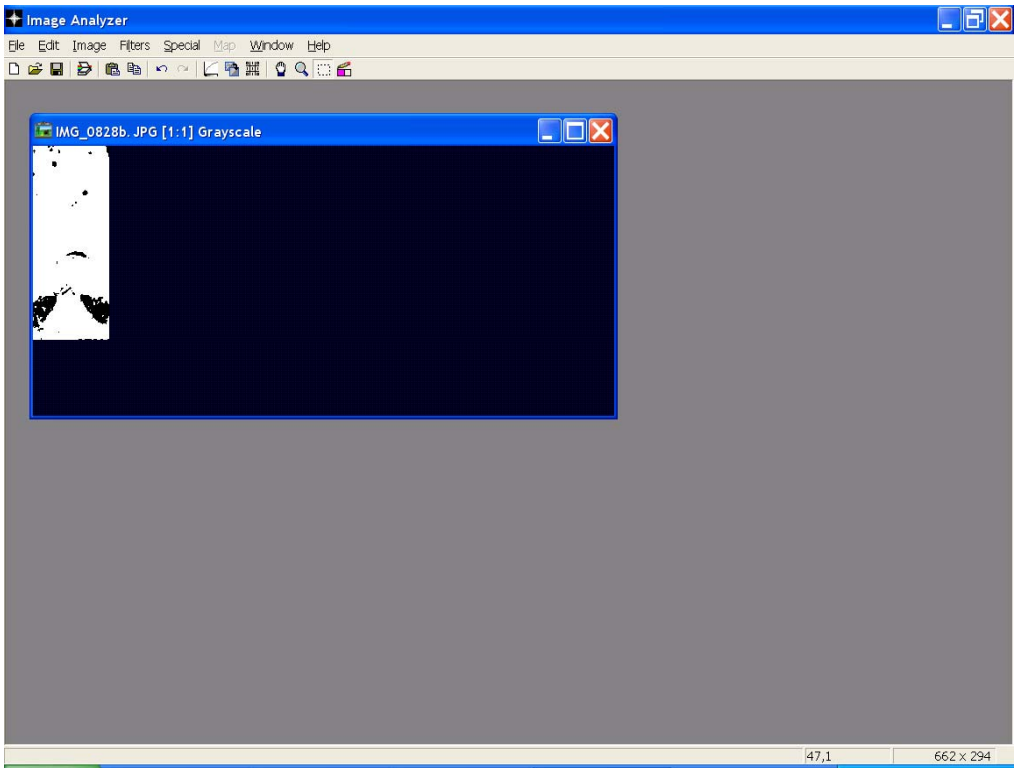

APPENDIX C 4/4. QUALITY INDEX MEASUREMENT BY USING IMAGE ANALYZER

c. Image→Color mapper

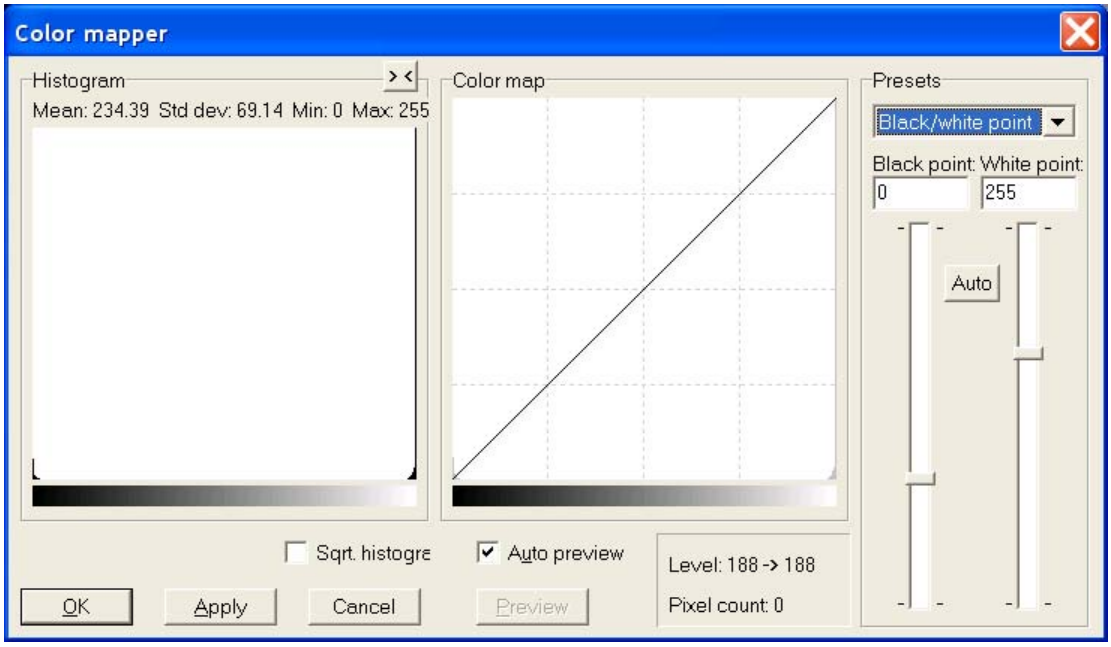

Mean value for the first piece is 234.39
Reacted area [(255-234)/255]x100 = 8.2%
Unreacted area (white) = 91.8%

d. Measure the other pieces similarly.

It is also possible to convert these readings to mm^2 or cm^2 "surface area reacted" and "surface area unreacted", if the total area of the test piece is known.

The removal of the grey areas (step 3) of the digital pictures reduces the errors. In the absence of this step, image analyzer will give smaller values for all pieces because it interprets the black pixels within the unreacted areas as reaction pixels.

APPENDIX D 1/4. The Values for the Free Energy of Formation for the Studied Oxides as Calculated by HSC Software

$Si + O_2 (g) = SiO_2$

T	deltaH	deltaS	deltaG	K
C	kcal	cal	kcal	
0.000	-217.668	-43.508	-205.784	4.607E+164
100.000	-217.741	-43.746	-201.417	9.499E+117
200.000	-217.706	-43.667	-197.045	1.055E+091
300.000	-217.589	-43.445	-192.689	3.026E+073
400.000	-217.392	-43.130	-188.359	1.443E+061
500.000	-217.110	-42.741	-184.065	1.083E+052
600.000	-216.619	-42.147	-179.818	1.029E+045
700.000	-216.429	-41.941	-175.614	2.771E+039
800.000	-216.235	-41.751	-171.430	8.222E+034
900.000	-215.543	-41.118	-167.306	1.481E+031
1000.000	-215.331	-40.944	-163.203	1.042E+028

Formula	FM	Conc.	Amount	Amount	Volume
	g/mol	wt-%	mol	g	l or ml
Si	28.086	46.743	1.000	28.086	12.054 ml
O_2(g)	31.999	53.257	1.000	31.999	22.414 1
	g/mol	wt-%	mol	g	l or ml
SiO_2	60.084	100.000	1.000	60.084	0.000 ml

$Al + 0.75\ O_2 (g) = 0.5\ Al_20_3$

T	deltaH	deltaS	deltaG	K
C	kcal	cal	kcal	
0.000	-200.155	-37.286	-189.970	1.022E+152
100.000	-200.273	-37.668	-186.217	1.187E+109
200.000	-200.280	-37.687	-182.448	1.908E+084
300.000	-200.228	-37.588	-178.684	1.381E+068
400.000	-200.145	-37.455	-174.932	6.299E+056
500.000	-200.051	-37.325	-171.193	2.488E+048
600.000	-199.964	-37.220	-167.466	8.322E+041
700.000	-202.444	-39.877	-163.638	5.661E+036
800.000	-202.327	-39.762	-159.656	3.289E+032
900.000	-202.196	-39.646	-155.686	1.013E+029
1000.000	-202.053	-39.529	-151.727	1.116E+026

Formula	FM	Conc.	Amount	Amount	Volume
	g/mol	wt-%	mol	g	l or ml
Al	26.982	52.925	1.000	26.982	9.993 ml
O_2(g)	31.999	47.075	0.750	23.999	16.810 1
	g/mol	wt-%	mol	g	l or ml
Al_20_3	101.961	100.000	0.500	50.981	12.858 ml

APPENDIX D 2/4. The Values for the Free Energy of Formation for the Studied Oxides as Calculated by HSC Software

$Y + 0.75\ O_2\ (g) = 0.5\ Y_2O_3$

T	deltaH	deltaS	deltaG	K
C	kcal	cal	kcal	
0.000	-227.667	-35.594	-217.945	2.479E+174
100.000	-227.575	-35.314	-214.398	3.811E+125
200.000	-227.426	-34.961	-210.884	2.609E+097
300.000	-227.252	-34.627	-207.405	1.239E+079
400.000	-227.066	-34.328	-203.958	1.675E+066
500.000	-226.878	-34.068	-200.538	4.918E+056
600.000	-226.694	-33.844	-197.143	2.234E+049
700.000	-226.518	-33.653	-193.769	3.312E+043
800.000	-226.354	-33.493	-190.411	6.040E+038
900.000	-226.200	-33.355	-187.069	7.122E+034
1000.000	-226.060	-33.240	-183.740	3.495E+031

Formula	FM	Conc.	Amount	Amount	Volume
	g/mol	wt-%	mol	g	l or ml
Y	88.906	78.744	1.000	88.906	19.894 ml
0_2(g)	31.999	21.256	0.750	23.999	16.810 l
	g/mol	wt-%	mol	g	l or ml
Y_20_3	225.810	100.000	0.500	112.905	22.536 ml

$Zr + O_2\ (g) = ZrO_2$

T	deltaH	deltaS	deltaG	K
C	kcal	cal	kcal	
0.000	-262.303	-46.295	249.657	5.886E+199
100.000	-262.227	-46.070	-245.036	3.362E+143
200.000	-262.045	-45.641	-240.450	1.185E+111
300.000	-261.816	-45.204	-235.908	9.167E+089
400.000	-261.568	-44.804	-231.408	1.370E+075
500.000	-261.311	-44.450	-226.945	1.435E+064
600.000	-261.056	-44.139	-222.516	5.018E+055
700.000	-260.807	-43.869	-218.116	9.739E+048
800.000	-260.570	-43.637	-213.741	3.408E+043
900.000	-261.264	-44.247	-209.356	1.011E+039
1000.000	-260.932	-43.975	-204.945	1.527E+035

Formula	FM	Conc.	Amount	Amount	Volume
	g/mol	wt-%	mol	g	l or ml
Zr	91.220	74.031	1.000	91.220	14.055 ml
02 (g)	31.999	25.969	1.000	31.999	22.414 1
	g/mol	wt-%	mol	g	l or ml
ZrO2	123.219	100.000	1.000	123.219	20.920 ml

APPENDIX D 3/4. The Values for the Free Energy of Formation for the Studied Oxides as Calculated by HSC Software

$Al + 0.5\ Si + 1.25\ O_2\ (g) = 0.5\ Al_2SiO_5$

T	deltaH	deltaS	deltaG	K
C	kcal	cal	kcal	
0.000	-321.034	-57.563	-305.310	2.004E+244
100.000	-321.193	-58.081	-299.520	2.755E+175
200.000	-321.169	-58.030	-293.712	4.764E+135
300.000	-321.057	-57.818	-287.919	6.259E+109
400.000	-320.903	-57.570	-282.150	4.096E+091
500.000	-320.732	-57.334	-276.405	1.377E+078
600.000	-320.567	-57.133	-270.682	5.719E+067
700.000	-322.957	-59.692	-264.868	3.082E+059
800.000	-322.739	-59.479	-258.909	5.394E+052
900.000	-322.496	-59.263	-252.972	1.352E+047
1000.000	-322.229	-59.044	-247.057	2.591E+042

Al_2SiO_5 Extrapolated from 398.000 K

Formula	FM	Conc.	Amount	Amount	Volume
	g/mol	wt-%	mol	g	l or ml
Al	26.982	33.301	1.000	26.982	9.993ml
Si	28.086	17.332	0.500	14.043	6.027 ml
O_2(g)	31.999	49.367	1.250	39.999	28.017 I
	g/mol	wt-%	mol	g	l or ml
Al_2SiO_5	162.046	100.000	0.500	81.023	0.000 ml

$Zr + Si + 2\ O_2(g) = ZrSiO_4$

T	deltaH	deltaS	deltaG	K
C	kcal	cal	kcal	
0.000	-483.654	-91.604	-458.632	1.000E+308
100.000	-483.702	-91.782	-449.453	1.827E+263
200.000	-483.506	-91.325	-440.296	2.461E+203
300.000	-483.180	-90.703	-431.194	2.714E+164
400.000	-482.777	-90.056	-422.156	1.179E+137
500.000	-482.326	-89.433	-413.182	6.392E+116
600.000	-481.850	-88.853	-404.268	1.573E+101
700.000	-481.364	-88.326	-395.409	6.431E+088
800.000	-480.883	-87.855	-386.601	5.480E+078
900.000	-481.336	-88.251	-377.804	2.445E+070
1000.000	-480.774	-87.791	-369.003	2.231E+063

Formula	FM	Conc.	Amount	Amount	Volume
	g/mol	wt-%	mol	g	l or ml
Zr	91.220	49.765	1.000	91.220	14.055 ml
Si	28.086	15.322	1.000	28.086	12.054 ml
O_2(g)	31.999	34.914	2.000	63.998	44.827 1
	g/mol	wt-%	mol	g	l or ml
$ZrSiO_4$	183.303	100.000	1.000	183.303	0.000 ml

APPENDIX D 4/4. The Values for the Free Energy of Formation for the Studied Oxides as Calculated by HSC Software

$Mg + 0.5O_2(g) = MgO$

T	deltaH	deltaS	deltaG	K
C	kcal	cal	kcal	
0.000	-143.681	-25.823	-136.627	2.117E+109
100.000	-143.711	-25.927	-134.036	3.237E+078
200.000	-143.672	-25.835	-131.448	5.264E+060
300.000	-143.610	-25.717	-128.870	1.393E+049
400.000	-143.546	-25.614	-126.304	1.024E+041
500.000	-143.490	-25.536	-123.747	9.614E+034
600.000	-143.446	-25.482	-121.196	2.177E+030
700.000	-145.558	-27.773	-118.531	4.186E+026
800.000	-145.528	-27.743	-115.755	3.765E+023
900.000	-145.488	-27.708	-112.982	1.121E+021
1000.000	-145.439	-27.669	-110.213	8.334E+018

Formula	FM	Conc.	Amount	Amount	Volume
	g/mol	wt-%	mol	g	l or ml
Mg	24.305	60.304	1.000	24.305	13.968 ml
O_2(g)	31.999	39.696	0.500	15.999	11.207 l
	g/mol	wt-%	mol	g	l or ml
MgO	40.304	100.000	1.000	40.304	11.258 ml

APPENDIX E. Free Energy Change in Silica Reactions Calculated by HSC Software

$2Mg + 2SiO_2 \rightarrow Mg_2SiO_4 + Si$ (dissolved in the Mg)

T	deltaH	deltaS	deltaG	K
C	kJ	J	kJ	
0.000	-319.330	-16.486	-314.827	1.620E+060
100.000	-320.167	-19.138	-313.026	6.637E+043
200.000	-320.774	-20.581	-311.037	2.191E+034
300.000	-321.481	-21.929	-308.912	1.430E+028
400.000	-322.488	-23.540	-306.642	6.260E+023
500.000	-323.950	-25.557	-304.191	3.357E+020
600.000	-326.966	-29.197	-301.473	1.088E+018
700.000	-327.285	-29.544	**-298.534**	1.060E+016
800.000	-327.485	-29.740	-295.569	2.442E+014
900.000	-331.715	-33.652	-292.236	1.030E+013
1000.000	-331.808	-33.729	-288.866	7.121E+011

Formula	FM	Conc.	Amount	Amount	Volume
	g/mol	wt-%	mol	g	l or ml
Mg(l)	24.305	28.801	2.000	48.610	27.937 ml
SiO_2(g)	60.084	71.199	2.000	120.169	0.000 ml
	g/mol	wt-%	mol	g	l or ml
Si(l)	28.086	16.640	1.000	28.086	12.054 ml
Mg_2SiO_4	140.693	83.360	1.000	140.693	0.000 ml

$2Mg(l)+O_2(g)+SiO_2 \rightarrow Mg_2SiO_4$

T	deltaH	deltaS	delta G	K
C	kJ	J	kJ	
0.000	-1278.336	-223.502	-1217.286	6.335E+232
100.000	-1280.137	-229.229	-1194.601	1.728E+167
200.000	-1281.072	-231.474	-1171.550	2.224E+129
300.000	-1281.655	-232.598	-1148.342	4.614E+104
400.000	-1282.128	-233.360	-1125.042	2.030E+087
500.000	-1282.637	-234.063	-1101.672	2.729E+074
600.000	-1283.767	-235.424	-1078.206	3.215E+064
700.000	-1283.414	-235.044	**-1054.681**	4.127E+056
800,000	-1282.880	-234.523	-103I.202	1.574E+050
900.000	-1284.248	-235.814	-1007.603	7.369E+044
1000.000	-1283.441	-235.155	-984.054	2.382E+040

Formula	FM	Conc.	Amount	Amount	Volume
	g/mol	wt-%	mol	g	l or ml
Mg(l)	24.305	34.550	2.000	48.610	27.937
02(g)	31.999	22.744	1.000	31.999	22.414
Si02	60.084	42.706	1.000	60.084	0.000
	g/mol	wt-%	mol	g	l or ml
Mg2Si04	140.693	100.000	1,000	140.693	

APPENDIX E. Free Energy Change in Silica Reactions Calculated by HSC Software

$2Mg(l)+O_2(g)=2MgO$

T	deltaH	deltaS	deltaG	K
C	kJ	J	kJ	
0.000	-1214.766	-223.427	-1153.737	4.449E+220
100.000	-1216.510	-228.963	-1131.072	2.208E+158
200.000	-1217.431	-231.175	-1108.050	2.169E+122
300.000	-1217.933	-232.147	-1084.878	7.581E+098
400.000	-1218.180	-232.549	-1061.639	2.439E+082
500.000	-1218.253	-232.653	-1038.377	1.444E+070
600.000	-1218.194	-232.583	-1015.115	5.401E+060
700.000	-1218.030	-232.405	**-991.865**	1.752E+053
800.000	-1217.775	-232.157	-968.636	1.417E+047
900.000	-1217.442	-231.861	-945.435	1.256E+042
1000.000	-1217.038	-231.580	-922.265	6.946E+037

Formula	FM	Conc.	Amount	Amount	Volume
	g/mol	wt-%	mol	g	l or ml
Mg(l)	24.305	60.304	2.000	48.610	27.937 ml
O_2(g)	31.999	22.744	1.000	31.999	22.414
	g/mol	wt-%	mol	g	l or ml
MgO	40.304	100.00	2.000	80.609	22.516 ml

$2\ MgO + SiO_2 \rightarrow Mg_2SiO_4$

T	deltaH	deltaS	deltaG	K
C	kJ	J	kJ	
0.000	-63.570	-0.076	-63.549	1.424E+012
100.000	-63.627	-0.266	-63.528	7.827E+008
200.000	-63.642	-0.299	-63.500	1.025E+007
300.000	-63.723	-0.451	-63.464	6.086E+005
400.000	-63.948	-0.810	-63.403	8.324E+004
500.000	-64.384	-1.410	-63.294	1.890E+004
600.000	-65.573	-2.842	-63.092	5.952E+003
700.000	-65.385	-2.639	**-62.817**	2.355E+003
800.000	-65.105	-2.366	-62.566	1.111E+003
900.000	-66.806	-3.953	-62.168	5.865E+002
1000.000	-66.403	-3.624	-61.789	3.430E+002

Formula	FM	Conc.	Amount	Amount	Volume
	g/mol	wt-%	mol	g	l or ml
MgO	40.304	57.294	2.000	80.609	22.516 ml
SiO_2	60.084	42.706	1.000	60.084	0.000 ml
	g/mol	wt-%	mol	g	l or ml
Mg_2SiO_4	140.693	100.00	1.000	140.693	0.000 ml